SYNTHESIS OF CARBON NANOMATERIALS AND THEIR APPLICATION TOWARDS FIELD ELECTRON EMISSION

カーボンナノ材料の合成とその電界電子放出応用

2008

PRADIP GHOSH

名古屋工業大学博士論文
甲第667号(課程修了による)
平成20年12月17日授与

Dedicated to my beloved parents

Table of Contents

Chapter 1

Introduction

1.1 General introduction

In the past decades carbon nanomaterials have drawn much attention to the researcher due to their unique structure and properties. It is the chemical genius of carbon that it can bond in different ways to form different material with completely different properties. Carbon nanomaterials are found in variety forms such as graphite, diamond, carbon nanofibers (CNFs), fullerenes and carbon nanotubes (CNTs). Fig. 1 shows the various allotropic forms of carbon. The arrangement of carbon atoms by forming several distinct types of valence bond in the lattice formed different kinds of structures of carbon material.

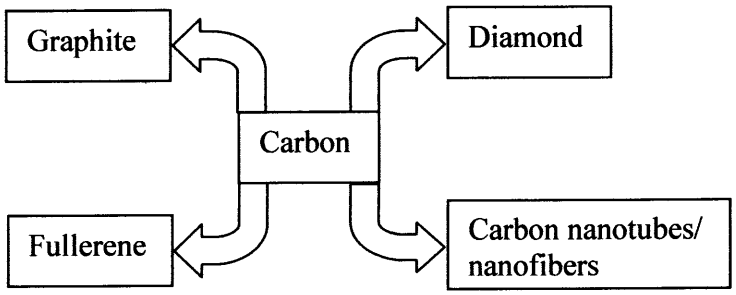

Fig. 1. Different forms of carbon.

Diamond

Diamond is the allotrope and one of the stable forms of carbon where the carbon atoms are arranged in an isometric-hexoctahedral crystal lattice. Diamond is one of the hardest known natural materials and the third-hardest known material after aggregated diamond nanorods and ultrahard fullerite. It can be synthesized from graphite at high temperatures and pressures [1]. In diamond, four valence electrons in the carbon atom are

shared equally through sp^3 hybridization. This material has been adapted for many uses because of its exceptional physical characteristics viz. high dispersion index, high thermal conductivity (900-2320 W/m K), high melting point of 3820 K (3547 °C/6420 °F) and a boiling point of 5100 K (4827 °C/8720 °F). Naturally occurring diamonds have a density ranging from 3.15 to 3.53 g/cm^3, with very pure diamond typically extremely close to 3.52 g/cm^3. The structure of the diamond is shown in Fig. 2.

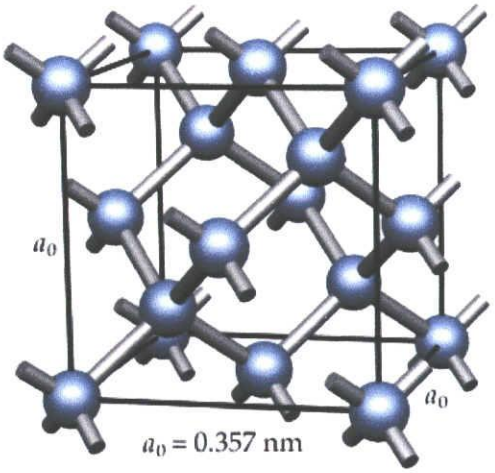

Fig. 2. Structure of diamond.

The bond length between two sp^3 carbon atoms is 1.54 Å. Due to highly symmetrical arrangememts of carbon atom, diamond can form different shapes of eight-sided octahedron cubes, dodecahedra, and combinations of these shapes.

Graphite

Graphite is the most stable form of carbon at room temperature and atmospheric pressure. In graphite each carbon atom is covalently bonded to three others in the same plane. The structure of the graphite is shown in Fig. 3. In the graphite structure, overlap

occurs between the 2(sp^2) orbital of neighboring atoms in the same plane. For such neighbors a side-to-side overlap also occurs between their unhybridized p orbital. A side-to-side bonding known as π-bonding and the electrons participating in this π-bonding seem able to move across these π-bonds from one atom to the next. This feature explains graphite's ability to conduct electricity along the sheets of carbon atom parallel to the (0001) direction. The distance between the sp^2 C-C is 1.42 Å.

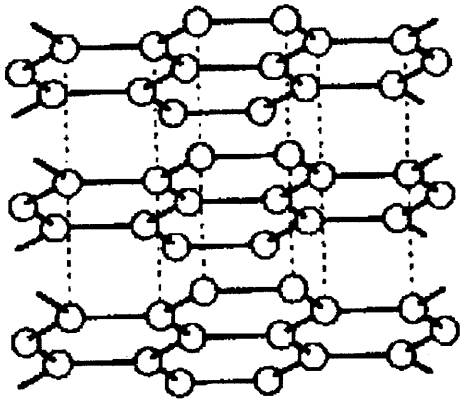

Fig. 3. Structure of graphite.

A distance 3.40 Å holds the adjacent sheets of carbon atoms together by the weak Van der Waals bonds. The bond angle between the carbon atoms is 120°. It has a high melting point, similar to that of diamond. It is used in pencils and as a dry lubricant for things like locks. Due to the presence of delocalized π electrons it can conduct electricity. However, the electricity is only conducted within the plane of the layers.

Fullerene

Eiji Osawa of Toyohashi University of Technology predicted the existence of C_{60}

in the year of 1970. He made some hypothesis about ball shape structure. He published that report in Japanese magazine and did not reach to the people of other country. Real breakthrough came when Robert Curl, Harold Kroto and Richard Smalley first reported the existence of fullerene in the year of 1985 [2].

The fullerene is one of the most well known allotropes of carbon (Fig. 4). This closed cage carbon molecule is completely composed of carbon atoms and exists in the form of sphere, ellipsoid and tubes. The best known example of fulllerene is C_{60}. This molecule is nearly spherical with truncated icosahedral structure formed by 12 pentagons and 20 hexagons with a carbon atom at the vertices of each polygon and a bond along each polygon edge. The presence of pentagons prevents the molecule to be planar and introduces curved structure. A greatly elongated fullerene can be produced with exactly 12 pentagons and millions of hexagons [3]. The coordination of carbon atom in fullerene is non planar but slightly pyramidalized with some sp^3 bonding present in the essentially sp^2 carbons. Not only C_{60} but also C_{70}, C_{72}, C_{76}, C_{84} and even up to 100 carbon atoms are also observed.

Fig. 4. Structure of fullerene.

Carbon nanofibers (CNFs)

Carbon nanofibers (CNFs) are an exciting new class of carbon nanomaterial and it has been the subject of numerous research studies. The interest in the structure of these filaments and their properties emerged in the 1970s with the development of the transmission electron microscopy, when the mechanistic proposals of Oberlin et al. [4] and Baker et al. [5] were reported.

There are different structural forms of CNFs. The widely accepted structures of CNFs are platelet, fishbone, ribbon, stacked cup CNFs (Fig. 5).

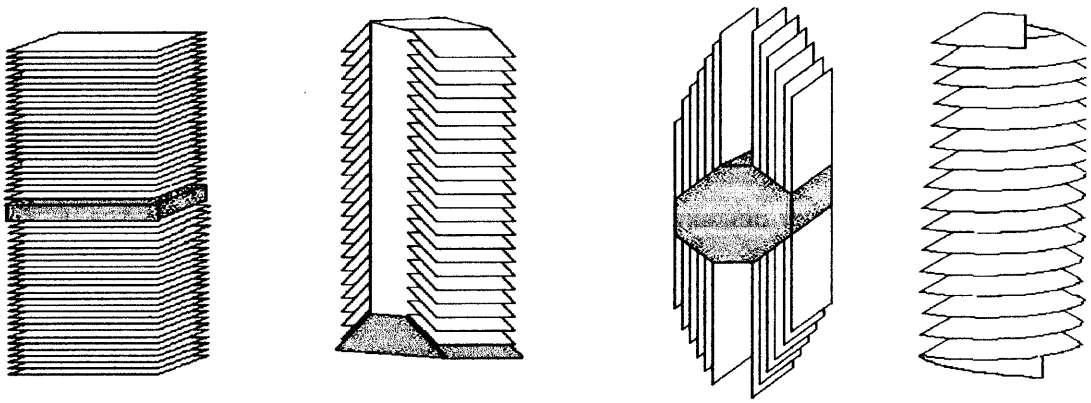

Fig. 5. Different forms of carbon nanofibers.

The structural differences of CNFs arise due to the arrangement of graphene layers with respect to the fiber axis of nanofibers. In platelet CNFs the graphene layers are perpendicular to the fiber axis. In fishbone nanofibers the graphene layers are inclined to some angle with respect to the fibril axis. Ribbon CNFs are comprised of straight, unrolled graphene layers that are parallel to the fibril axis with non-cylindrical cross-sections. This form of nanofiber is a continuous layer of rolled (spiral) graphene along the fiber axis.

Carbon nanotubes (CNTs)

In 1952 Radushkevich and Lukyanovich published clear images of 50 nanometer diameter tubes made of carbon [6]. The discovery of this material was largely unnoticed, as the article was published in the Russian language. Although CNTs were produced before 1991, but the invention of the transmission electron microscope allowed the direct visualization of these structures by S. Iijima in 1991 [7]. After the discovery of this novel material it gave us lot of hopes regarding the new technology progress. CNTs have been attracting considerable attention because of their unique physical and chemical properties. There are two kinds of CNTs: single-walled (SWNTs) and multi-walled carbon nanotubes (MWNTs). They are made of concentric cylinders placed around a common central hollow, with spacing between the layers close to that of the interlayer distance in graphite (0.34 nm). The interlayer distance in MWNTs is little bit higher to the distance between graphene layers in graphite, approximately 3.3 Å due to severe geometrical constraint when forming the concentric seamless cylinders while maintaining the graphite spacing between them. A SWNT is formed by rolling a sheet of graphene into a cylinder along a lattice vector in the graphene plane. Depending on the chirality (the chiral angle between hexagons and the tube axis), SWNTs can be either metallic or semiconductors, with band gaps that are relatively large (0.5 eV for typical diameter of 1.5 nm) or small (10 meV), even if they have nearly identical diameters [8]. The chemical bonding of CNTs are composed entirely of sp^2 bonds, similar to those of graphite. This sp^2 bonding structure makes the molecule with their unique strength. Both SWNTs and MWNTs can be regarded as aggregates of nanotube units (cylinders), the MWNTs consisting of

concentric assembly and SWNTs ropes of close packed nanotube units. The aspect ratios of both MWNTs and SWNTs are high because their lengths are in the range of several micrometers. SWNTs have a diameter of close to 1 nanometer, with a tube length that can be many thousands of times longer and MWNTs have the diameter is in the range of 2 to 25 nm. Apart from SWNTs and MWNTs, double-walled carbon nanotubes (DWNTs) are considered as one special type of material and can be considered as two co-axial SWNTs, which are expected to be utilized as memory devices, magnetic devices etc [9]. Recent studies showed that DWNTs have higher thermal and chemical stability than SWNTs, and can be applied to gas sensors, dielectric devices, nanoelectronic devices, nanocomposites and emitters etc. The DWNTs have a co-axial structure and made of two concentric graphene cylinders.

1.2 Synthesis methods of carbon nanofibers (CNFs)

Till date, numerous methods have been developed to synthesize CNFs for many potential applications (field emission devices, sensors, fuel cells, supercapacitors etc). These include:

A. Floating catalyst method, in which fibers seems to grow on vapor phase [10-12].

B. Substrate methods, where fibers grow on catalyst deposit on substrate [13,14].

C. Microwave pyrolysis chemical vapor deposition (MCVD) [15].

D. Low-Power Microwave Plasma-Assisted CVD [16].

E. Ion irradiation technique [17,18].

F. Pulsed laser ablation method [19].

1.3 Synthesis methods of carbon nanotubes (CNTs)

There are three principle methods to synthesize CNTs. These are arc discharge [20], laser ablation [21], and chemical vapor deposition method (CVD [22]. The first two methods are modified physical vapor deposition method and involve carbon vaporization at high temperatures. These two methods are very well known to produce high quality CNTs with lot of other byproducts (amorphous carbon, metal impurities). The main disadvantages of these methods are that the equipments requirements and large amounts of energy consumed by these methods make them hinder for large-scale production. CVD method offer one of the most viable techniques to prepare large-scale synthesis of CNTs in low cost. This method can be easily scaled up to industrial production. This method is a continuous process and considered for high yield and low impurity production of CNTs at moderate temperature.

1.3.1 Arc discharge method

In 1991, Sumio Iijima first prepared CNTs [7] by arc discharge method and the macroscopic production of CNTs was made in 1992 [23]. This method is very well known method to prepare SWNTs, DWNTs and MWNTs. In arc discharge method, direct current (DC) arc discharge experiments were carried out in a stainless steel chamber that was filled with hydrogen/helium, or their mixture at certain pressure. The anode is a graphite rod in which a hole had been drilled and filled with some metal catalyst. The anode and cathode was kept at certain distance. When current was passed through the

electrodes, plasma will be generated. This plasma will evaporate the carbon on the anode and the material will be deposited on the cathode surface. Using this method Iijima et al. [24] and Bethune et al. [25] synthesized SWNTs. Not only SWNTs and MWNTs, but also DWNTs have been also synthesized by this method [26,27].

1.3.2 Laser ablation techniques

This method is almost similar to arc discharge method, as the optimum background gas and catalyst mixture is same as in the arc discharge method. In the year of 1995, Smalley's group prepared CNTs by laser ablation method [28]. There are two kinds of laser to vaporize the graphite target. These are continuous laser and pulsed laser. The light intensity of pulsed laser is much higher than the continuous laser. The chamber is filled with inert gas (helium or argon) in order to keep the pressure at 500 Torr. Continuous or pulsed laser was used to vaporize a target consisting of a mixture of graphite and metal catalyst (cobalt or nickel). As the vaporized species cooled down, small carbon molecule quickly condense to form large clusters. The catalyst also started to condense and adheres to carbon clusters to prevent their closing into cage structures. The SWNTs formed in this case are bundle together by Van der Walls forces. In the case of pure graphite electrodes, MWNTs would be synthesized but SWNTs can be synthesized using a mixture of graphite with transition metals as a catalyst.

1.3.3 Chemical vapor deposition method (CVD)

CVD method is cost effective and viable techniques for large-scale production of CNTs. Recently this method has created a lot of attention to the researchers because of high yield, low impurity and bulk production of CNTs at moderate temperature. This method is capable to control the diameter, length, and alignment of the CNTs by choosing the suitable catalyst on substrate. This method mainly involves the decomposition of hydrocarbon (ethylene, acetylene, methane, alcohol etc) over the transition metal catalyst at the desired temperature. CVD method is essentially a two-step process consisting of a catalyst preparation followed by the synthesis of CNTs. There are different kinds of CVD techniques are developed to synthesize carbon nanotubes (SWNTs, DWNTs, MWNTs). These are plasma enhanced CVD [29-31], thermal CVD [32], alcohol catalytic CVD [33,34], aero gel supported CVD [35]. In some applications, the deposition of CNTs on substrate is highly desirable. In this regard CVD method is superior compared to laser ablation and arc discharge method. The CNTs deposited on the substrate are highly aligned due to Van der Walls interaction between the neighboring CNTs. Various groups reported the highly aligned CNTs on different substrates by this simple method [36-40].

1.3.4 Spray pyrolysis method

This method is very simple method compared to that of CVD method and is effective for synthesis of CNTs. This method is the sister method of CVD method and relatively inexpensive and simpler than CVD method. Using this method Afre et al.

synthesized well-aligned MWNTs by spray pyrolysis of natural precursor [41]. Thus it has been indicated that spray pyrolysis method is also a promising method for the growth of different kinds of CNTs.

1.4 Y-junction carbon nanotubes (Y-CNTs)

CNTs with junctions have been attracting a considerable attention because these materials are potentially able to bring in new mechanical and electrical properties. Many theoretical and experimental works have been carried out to explore the atomic structure and electrical properties of Y-CNTs [42-46]. For device application it is desirable to connect the CNTs with different diameters and chiralities [47]. However, these special kinds of CNTs are relatively difficult to synthesize than normal CNTs. The first synthesis of Y-CNTs was reported in 1995 [48] by Zhou et al. Since then, most of the work has been carried out by CVD using different carbon source and transition metal as the catalyst [49-55]. Recently, it has been observed that gold nano-particles are also effective for growing Y-CNTs. Since gold has the merits of excellent electric conductivity, resistance to oxidation, and compatible with IC process, it would be an ideal choice for the fabrication of CNT devices. Recently Luo et al. prepared Y-CNTs on Si substrate by Au-catalyzed CVD method [56].

1.5 Doped carbon nanotubes

Heteroatom doping (e.g., boron, sulfur, phosphorous, and nitrogen) of graphitic carbon lattices effects various physicochemical properties of sp^2 carbon materials [57,58].

It has been predicted theoretically and experimentally that the substitution of carbon atom by heteroatom in the graphite framework changes the electrical conductivity, chemical reactivity and hardness of the CNTs [59,60]. Thus the tuning of their electronic properties in a controlled manner is required, and in this context, doping represents a suitable choice. Analogous to the processes employed in the silicon industry, an effective approach to generate n-and p-type semiconductors with a controlled doping level is the substitution with heteroatoms such as N, B, or P. The doping of CNTs with boron and nitrogen is relatively easy because of their smaller atomic radius. The doping of CNTs with boron and nitrogen atom renders them p-type and n-type, respectively.

Synthesis of nitrogen-doped CNTs (CN_x) has recently been considered as a possible method to control the electronic properties of CNTs in a well-defined way. An enhancement of conductivity is expected, because the additional electrons contributed by the nitrogen atom provide electron carriers for the conduction band [61]. The advantage of such nanotube is that their electronic properties are primarily determined by the composition and are thus relatively easy to control. CN_x nanotubes are very effective material for field emission [62], hydrogen storage media [63] and in microelectronics [64,65]. For this reason, much effort has been devoted to the synthesis of CN_x nanotubes of good quality via simple and reliable techniques. Several groups have reported the synthesis of the CN_x nanotubes [66-74]. Substitution of nitrogen atom on CNTs induces different features on these structures. The first is an sp^2 configuration where one N atom substitutes C atom in the walls and has an extra electron, thereby generating an n-type semiconductor. The second expected configuration is a pyridine-like bond, which involves the removal of a C atom from the nanotube walls inducing structural defects.

CN_x nanotubes show a bamboo-like morphology with transverse carbon bridges forming compartments due to incorporation of nitrogen atom on CNTs.

1.6 Field emission properties of carbon nanotubes/nanofibers

The remarkable field emission characteristics of CNTs/CNFs have generated considerable interest in their application for vacuum microelectronic devices [75-78]. This is due to their high aspect ratio, good mechanical/electrical properties, and thermal/chemical stability. New X-ray tubes have recently been developed using CNTs and CNFs as field electron sources [79,80]. Various methods have been developed to synthesize CNFs on various substrates (silicon, nickel, quartz, glass, plastic etc) to study their field electron emission properties. Chen et al. [81] prepared aligned high aspect ratio CNFs in-situ using modified hot filament chemical vapor deposition. The field emission properties were then studied. A Fe–Cr wire filament acted as a catalytic source and a heat source. CNFs were deposited on a Si substrate with CO_2 as a carrier gas through ethanol. The experimental results indicate that the flow in the horizontal direction to the substrate produces CNFs with diameters of less than 10 nm. The field emission current of 2 V/μm was 0.54 mA/cm^2; the turn-on field of the sample was 1.1 V/μm. The direct growth of vertically aligned CNTs onto flexible plastic substrates using plasma-enhanced chemical vapor deposition has been reported by Hofmann et al. [82]. Field emission measurements show a low turn-on field of ~3.2 V/μm and a low threshold field of ~4.2 V/μm. The result establishes a method of flexible field emitter fabrication, which is well suited for display production and integration of CNTs into plastic electronics. Recently Tan et al. fabricated

carbon nanofiber-based flexible field emitters prepared by an ion beam technique. The flexible emitters are extremely robust under various stress conditions and show no sign of degradation after 16 h long lifetime test. The advantages of flexible substrate, among many, are lower cost of producing the emitter and allowing emitter of any geometry and shape to be made for use in field emission applications [83]. For the practical application of CNTs and CNFs to field electron sources, their synthesis on large substrates is indispensable. In the conventional synthesis methods, such as arc discharge, laser ablation, CVD, growth temperatures higher than 500 °C are generally required. Such a high growth-temperature is, however, a serious drawback for commercialization. They should be grown at lower temperatures, ideally at room temperature. Tanemura et al. synthesized CNFs on graphite, carbon-coated silicon, and carbon-coated nickel surfaces were bombarded with obliquely incident Ar^+ ions at room temperature. The field electron emission measurements for the CNFs thus grown on the carbon-coated silicon substrate showed the threshold field of 1.8 V/μm with a current density of 1 mA/cm^2, and the field enhancement factor was estimated to be 1951 [84]. Smith et al. prepared CNFs by plasma enhanced chemical vapor deposition of CH_4 at room temperature on Ni catalyzed glass substrates. The observed structures displayed excellent electron field emission with a threshold field of 5 V/μm and field enhancement factor was found to be about 4200 [85]. Extensive studies on the electron field emission characteristics of CNTs (SWNTs, DWNTs, MWNTs and vertically aligned one) have been carried out in recent years due to the potential applications of CNT field emitters in flat TV and large panel display [86-88]. The first working flat panel display based on carbon nanotube field emitters has been reported [89]. Recent studies showed that aligned CNTs are very effective field emitter.

Pan et al. measured the field emission performance from aligned and opened carbon nanotube arrays. Field emission current densities of 10 $\mu A/cm^2$ were observed at applied field of 0.6-1 V/μm, and current densities of 10 mA/cm^2 have been realized at applied fields as low as 2-2.7 V/μm [90]. Yoon et al. prepared high-purity vertically aligned CNTs via pyrolysis of ferrocene ($FeC_{10}H_{10}$) and acetylene (C_2H_2) in the wide temperature range of 600-1000 °C and studied their field emission property. A typical turn-on field, which produces a current density of 0.1 $\mu A/cm^2$, is about 2.9, 1.4, and 1.2 V/μm respectively, for the CNTs prepared at 600, 800, and 1000 °C. The respective emission current density reaches 1 mA/cm^2 at an applied field of about 6.0, 3.0, and 2.5 V/μm. This indicates that field emission property was improved with increasing the growth temperature. This can be attributed to the enhancement of graphitization of CNTs with increasing the growth temperature [91].

SWNTs and DWNTs are also a potential candidate for application on the field emission display. Yang et al. prepared large-area, high-uniformity, and high-density SWNTs by catalytic pyrolysis of ethanol at 900 °C in a tubular furnace. The field emission measurements indicated that they are excellent emitter with extremely low turn-on field of 0.008 V/μm and threshold field of 0.07 V/μm [92]. Jung et al. studied the field emission characteristics of annealed and non-annealed DWNTs. It was observed that the annealed DWNTs had enhanced crystallinity and reduced defects. DWNTs showed better field emission performance after high-temperature thermal annealing. The annealed DWNTs indicated the turn-on field of about 1.16 V/μm at 0.1 $\mu A/cm^2$ and the threshold field of about 2.12 V/μm at 1.0 mA/cm^2. Moreover, the annealed DWNTs exhibited better emission stability in relative to the nonannealed DWNTs. Such a remarkable

improvement of field emission performance was attributed to the enhanced crystallinity and reduced defects of the annealed DWNTs [93].

1.7 Field emission properties of CN_x nanotubes

As mentioned earlier that the electronic properties of CNTs can be modified by introducing topological defects. Theoretical and experimental studies revealed that doping CNTs by N or B atoms could alter the structural and electronic properties significantly. These studied showed that nitrogen doping in CNTs enhances the local density of states near the Fermi level which in turn enhance the field emission characteristics at relatively lower applied voltage [94,95]. It is observed that aligned CN_x nanotubes showed better field emission properties than pure CNTs. The Doping of CNTs with N atom enhances their electron-conducting properties because of the presence of additional lone pairs of electrons that act as donors with respect to the delocalized π system of the hexagonal framework. The controllable synthesis of well-aligned CN_x nanotubes with high N ratio may open a route to improve the field emission properties of CNTs [96].

Till date, there are only few reports of the field emission properties of CN_x nanotubes. Sharma et al. studied the field emission properties of CN_x nanotubes grown in-situ on tungsten (W) tips and flat silicon substrate. Field emission measurement showed that CN_x nanotubes exhibited better field emission performance than the undoped CNTs. It has been suggested that in CN_x nanotubes, the nitrogen atoms substitute the carbon atoms in the graphene sheet and modify the conduction band [97]. Wang et al.

synthesized highly aligned CN_x nanotubes with a high content of nitrogen ($x \leq 9\%$) by pyrolyzing metal phthalocyanine on an n-type Si(100) substrate. Field emission measurements suggest that the CN_x nanotubes began to emit electrons at an electric field of 1.5 V/μm, and current densities of 80 $\mu A/cm^2$ have been realized at an applied field as low as 2.6 V/μm [98]. Srivastava et al. synthesized CN_x nanotubes on mirror polished and mechanical polished Si substrates. All the CNTs were found to have bamboo structure with very sharp tips. These films showed very good field emission characteristics with threshold field in the range of 2.65–3.55 V/μm [99]. Thus various studies indicated that CN_x nanotubes are effective material for field electron emission applications.

1.8 Purpose and organization of dissertation

The chief purpose of this thesis is to synthesize CNTs/CNFs and CN_x nanotubes from eco-friendly, regenerative and organic precursors by cost effective methods (spray pyrolysis, CVD method) for potential application and enhancements in the field electron emission superior to earlier reports. We have successfully gown CNTs/CNFs from botanical hydrocarbons by simple spray pyrolysis method. For field emission displays it is highly desirable to grow well-aligned CNTs by simple method. Our target was to prepare vertically aligned CNTs from botanical hydrocarbons (turpentine oil, eucalyptus oil) by a viable and cost effective spray pyrolysis method and studied their field electron emission. Using these botanical hydrocarbons, aligned CNTs were grown nicely on silicon and quartz substrate. Our purpose was to achieve low turn-on, threshold field and

high current density using natural precursors grown aligned CNTs. It has been observed that these kinds of CNTs are effective field emitter with low turn-on and threshold field. The results indicated that the field emission behaviors of turpentine oil and eucalyptus oil grown CNTs are comparable or better than the some of the recently published natural precursor (camphor) grown field emission data.

CN_x nanotubes are thought to be one of the promising materials for field electron emission devices. Keeping this in mind, highly dense well-aligned bamboo-shaped CN_x nanotubes were synthesized via pyrolysis of a single feedstock (monoethanolamine) on silicon and quartz substrate. The difficulty of using multi precursors during CVD can be easily avoided using monoethanolamine as a single C/N feedstock to grow CN_x nanotubes. The as-grown CN_x nanotubes show superior field emission characteristics and high current density at low field.

Y-junction CNTs are also considered to be potential use in the FE displays and also in the upcoming field of nanoelectronics. Y-junction N-doped CNTs (Y-CN_x) are thought to be more conducting than normal Y-junction CNTs. However, there have been few reports on the electronic properties of junction CNTs. Again the geometry of the as-grown CNTs is very important for getting high field emission performance. In this regards, Y-junction CNTs are assumed to be quite promising to reduce the screening effect due to sufficient distance between the adjacent CNTs. That is why we tried to grow Y-CN_x nanotubes for future application in nanoelectronic devices especially in FE displays. We successfully achieved to grow Y-CN_x nanotubes on GaAs substrate by catalytic decomposition of a single feedstock (monoethanolamine) by CVD method. FE measurements indicated that they were effective emitter with low turn-on and threshold

field. The results demonstrate that monoethanolamine is an effective precursor for growing CN_x nanotubes, which might be a promising material for field electron emission applications. Our results indicated that the FE behaviors of these materials are better than the some of the earlier reported value.

In the first chapter, a brief introduction of carbon nanomaterials (diamond, graphite, fullerene, CNFs, and CNTs, doped CNTs) has been discussed. The application of CNTs and CNFs in the field electron emission has been described intensively. This chapter also discussed the synthesis of CN_x nanotubes and their application in field electron emission.

Second chapter deals with the synthesis of SWNTs from natural precursors: turpentine oil and eucalyptus oil. These precursors have been found to be an effective precursor for SWNTs synthesis. SWNTs were grown on high silica Y-type zeolite using transition metal catalyst by spray pyrolysis method with a reaction time 25 minutes. The as-grown SWNTs were characterized by SEM, TEM, TGA/DTA and Raman spectroscopy. The growth of SWNTs depends upon various factors (temperature, flow rate of oil, flow rate of gas, catalyst concentration). The parameters are well optimized for the growth of SWNTs.

Third chapter describes the synthesis of CNFs using a botanical hydrocarbon: turpentine oil, a carbon feedstock, ferrocene as dissolved catalyst and sulfur as a promoter by simple spray pyrolysis method at 1000 °C. The influence of sulfur concentration on the morphology of the CNFs was investigated. SEM, TEM, Raman, TGA/DTA, BET surface area were employed to characterize the as-prepared samples. TEM analysis confirm that as-prepared CNFs have a very sharp tip, bamboo-shaped,

open end, hemispherical cap, pipe-like morphology and metal particle trapped inside the wide hollow core. It is observed that sulfur plays an important role to promote or inhibit the CNF growth. Addition of sulfur to the solution of ferrocene and turpentine oil mixture was found to be very effective in promoting the growth of CNF. Without addition of sulfur, carbonaceous product was very less. At high concentration of sulfur inhibit the growth of CNFs. So the yield of CNFs was optimized for a given sulfur concentration.

In the fourth chapter, vertically aligned CN_x nanotubes were synthesized on silicon and quartz substrate using turpentine oil as carbon source, 4-tert-butylpyridine ($C_9H_{13}N$) as nitrogen precursor and ferrocene as dissolved catalyst in nitrogen atmosphere at 700 °C by simple spray pyrolysis technique. SEM, TEM, TGA/DTA, Raman spectroscopy, X-ray photoelectron spectroscopy (XPS) and electron probe micro analysis (EPMA) technique were used to characterize the structural analysis and composition of the as-grown CN_x nanotubes. Morphology of the films was greatly affected by the nature of the substrate. From XPS and EPMA data, it was found that nitrogen content of the CN_x nanotubes were 1.6 and 2 at. % on silicon and quartz substrate, respectively. Our studies show that two different types of N atoms can be present in these materials. Raman spectroscopy reveals that graphitization of CN_x nanotubes grown on silicon is better than quartz substrate. Thermogravimetric analysis showed that the thermal stability of as-prepared CN_x nanotubes grown on silicon substrate is higher than the CN_x nanotubes deposited on quartz substrate.

Chapter 5 describes the synthesis of vertically aligned CNTs from botanical hydrocarbons: turpentine oil and eucalyptus oil on n-type Si(100) substrate using Fe catalyst by simple spray pyrolysis method at 700 °C at atmospheric pressure. The

as-grown CNTs were characterized by SEM, TEM/HRTEM, TGA/DTA and Raman spectroscopy. It was observed that CNTs grown from turpentine oil had better degree of graphitization and field emission performance than eucalyptus oil grown CNTs. The turpentine oil and eucalyptus oil grown CNTs indicated that the turn-on field of about 1.7 and 1.93 V/μm, respectively at 10 $\mu A/cm^2$. The threshold field was observed to be about 2.13 and 2.9 V/μm at 1 mA/cm^2 of CNTs grown from turpentine oil and eucalyptus oil, respectively. Moreover, turpentine oil grown CNTs shows higher current density in relative to eucalyptus oil grown CNTs. The maximum current density 15.3 mA/cm^2 was obtained for ~3 V/μm corresponds to the CNTs grown from turpentine oil. The improvement of field emission performance was attributed to the enhanced crystallinity and greater length of turpentine oil grown CNTs.

Chapter 6 describes the synthesis of aligned bamboo-shaped CN_x nanotubes by chemical vapor deposition of monoethanolamine/ferrocene mixture on silicon and quartz substrate and studied their field electron emission. All CNTs exhibited bamboo-like morphology with transverse carbon bridges forming compartments. The concentration of nitrogen content has been controlled in the range of 4.8 to 6.6 at.% by controlling the deposition temperature. High resolution transmission electron microscopy revealed that CN_x nanotubes prepared at high temperature with low nitrogen content have high graphitization degree. The decomposition of monoethanolamine at reaction temperature produces ammonia which may provides an efficient route of higher nitrogen content on CN_x nanotubes. Field emission measurements indicated that CN_x nanotubes prepared at 800 °C showed nice field emission performance with turn-on and threshold field of 1.6 and 2.3 V/μm, respectively.

In chapter 7, Y-CN_x nanotube has been synthesized by catalytic pyrolysis of monoethanolamine/ferrocene mixture on GaAs substrate at 950 °C by CVD method. The presence of Y-junction has been confirmed by SEM analysis. SEM analysis also indicated that most of the metal particle present at the tip of the Y-CN_x. The nitrogen concentration of Y-CN_x nanotubes was found to be 7.8 at.% by XPS analysis. TEM observation indicated that junction CN_x nanotubes have bamboo-like morphology with transverse bridge compartments. Field emission measurements suggested that as-grown Y-CN_x nanotube is good field emitter with turn-on and threshold field is 1.6 and 2.63 V/μm, respectively.

In the last chapter, summary of the present work and suggestion for future work have been discussed.

References

1. F.P. Bundy, Journal of Chemical Physics, 38 (1963) 631.
2. H.W. Kroto, J.R. Heath, S.C. ÓBrien, R.F. Curl, R.E. Smalley, Nature 318 (1985) 162.
3. T.W. Ebbesen, Carbon Nanotubes: Preparation and Properties (CRC Press: Boca Raton, FL, 1997).
4. A. Oberlin, M. Endo, T. Koyama, J. Crystal Growth 32 (1976) 335.
5. R.T.K. Baker, M.A. Barber, P.S. Harris, F.S. Feates, R.J. Waite, J. Catal. 26 (1972) 51.
6. L.V. Radushkevich and V.M. Lukyanovich, Zurn Fisic Chim 111 (1952) 24.
7. S. Iijima, Nature 354 (1991) 56.
8. M.S. Dresselhaus, G. Dresselhaus, P.C. Eklund, Science of Fullerenes and Carbon Nanotubes; Academic Press: San Diego, 1996; p 985.
9. R. Saito, G. Dresselhaus, M.S. Dresselhaus, J. Appl. Phys. 73 (1993) 494.
10. M. Endo, M. Shikata, M. Momose, M. Shiraishi, Extended abstracts of the 17th Biennial Conference on Carbon, Lexington, USA. 1985, p. 295.
11. T. Kato, K. Kusakabe, S. Morooka, J. Mater. Sci. Lett. 11 (1992) 674.
12. G.G. Tibbetts and D.W. Gorkiewicz, Carbon 31 (1993) 809.
13. H. Katsuki, K. Matsunaga, M. Egashira, S. Kawasumi, Carbon 19 (1981) 148.
14. M. Egashira, H. Katsuki, Y. Ogawa, S. Kawasumi, Carbon 21 (1983) 89.
15. Ji-zhao Zou, Xie-rong Zeng, Xin-bo Xiong, Han-ling Tang, Long Li, Qiang Liu, Zhi-qiang Li, Carbon 45 (2007) 828.

16. G. Zhong, M. Tachiki, H. Umezawa, T. Fujisaki, H. Kawarada, I. Ohdomari, Chem. Vapor Depos. 10 (2004) 125.

17. M. Tanemura, H. Hatano, M. Kitazawa, J. Tanaka, T. Okita, S.P. Lau, H.Y. Yang, S.F. Yu, L. Huang, L. Miao, S. Tanemura, Surface Science 600 (2006) 3663.

18. M. Tanemura, T. Okita, H. Yamauchi, S. Tanemura, R. Morishima, Appl. Phys. Lett. 84 (2004) 3831.

19. Y. Suda, A. Tanaka, A. Okita, Y. Sakai, H. Sugawara, J. Phys. Conf. Ser. 59 (2007) 48.

20. C. Journet, W.K. Maser, P. Bernier, A. Loiseau, M. Lamy de la Chapelle, S. Lefrant, P. Deniard, R. Lee, J.E. Fischer, Nature 388 (1997) 756.

21. T. Guo, P. Nikolaev, A. Thess, D.T. Colbert, R.E. Smalley, Chem. Phys. Lett. 243 (1995) 49.

22. C.J. Lee and J. Park, Carbon 39 (2001) 1891.

23. T.W. Ebbesen and P.M. Ajayan, Nature 358 (1992) 220.

24. S. Iijima and T. Ichihashi, Nature 363 (1993) 603.

25. D.S. Bethune, C.H. Klang, M.S. DeVries, G. Gorman, R. Savoy, J. Vazquez, R. Beyers, Nature 363 (1993) 605.

26. J.L. Hutchison, N.A. Kiselev, E.P. Krinichnaya, A.V. Krestinin, R.O. Loutfy, A.P. Morawsky, V.E. Muradyan, E.D. Obraztsova, J. Sloan, S.V. Terekhov, D.N. Zakharov, Carbon 39 (2001) 761.

27. Y. Saito, T. Nakahira, S. Uemura, J. Phys. Chem. B 107 (2003) 931.

28. T. Guo, P. Nikolaev, A.G. Rinzler, D. Tomanek, D.T. Colbert, R.E. Smalley, J. Phys. Chem. 99 (1995) 10694.

29. Y. Li, D. Mann, M. Rolandi, W. Kim, A. Ural, S. Hung, A. Javey, J. Cao, D. Wang, E. Yenilmez, Q. Wang, J.F. Gibbons, Y. Nishi, H. Dai, Nano Lett. 4 (2004) 317.

30. Yo-Sep Min, Eun Ju Bae, Byung Seok Oh, Donghun Kang, Wanjun Park, J. Am. Chem. Soc. 127 (2005) 12498.

31. N.A. Kiselev, J.L. Hutchison, A.P. Moravsky, E.V. Rakova, E.V. Dreval, C.J.D. Hetherington, D.N. Zakharov, J. Sloan, R.O. Loutfy, Carbon 42 (2004) 149.

32. H. Liao and J.H. Hafner, J. Phys. Chem. B 108 (2004) 6941.

33. Y. Murakami, Y. Miyauchi, S. Chiashi, S. Maruyama, Chem. Phys. Lett. 377 (2003) 49.

34. S. Maruyama, R. Kojima, Y. Miyauchi, S. Chiashi, M. Kohno, Chem. Phys. Lett. 360 (2002) 229.

35. M. Su, B. Zheng, J. Liu, Chem. Phys. Lett. 322 (2000) 321.

36. J. Liu, X. Li, A. Schrand, T. Ohashi, L. Dai, Chem. Mater. 17 (2005) 6599.

37. Y.H. Li, C. Xu, B. Wei, X. Zhang, M. Zheng, D. Wu, P.M. Ajayan, Chem. Mater.14 (2002) 483.

38. Y. Yang, S. Huang, H. He, A.W.H. Mau, L. Dai, J. Am. Chem. Soc. 121 (1999) 10832.

39. S. Fan, M. Chapline, N. Franklin, T. Tombler, A. Cassell, H. Dai, Science 283 (1999) 512.

40. M. Terrones, N. Grobert, J. Olivares, J.P. Zhang, H. Terrones, K. Kordatos, W.K. Hsu, J.P. Hare, P.D. Townsend, K. Prassides, A.K. Cheetham, H.W. Kroto, D.R.M. Walton, Nature 388 (1997) 52.

41. R.A. Afre, T. Soga, T. Jimbo, M. Kumar, Y. Ando, M. Sharon, Chem. Phys. Lett.

414 (2005) 6.

42. C. Papadopoulos, A. Rakitin, J. Li, A.S. Vedeneev, J.M. Xu, Phys. Rev. Lett. 85 (2000) 3476.

43. G. Treboux, P. Lapstun, K. Silverbrook, Chem. Phys. Lett. 306 (1999) 402.

44. B. Gan, J. Ahn, Q. Zhang, et al., Diamond Relat. Mater. 9 (2000) 897.

45. B. Gan, J. Ahn, Q. Zhang, et al., Mater. Lett. 45 (2000) 315.

46. B.C. Satishkumar, P.J. Thomas, A. Govindaraj, C.N.R. Rao, Appl. Phys. Lett. 77 (2000) 2350.

47. P.L. McEuen, Nature 393 (1998) 494.

48. D. Zhou and S. Seraphin, Chem. Phys. Lett. 238 (1995) 286.

49. F.L. Deepak, A. Govindaraj, C.N.R. Rao, Chem. Phys. Lett. 345 (2001) 5.

50. D.Y. Ding, J.N. Wang, F. Yu, L.F. Su, Appl. Phys. A-Mater. 81 (2005) 805.

51. W.Z. Li, J.G. Wen, Z.F. Ren, Appl. Phys. Lett. 79 (2001) 1879.

52. N. Gothard, C. Daraio, J. Gaillard, R. Zidan, S. Jin, A.M. Rao, Nano Lett. 4 (2004) 213.

53. S.M. Huang, L.M. Dai, A. Mau, Physica B 323 (2002) 336.

54. J.M. Ting and C.C. Chang, Appl. Phys. Lett. 80 (2002) 324.

55. T.J. Lee, S.I. Jung, C.Y. Park, Y.H. Choa, C.J. Lee, Carbon 43 (2005) 1341.

56. C. Luo, L. Liu, K. Jiang, L. Zhang, Q. Li, S. Fan, Carbon 46 (2008) 440.

57. M. Endo, T. Hayashi, S.H. Hong, T. Enoki, M.S. Dresselhaus, J. Appl. Phys. 90 (2001) 5670.

58. S. Glenis, A.J. Nelson, M.M. Labes, J. Appl. Phys. 86 (1999) 4464.

59. M.C. dos Santos and F. Alvarez, Phys. Rev. B 58 (1998) 13918.

60. A.H. Nevidomskyy, G. Csanyi, M.C. Payne, Phys. Rev. Lett. 91 (2003) 1055021.

61. M. Terrones, P.M. Ajayan, F. Banhart, X.D. Blase, L. Carroll, J.C. Charlier, R. Czerw, B. Foley, N. Grobert, R. Kamalakaran, P. Redlich, M. Rühle, T. Seeger, H. Terrones, Appl. Phys. A. materials science & Processing 74 (2002) 355.

62. S. Fan, M.G. Chapline, N.R. Franklin, T.W. Tombler, A.M. Cassell, H. Dai, Science 283 (1999) 512.

63. P. Chen, X. Wu, J. Lin, K.L. Tan, Science 285 (1999) 91.

64. T. Rueckes, K. Kim, E. Joselevich, G.Y. Tseng, C.L. Cheung, C.M. Lieber, Science 289 (2000) 94.

65. H. Dai, E.W. Wong, C.M. Lieber, Science 272 (1996) 523.

66. D. Zhong, S. Liu, G. Zhang, E.G. Wang, J. Appl. Phys. 89 (2001) 5939.

67. X. Ma, E. Wang, W. Zhou, D.A. Jefferson, J. Chen, S. Deng, N. Xu, J. Yuan, Appl. Phys. Lett. 75 (1999) 3105.

68. R. Sen, B.C. Satishkumar, A. Govindaraj, K.R. Harikumar, G. Raina, J.P. Zhang, A.K. Cheetham, C.N.R. Rao, Chem. Phys. Lett. 287 (1998) 671.

69. X. Ma and E.G. Wang, Appl. Phys. Lett. 78 (2001) 978.

70. M. Nath, B.C. Satishkumar, A. Govindaraj, C.P. Vinod, C.N.R. Rao, Chem. Phys. Lett. 322 (2000) 333.

71. S.L. Sung, S.H. Tsai, C.H. Tseng, F.K. Chiang, X.W. Liu, H.C. Shin, Appl. Phys. Lett. 74 (1999) 197.

72. M. Yudasaka, R. Kikuchi, Y. Ohki, S. Yoshimura, Carbon 35 (1997) 195.

73. K. Suenaga, M. Yudasaka, C. Colliex, S. Iijima, Chem. Phys. Lett. 316 (2000) 365.

74. W.Q. Han, P. Redlich, T. Seeger, F. Ernst, M. Rühle, N. Grobert, W.K. Hsu, B.H.

Chang, Y.Q. Zhu, H.W. Kroto, D.R.M. Walton, M. Terrones, H. Terrones, Appl. Phys. Lett. 77 (2000) 1807.

75. W.A. de Heer, A. Chatelaine, D. Ugarte, Science 270 (1995) 1179.

76. P.G. Collins and A. Zettl, Appl. Phys. Lett. 69 (1996) 1969.

77. W. Zhu, C. Bower, O. Zhou, G. Kochanski, S. Jin, Appl. Phys. Lett. 75 (1999) 873.

78. J.M. Kim, W.B. Choi, N.S. Lee, J.E. Jung, Diamond Relat. Mater. 9 (2000) 1184.

79. H. Sugie, M. Tanemura, V. Filip, K. Iwata, K. Takahashi, F. Okuyama, Appl. Phys. Lett. 78 (2001) 2578.

80. G.Z. Yue, Q. Qiu, B. Gao, Y. Cheng, J. Zhang, H. Shimoda, S. Chang, J.P. Lu, O. Zhou, Appl. Phys. Lett. 81 (2002) 355.

81. C.F. Chen, C.L. Lin, C.M. Wang, Appl. Phys. Lett. 82 (2003) 2515.

82. S. Hofmann, C. Ducati, B. Kleinsorge, J. Robertson, Appl. Phys. Lett. 83 (2003) 4661.

83. T.T. Tan, H.S. Sim, S.P. Lau, H.Y. Yang, M. Tanemura, J. Tanaka, Appl. Phys. Lett. 88 (2006) 103105.

84. M. Tanemura, J. Tanaka, K. Itoh, Y. Fujimoto, Y. Agawa, L. Miao, S. Tanemura, Appl. Phys. Lett. 86 (2005) 113107.

85. R.C. Smith, J.D. Carey, C.H. Poa, D.C. Cox, S.R.P. Silva, J. Appl. Phys. 95 (2004) 3153.

86. J.M. Bonard, H. Kind, T. Stockli, L.O. Nilsson, Solid State Electron. 45 (2001) 893.

87. Y. Saito et al., Nature 389 (1997) 554.

88. K.A. Dean, B.R. Chalamala, Appl. Phys. Lett. 76 (2000) 375.

89. Q.H. Wang, A.A. Setlur, J.M. Lauerhaas, J.Y. Dai, E.W. Seeling, R.P.H. Chang, Appl. Phys. Lett. 72 (1998) 2912.

90. Z.W. Pan, Frederick C. K. Au, H.L. Lai, W.Y. Zhou, L.F. Sun, Z.Q. Liu, D.S. Tang, C.S. Lee, S.T. Lee, S.S. Xie, J. Phys. Chem. B 105 (2001) 1519.

91. S.W. Yoon, S.Y. Kim, J. Park, C.J. Park, C.J. Lee, J. Phys. Chem. B 109 (2005) 20403.

92. Yu H. Yang, Chih Y. Wang, Uei S. Chen, Wei J. Hsieh, Yee S. Chang, Han C. Shih, J. Phys. Chem. C 111 (2007) 1601.

93. Seung Il Jung, S.H. Jo, H.S. Moon, J.M. Kim, D.S. Zang, C.J. Lee, J. Phys. Chem. C 111 (2007) 4175.

94. G. Zhang, W. Duan, B. Gu, Appl. Phys. Lett. 80 (2002) 2589.

95. H.L. Sun, J.F. Jia, D. Zhong, Q.T. Shen, M. Sun, Q.K. Xue, E.G. Wang, Phys. Rev. B 66 (2002) 085423.

96. M. Terrones, P. Redlich, N. Grobert, S. Trasobares, W.K. Hsu, H. Terrones, Y.Q. Zhu, J.P. Hare, C.L. Reeves, A.K. Cheetham, M. Rühle, H.W. Kroto, D.R.M. Walton, Adv. Mater. 11 (1999) 655.

97. R.B. Sharma, D.J. Late, D.S. Joag, A. Govindaraj, C.N.R. Rao, Chem. Phys. Lett. 428 (2006) 102.

98. X. Wang, Y. Liu, D. Zhu, L. Zhang, H. Ma, N. Yao, B. Zhang, J. Phys. Chem. B 106 (2002) 2186.

99. S.K. Srivastava, V.D. Vankar, D.V. Sridhar Rao, V. Kumar, Thin Solid Films 515 (2006) 1851.

Chapter 2

Synthesis of single-walled carbon nanotubes from botanical hydrocarbons

2.1 Introduction

Since their discovery in 1993 [1], single-walled carbon nanotubes (SWNTs) have attracted a great attention due to their unique physical properties and potential application in devices. Till date, several precursors such as carbon monoxide [2], methane [3], acetylene [4], benzene [5], alcohol [6] etc. have been used as a carbon feedstock to synthesize SWNTs. These precursors are related to the fossil fuels and there may be crisis for these precursors in near future. Scarce work has been published about the synthesis of carbon nanotubes (CNTs) from natural precursors. The advantages of using natural precursor as a carbon feedstock for synthesizing CNTs are that they are eco-friendly and no chance of shortage in near future. Using these natural precursors as a carbon feedstock Afre et al. and Kumar et al. prepared good quality of multi-walled carbon nanotubes (MWNTs) and vertically aligned ones by thermal decomposition of turpentine oil and camphor [7-10]. But the synthesis of SWNTs from these kinds of natural precursors is very rare. Recently Andrews et al. synthesized SWNTs by catalytic decomposition of camphor and its analogs [11]. Our target was to prepare SWNTs by this simple method using this ecologically advantageous and regenerative material. Turpentine oil ($C_{10}H_{16}$) and eucalyptus oil ($C_{10}H_{18}O$), botanical hydrocarbons, has been found to be a promising precursor for SWNTs synthesis. Turpentine oil is a yellow to brown fluid obtained by the complex distillation of resin obtained from trees, mainly various species of pine (Pinus), extensively planted in many parts of the Southern Hemisphere. Turpentine oil is composed of terpenes, mainly α- pinene and β- pinene with a boiling point of ~170 °C. It is used chiefly as a solvent and drying agent in paints and varnishes. This oil also used for

medicinal purposes. Eucalyptus oil is a colorless to pale yellow liquid with a boiling point of 176-177 °C.

Most well known methods for synthesizing CNTs are arc discharge [12], laser ablation [13] and CVD method [14]. However, the arc discharge grown CNTs are highly impure and yield is very low. Laser ablation process could produce high-quality SWNTs. But the laser vaporization of a graphite target doped with transition metal is a high energy process and not cost effective. CVD method is a very popular technique for synthesizing CNTs and this method is economical and scaleable technique for mass production of CNTs. However, spray pyrolysis method is a very simple and inexpensive compared to that of other methods. This method is a sister method of CVD. The basic difference between CVD and spray pyrolysis method is that in spray pyrolysis method pyrolysis of carbon feedstock and the deposition of CNTs occur in one furnace whereas in CVD method two furnaces are required for two different temperature zones to grow CNTs. One temperature zone is used for the vaporization of carbon containing precursor and second temperature zone is used for the pyrolysis of carbon precursor and deposition of CNTs. Recently spray pyrolysis method has attracted attention due to possibility to produce CNTs on a commercial scale [15]. Su et al. reported the synthesis of SWNTs by this method using alcohol as carbon source and ferrocene as a dissolved catalyst [16].

Synthesis of SWNTs by this simple method using natural precursor remained as a challenge. In this chapter, we have reported the synthesis of SWNTs from botanical hydrocarbons: turpentine oil and eucalyptus oil over Fe-Co and Fe-Mo/zeolite catalyst by spray pyrolysis technique.

2.2 Experimental

Iron nitrate ($Fe(NO_3)_3.9H_2O$), cobalt nitrate ($Co(NO_3)_2.6H_2O$) and iron nitrate ($Fe(NO_3)_3.9H_2O$), molybdenum acetate $[Mo(OCOCH_3)_2]_2$ were used as the Fe-Co or Fe-Mo precursor and high silica zeolite (HSZ-390HUA) as the catalyst support. All chemicals were purchased from Nacalai Tesque and used without further purification. Desired amount of iron nitrate and cobalt nitrate was dissolved in ethanol and then high silica zeolite was added to this mixture. To prepare Fe-Mo catalyst, 0.15 g of $Fe(NO_3)_3.9H_2O$ and 0.02 g of $[Mo(OCOCH_3)_2]_2$ was dissolved in ethanol and 1g of Y-type zeolite was added to this mixture. The mixture was sonicated for 15 minutes and dried at 65 °C for 24 hr. and ball milled for few hours to break apart any agglomerates that may have formed. The concentration of the each metal species for Fe-Co catalyst was 2.5 wt% with respect to the weight of the supported material. The schematic diagram of spray pyrolysis system is illustrated in Fig. 1. In the spray pyrolysis method, 100 mg of the catalyst powder was placed on quartz boat, which was then kept at the center of the quartz tube. The one end of the quartz tube of inner diameter 25 mm and length of 500 mm was attached with the spray nozzle and the other end was connected with the water bubbler. The inlet of the spray nozzle was connected with the turpentine oil container. The flow of the oil was maintained by stop cock of the separating funnel. Nitrogen gas was used as a carrier gas. It directs the oil to flow into the reaction zone.

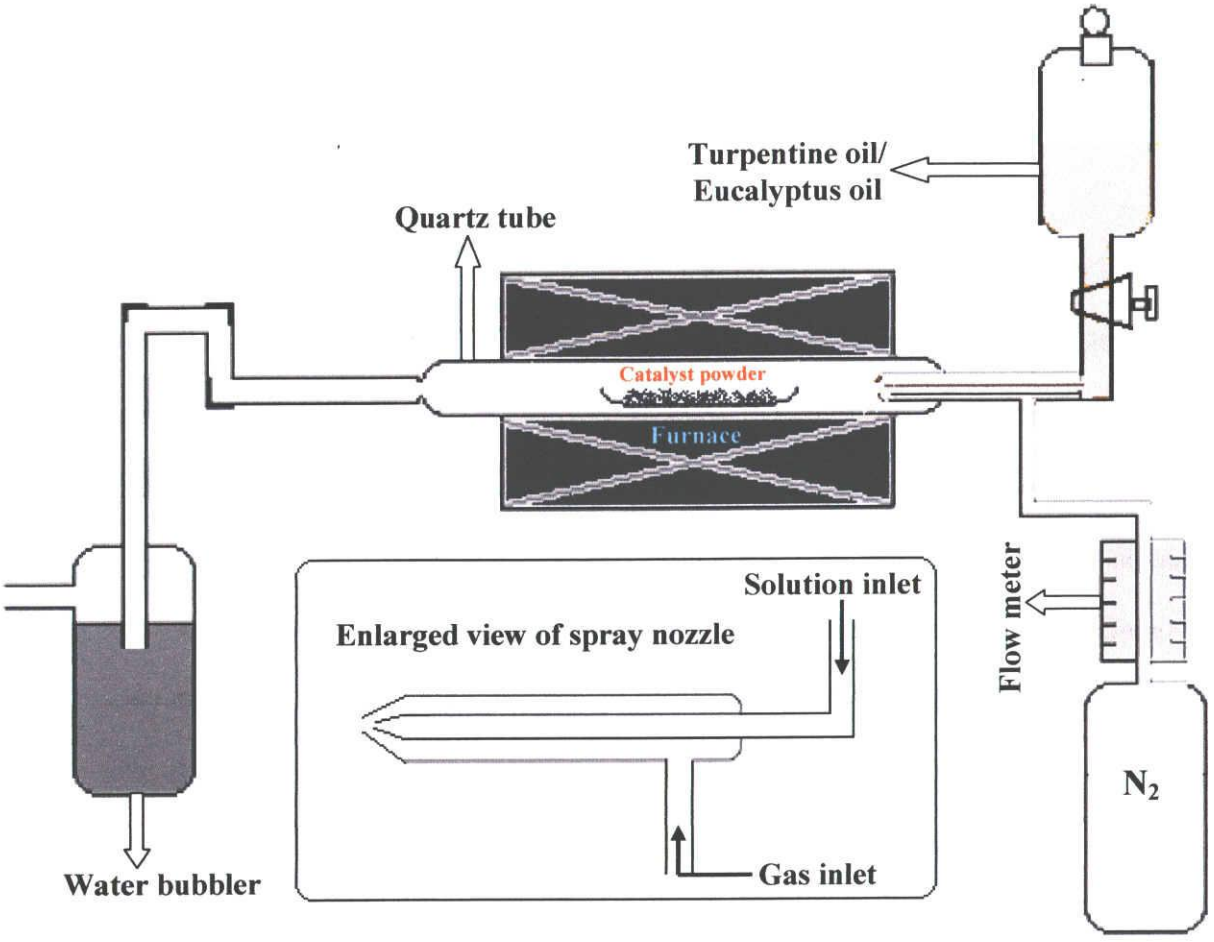

Fig. 1. Schematic diagram of spray pyrolysis system.

Before switch on the furnace, nitrogen gas was purged for few minutes for complete removal of air from the reaction chamber. The furnace was then switched on and heated to the reaction temperature. Syntheses were conducted at different temperatures at atmospheric pressure, with a typical reaction time of 25 minutes for each deposition. When furnace attained the desire temperature the N_2 gas flow was initiated at the rate of 100 cm^3/min. Then stop cock of the oil container was opened to allow oil to come inside the quartz tube by flow of nitrogen gas. The flow rate of the oil was maintained 0.1g/min. After deposition the furnace was switched off and allowed to cool down to room temperature.

2.2.1 Material characterization

The as-grown CNTs were characterized by using SEM (Hitachi S-3000H, scanning electron microscope), transmission electron microscope (JEOL JEM-3010) and thermogravimetric analysis (TGA). TGA was performed with DTG-60, Shimadzu, TA-60 WS thermal analyzer with a heating rate of 10 °C/min with 100 cm^3/min flow of air. Raman spectroscopy (JASCO, NRS-1500W) was measured with an excitation wavelength of 532 nm from a green laser with typical acquisition time of 300 s. The relation $d = 248/\omega$, where ω (cm^{-1}) is Raman Shift, was used to correlate the radial breathing mode frequencies and SWNTs diameter.

2.3 Results and discussion

2.3.1 Electron microscopy characterization

The formations of SWNTs were confirmed by direct observation under transmission electron microscopy. For TEM observation, the as-grown material was sonicated in methanol for few seconds and then the suspension was dropped onto the holey carbon grid and dried. Fig. 2a shows HRTEM image of isolated SWNTs prepared at 800 °C by pyrolysis of turpentine oil over Fe-Co/zeolite catalyst. Fig. 2b and 2c shows SWNTs grown from turpentine and eucalyptus oil, respectively at 850 °C using Fe-Co/zeolite catalyst. From TEM images it has been observed that the amount of SWNTs is very less at 800 °C than at 850 °C. Fig. 2b shows that sample is actually made up of SWNT bundles and isolated SWNT.

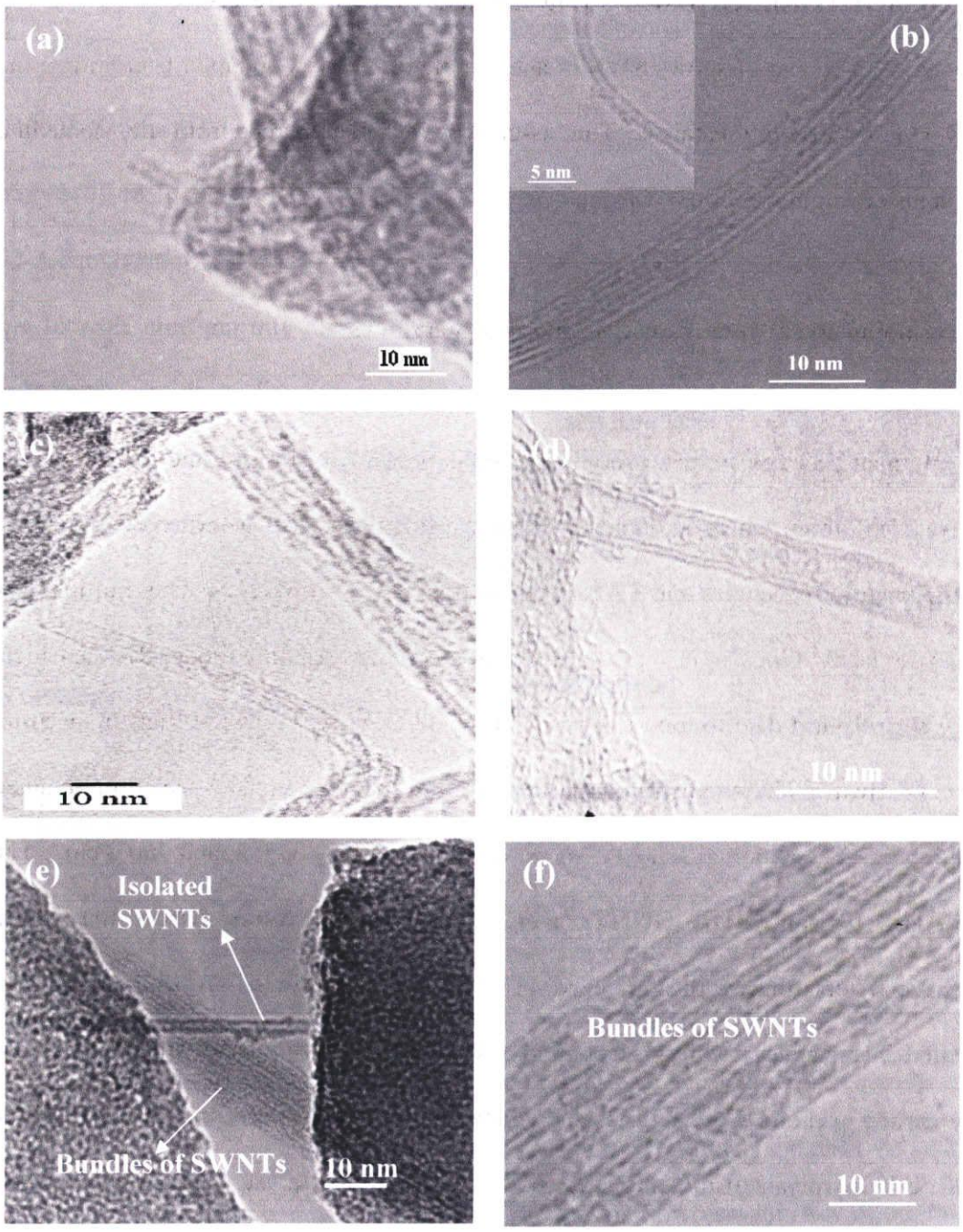

Fig. 2. HRTEM images of as-grown SWNTs grown from turpentine oil using bimetallic Fe-co/zeolite at (a) 800 °C and (b) 850 °C (c) SWNTs grown from eucalyptus oil at 850 °C (d) turpentine oil grown isolated DWNTs at 850 °C (e) turpentine oil grown SWNTs over Fe-Mo/zeolite at 850 °C (f) bundle of SWNTs from turpentine oil over Fe-Mo/zeolite at 850 °C.

Not only SWNTs but few DWNTs (Fig. 2d) and MWNTs were also observed in our specimen. Fig. 2e and 2f shows SWNTs and bundle of SWNTs obtained from turpentine oil over Fe-Mo/zeolite catalyst. The as-grown CNTs prepared from Fe-Mo/zeolite catalyst also contain some MWNTs.

2.3.2 Raman spectroscopy analysis of as-grown CNTs

Raman spectroscopy is a simple and good tool for confirming the formation of a single-walled structured and for determining the diameter of as-grown SWNTs. Three modes are very useful in the Raman spectra of the as-grown SWNTs. The multiple low frequencies (100-400 cm^{-1}) [17] associated with the radial breathing mode (RBM), which is inversely proportional to the diameter of the tube. Fig. 3a shows the Raman spectrum of the as-grown CNTs, synthesized at 800 °C from turpentine oil. The spectrum obtained in the low-frequency domain shows several components at 180, 202, and 300.6 cm^{-1}. The two intense bands near 500 cm^{-1} are characteristics peak of zeolite. Inset of the Fig. 3a shows the Raman spectra of Fe-Co/zeolite. This spectrum shows two bands at 488 and 507 cm^{-1}. The Raman spectrum of as-grown CNTs synthesized at 800 and 850 °C also shows similar peaks in this region. The diameter of SWNTs could be calculated from RBM peak frequency using the relation $d = 248/\omega$ [18,19]. According to the above expression, the radial breathing modes (RBM) frequencies of 180, 202, 300.6 cm^{-1} correspond to the SWNTs with the diameter of 1.37, 1.23, 0.82 nm, respectively. The relatively broad D-peak at 1359 cm^{-1} is related to the presence of defects within the graphene tubes or amorphous carbon. The G-peak at 1584 cm^{-1} is not so strong and broad

(Fig. 3a). For checking the purity of the samples we took the spectra at different positions, selected randomly but only in few positions we got the characteristic peaks of SWNTs.

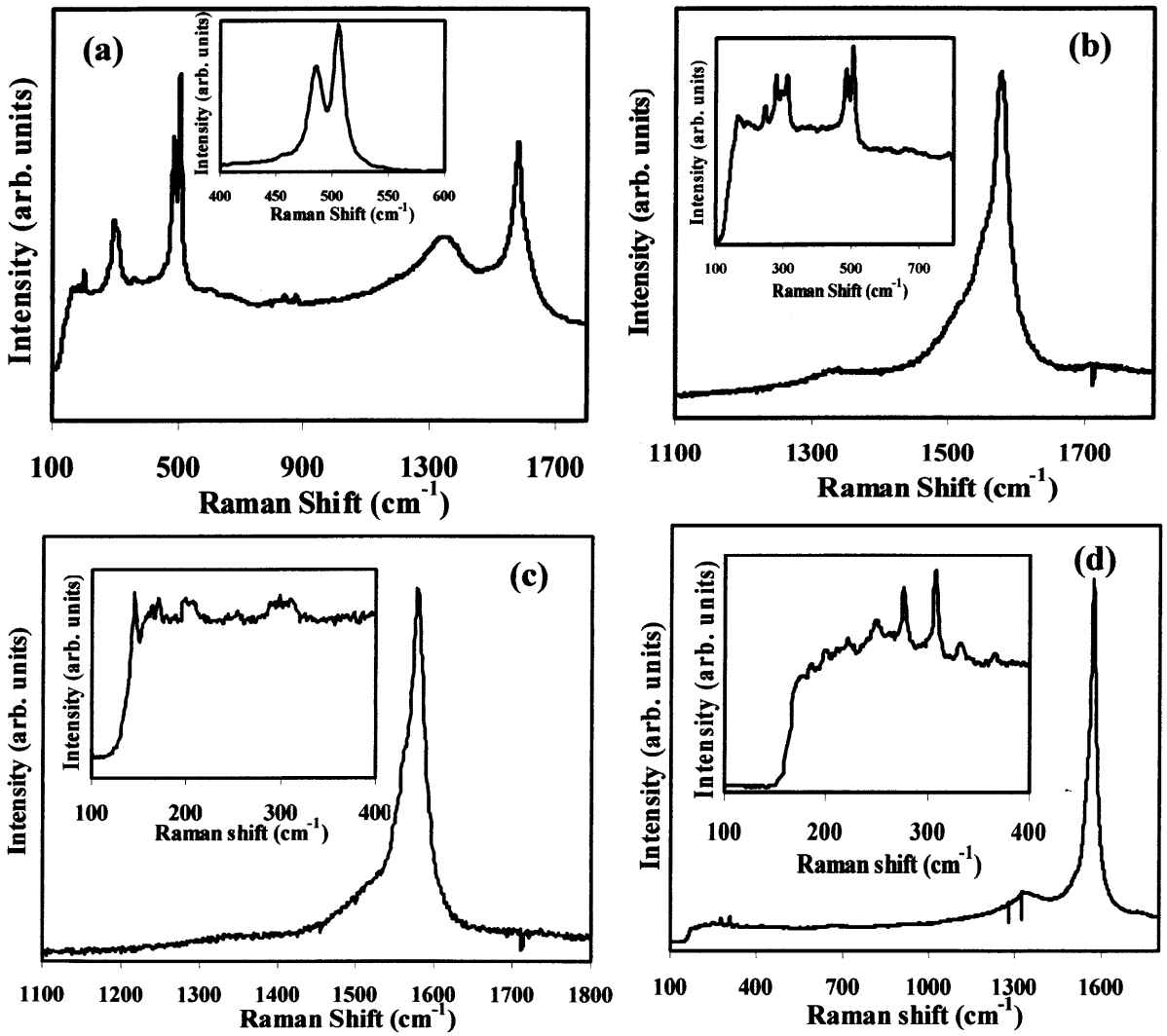

Fig. 3. Typical Raman spectrum (green laser, wavelength = 532 nm) of as-grown SWNTs obtained from turpentine oil (a) at 800 °C using bimetallic Fe-Co/zeolite catalyst. Inset shows spectra of Fe-Co/zeolite catalyst (b) at 850 °C. (c) Eucalyptus oil grown SWNTs at 850 °C using bimetallic Fe-Co/zeolite catalyst (d) Raman spectra of turpentine oil grown SWNTs using Fe-Mo/zeolite catalyst.

This indicates that at this temperature mixture of SWNTs and MWNTs were formed. Fig. 3b and 3c is the Raman spectra of SWNTs synthesized at 850 °C from turpentine oil and

eucalyptus oil, respectively over Fe-Co/zeolite catalyst. Spectra were recorded at different positions and most of the position gave rise to SWNTs spectrum, indicating the formation of mostly SWNTs. As shown in the inset of Fig. 3b, four main peaks was observed, the first peak is at 166.4, second is at 247.4, third is at 279.3, and the fourth peak is at 313.8 cm^{-1}. The diameter of the as-grown SWNTs is dependent on RBM frequency. The calculation indicated that these four peaks correspond to SWNTs with diameter of 1.49, ~1, 0.89 and 0.79 nm, respectively. The G-line mode located around 1577 cm^{-1} is assigned to the C-C bond motion due to the introduction of curvature into a graphite sheet, and the D-line present around 1338 cm^{-1} is ascribed to the existence of the disordered carbon in the bulk samples [20,21]. The 1558 cm^{-1} band is characteristic of SWNTs and appear for both semiconductor and metallic tubes.

The intensity ratio of the G- and D-band often regarded as an indicator of the purity of as-prepared CNTs [22]. The I_D/I_G ratio measures the quality of the CNTs. Generally, lower I_D/I_G value corresponds to the high-purity CNTs. The relatively low intensity of the D-band relative to the G-band indicates a low amount of amorphous carbon content or a lower defect concentration in the SWNTs. In order to obtain the structural information of as-grown CNTs, we calculated the I_D/I_G values from the Raman spectra of CNTs. It can be seen that the I_D/I_G value of as-grown sample, synthesized at 850 °C is ~0.3 whereas it is 0.67 for sample prepared at 800 °C. The graphitization of the as-grown CNTs at 850 °C is far better than the sample prepared at 800 °C. Preferably, I_D/I_G is sought to be as low as possible. But it is much lower than many other reports of CNTs by thermal decomposition of acetylene etc. showing I_D/I_G = 0.85-1.3 [23]. The I_D/I_G value is almost similar for turpentine and eucalyptus oil grown CNTs. This indicates

that presence of oxygen atom does not help to improve the quality of as-grown CNTs for eucalyptus oil. Fig. 3d shows the Raman spectra of as-grown CNTs obtained by pyrolysis of turpentine oil over Fe-Mo/zeolite catalyst. The CNTs prepared from this catalyst produces good quality of SWNTs with I_D/I_G value of ~0.15.

2.3.3 Thermogravimetric analysis of as-grown CNTs

Fig. 4a and 4b shows the TGA and DTA curves of the as-prepared material synthesized from turpentine oil over Fe-Co/zeolite catalyst at 800 and 850 °C, respectively. From TGA curve it was observed that the slight weight loss up to 400 °C is due to the burning of amorphous carbon. We assigned that weight loss between 400 and 677 °C is due to burning of mostly SWNTs, few DWNTs and MWNTs (Fig. 4b) whereas the weight loss between 400 and 652 °C is due to burning of few SWNTs and abundant MWNTs (Fig. 4a). The DTA peak for the sample synthesized at 800 °C is shifted toward higher temperature than the sample prepared at 850 °C.

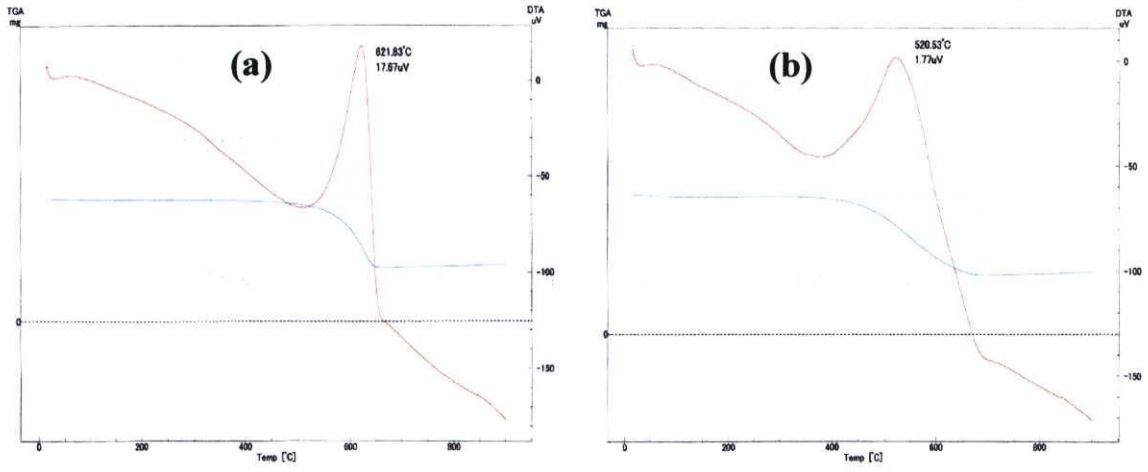

Fig. 4. TGA/DTA curve of the as-prepared CNTs grown from turpentine oil over Fe-Co/zeolite catalyst at (a) 800 °C (b) 850 °C.

This higher shift of DTA maxima is attributed to the formation of abundant MWNTs at 800 °C. This TGA and DTA analysis was repeated few times to check the reproducibility of the results.

The structure of the major components of turpentine and eucalyptus oil is shown in Fig. 5. Turpentine oil contains 58-65% α- pinene and about 30% of β- pinene. Both are composed of four and six memebered ring structures. The experiments indicated that synthesis temperature, flow rate of the inert gas, flow rate of the oil and catalyst loading greatly influence the growth of SWNTs. Catalyst (Fe-Co/zeolite) concentration of 5 wt% with respect to the weight of the supported material is suitable for formation of SWNTs. Syntheses were carried out using lower metal loading (2.5 wt%), formed mixture of SWNTs, abundant MWNTs and amorphous carbon at 850 °C and too lower concentration formed mainly amorphous carbon. Increasing the concentration above 5 wt% will increase the population of the metal particles, and mostly MWNTs are formed.

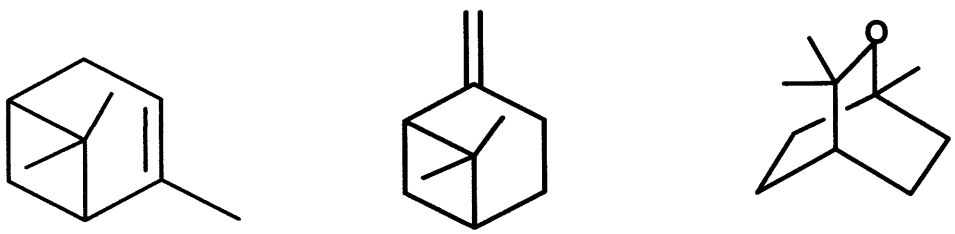

α- pinene β- pinene Cineole

Fig. 5. Chemical structure of the major components of turpentine and eucalyptus oil.

Temperature is one of the most important parameter for effective growth of SWNTs. Our experiment showed that, with 5 wt% metal concentration, mostly SWNTs were formed at 850 °C, whilst MWNTs formed at 900 °C. Raman spectroscopy did not

give any characteristic RBM peak at 900 °C (a spectrum is not shown here). Therefore, it can be supposed that metal particle produced at higher temperature (900 °C) were too large because of agglomeration which are not suitable for formation of SWNTs. Flow rate of the oil also plays an important role for the growth of SWNTs. Flow rate of the oil was adjusted to 0.1 g/min. Higher flow rate formed lot of amorphous carbon instead of abundant SWNTs. Lower flow rate formed mainly MWNTs. We tried to keep constant the experimental parameters for both eucalyptus oil and turpentine oil. It has been observed that there is not much difference in the I_D/I_G value corresponding to eucalyptus oil (containing one oxygen atom per molecule) and turpentine oil grown SWNTs. This indicates that oxygen atom on eucalyptus oil does not improve the quality of as-grown CNTs.

2.4 Conclusion

We have demonstrated a simple technique for the production of SWNTs by catalytic decomposition of turpentine oil and eucalyptus oil, green and regenerative precursors. Using these botanical hydrocarbons as a carbon feedstock, we simply avoided toxic organic precursors like benzene, toluene and harmful gas like carbon monoxide. Unlike previous approach [24] we did not do any pretreatment of the catalyst to generate the active catalyst by use of H_2 gas. Although the yield of SWNTs is low but we believe that if reaction conditions are carefully chosen, then it is possible to produce SWNTs in higher quantity by this simple method. This technique is so simple that it can be applied in any laboratory.

References

1. S. Iijima and T. Ichihashi, Nature 363 (1993) 603.
2. H. Dai, A.G. Rinzler, P. Nikolaev, A. Thess, D.T. Colbert, R.E. Smalley, Chem. Phys. Lett. 260 (1996) 471.
3. J.F. Colomer, C. Stephan, S. Lefrant, G. Van Tendeloo, I. Willems, Z. Konya, et al., Chem. Phys. Lett. 317 (2000) 83.
4. H.J. Jeong, K. Hyeok An, S.C. Lim, M.-S. Park, J.-S. Chang, S.-E. Park, S.J. Eum, C.W. Yang, C.-Y. Park, Y.-H. Lee, Chem. Phys. Lett. 380 (2003) 263.
5. A.M. Benito, Y. Maniette, E. Mũnoz, M.T. Mart´ınez, Carbon 36 (1998) 681.
6. Y. Murakami, Y. Miyauchi, S. Chiashi, S. Maruyama, Chem. Phys. Lett. 360 (2002) 229.
7. R.A. Afre, T. Soga, T. Jimbo, M. Kumar, Y. Ando, M. Sharon, Chem. Phys. Lett. 414 (2005) 6.
8. R.A. Afre, T. Soga, T. Jimbo, M. Kumar, Y. Ando, M. Sharon, P.R. Somani, M. Umeno, Microporous and Mesoporous Mater. 96 (2006) 184.
9. M. Kumar, K. Kakamu, T. Okazaki, Y. Ando, Chem. Phys. Lett. 385 (2004) 161.
10. M. Kumar and Y. Ando, Diamond Relat. Mater. 12 (2003) 1845.
11. R.J. Andrews, C.F. Smith, A.J. Alexander, Carbon 44 (2006) 341.
12. C. Journet, W.K. Maser, P. Bernier, A. Loiseau, M.L. de la Chapelle, S. Lefrant, et al., Nature 388 (1998) 756.
13. T. Guo, P. Nikoleav, A. Thess, D.T. Colbert, R.E. Smalley, Chem. Phys. Lett. 243 (1995) 49.

14. A. Cassell, N. Franklin, E. Chan, J. Han, H. Dai, J. Am. Chem. Soc. 121 (1999) 7959.

15. S.R.C. Vivekchand, L.M. Cele, F.L. Deepak, A.R. Raju, A. Govindaraj, Chem. Phys. Lett. 386 (2004) 313.

16. L.F. Su, J.N. Wang, F. Yu, Z.M. Sheng, H. Chang, C. Pak, Chem. Phys. Lett. 420 (2006) 421.

17. A.M. Rao, E. Richter, S. Bandow, B. Chase, P.C. Eklund, K.A. Williams, S. Fang, K.R. Subbaswamy, M. Menon, A. Thess, R.E. Smalley, G. Dresselhaus, M.S. Dresselhaus, Science 275 (1997) 187.

18. R. Saito, G. Dresselhaus, M.S. Dresselhaus, Phys. Rev. B 61 (2000) 2981.

19. A. Jorio, R. Saito, J.H. Hafner, C.M. Lieber, M. Hunter, T. McClure, et al., Phys. Rev. Lett. 86 (2001) 1118.

20. A.M. Rao, S. Bandow, E. Ritcher, Thin Solid Films 331 (1998) 141.

21. A. Claye, S. Rahman, J.E. Fischer, Chem. Phys. Lett. 333 (2001) 16.

22. G.S. Duesberg, W.J. Blau, H.J. Byrne, Chem. Phys. Lett. 8 (1999) 310.

23. M. Sveningsson, R.E. Morjan, O.A. Nerushev, et al., Appl. Phys. A 73 (2001) 521.

24. E. Flahaut, A. Govindaraj, A. Peigney, Ch. Laurent, A. Rousset, C.N.R. Rao, Chem. Phys. Lett. 300 (1999) 236.

Chapter 3

Synthesis of carbon nanofibers using a botanical hydrocarbon

3.1 Introduction

CNFs have attracted the tremendous attention because of their potential applications in the field of science and technology. They can be used in hydrogen storage materials [1], filler for polymer composites [2], field emission devices, sensors, fuel cells and supercapacitors [3]. Therefore extensive effort was made to develop CNFs by different methods using different metal catalyst (Fe, Co, Ni, Cu etc.) and different carbon feedstock. However, most of the work was done with zero valence iron compounds such as $Fe(C_5H_5)_2$ or $Fe(CO)_5$ in order to favor and control the catalyst particle size [4] to grow selective nanofiber. There are different kinds of CNF viz. platelet CNF, fishbone CNF, ribbon CNF, herringbone CNF, stacked cup CNF etc. They are classified according to their arrangement of graphene layer with respect to the fibril axis.

CNFs are mainly synthesized by CVD method from organic feedstock using transition metal as catalyst. The CNFs seem to form either in the vapor phase [5,6] or over catalyst deposited on supported material [7,8]. A sulfur compound (elemental sulfur, hydrogen sulfides, and thiophene) is essential with metal catalyst to promote the catalytic growth for CNFs formation [6,9]. It helps to increase the reaction kinetics which leads to formation of thickened CNF [6]. Small amount of such impurity helps to produce CNFs of reasonable quality and good yields. In an earlier study it was observed that without any hydrogen sulfides in the carbon feedstock, a negligible amount of CNFs were formed [9]. Sulfur plays an important role for the formation of CNFs as it liquefies iron particle that enhances CNFs formation. This liquefaction considerably increases the formation of

CNFs by VLS process, due to formation of eutectic between iron and iron-sulfur compounds at 988 °C [6].

To date, various petroleum products such as methane [10], xylene [11], benzene [12] etc. are in practice to synthesize CNFs. However, in view of foreseen crisis of fossil fuels in the near future, it is desirable to look for alternative carbon feedstock to synthesize this kind of nanomaterials. Turpentine oil is very effective precursor to synthesize CNFs. This precursor is very cheap and eco-friendly. One of the most advantages of this precursor is that there is no chance of crisis of this carbon feedstock in near future. This precursor is very effective to produce vertically aligned CNTs [13,14], MWNTs and SWNTs [15,16].

In this chapter, we have studied the effect of sulfur concentration on the morphology of CNFs using a natural precursor: turpentine oil, a carbon feedstock, ferrocene as a catalyst and sulfur as a promoting agent. This is the first report of synthesis of CNFs from a botanical hydrocarbon: turpentine oil using sulfur as a promoter by a simple, viable and cost effective spray pyrolysis method.

3.2 Experimental

3.2.1 Production of CNFs

CNFs were produced in a horizontal furnace, using ferrocene as a catalyst, turpentine oil as hydrocarbon feedstock and sulfur as a promoter at 1000 °C by spray pyrolysis method. The only variable in our experiment was the concentration of sulfur, keeping other experimental parameters (temperature, flow rate of gas, flow rate of oil,

ferrocene concentration) same. Detail information of this spray pyrolysis system was described in chapter 2. A quartz tube of one meter length and 25 mm diameter which is serving as spray pyrolysis reactor was kept inside one horizontal furnace. The inlet of the quartz tube was attached with the spray nozzle that helps to spray the precursor solution containing mixture or turpentine oil, ferrocene and small amount of sulfur by nitrogen gas. The outlet of the tube was connected with the water bubbler. At the initial stage, nitrogen gas was passed for few minutes to expel out atmospheric air from the tube. The furnace was then switched on with a desire deposition temperature (1000 °C). When the furnace attains the desire temperature, precursor solution was sprayed through spray nozzle by the help of nitrogen gas. The flow rate of nitrogen gas was 2.5 l/min and deposition time was lasted for 5 minutes. During the deposition process, the catalyst particles decomposed and formed sulfur-contaminated iron nanoparticles and CNFs started to grew. After 5 minutes, furnace was cooled down naturally to room temperature. The CNFs mainly deposited on the inner wall of the exit part of the reactor which was easily peeled off and used for characterization.

3.2.2 Characterization techniques

Several characterization techniques (SEM, TEM, Raman spectroscopy, TGA/ DTA, BET surface area) were employed of the as-grown samples. The morphology of the as-grown CNFs was analyzed by electron microscopy. Scanning electron microscopy (SEM) studies were carried out by SEM (Hitachi S-3000H, scanning electron microscope). Transmission electron microscopy was performed by HITACHI, HF-2000

with an acceleration voltage 200 kV. For TEM observation, the sample was prepared by sonication of the as-synthesized product in methanol, and a few drops of the resultant suspension were put onto a holey carbon TEM grid. TGA/DTA was performed with DTG-60, Shimadzu, TA-60 WS thermal analyzer with a heating rate of 10 °C/min with 100 cm^3/min flow of air. Raman spectroscopy (JASCO, NRS-1500W) was measured with an excitation wavelength of 532 nm from a green laser with typical acquisition time of 30 s. The microporous properties of the samples were determined by SHIMADZU Tristar 3000 to get the BET surface area of the as-grown CNFs.

3.3 Results and discussion

3.3.1 Electron microscopy characterization

Fig. 1a-d shows the SEM images of CNFs prepared at different sulfur concentrations varies from 10.5 to 40 at.%. These images clearly show that the morphology of product is strongly influenced by the atomic ratio of Fe and S. At 10.5 at.% and 40 at.% of sulfur concentration, the density of as-grown fiber is lower compared to that of 21 at.% and 31.5 at.% sulfur grown CNFs. Fig. 1b and 1c depict the SEM images of as-prepared CNFs grown by using 21 at.% and 31.5 at.% of sulfur. SEM images indicate that diameter of as-prepared CNFs is almost uniform. Moreover, it can be observed that 21 at.% and 31.5 at.% sulfur grown CNFs have a smooth surface. The density of 40 at.% sulfur grown CNFs is very less and CNFs are quite straight. This might be due to poison of the catalyst which leads to product of low yield.

TEM images of as-prepared CNFs grown from 21 at.% and 31.5 at.% of sulfur concentration are shown in Fig. 2. It is revealed that decomposition of turpentine oil generates different kinds of CNFs viz. bamboo-like, tubular and sharp tip geometrical pattern at different sulfur concentration. It can be clearly seen from TEM images that at lower sulfur concentration, the as-grown CNFs are relatively thicker than the CNFs prepared at high sulfur concentration. It is very clear from TEM analysis that as-grown CNFs are well-graphitized and amorphous carbon coating on the surface of the CNFs is very less which is also confirmed from TGA/DTA analysis. The structure of CNFs with 31.5 at.% of sulfur have variable diameter (from 80 nm to 112 nm) along graphene layer direction as shown in Fig. 2a. Some of the CNFs are bamboo-like with some transverse

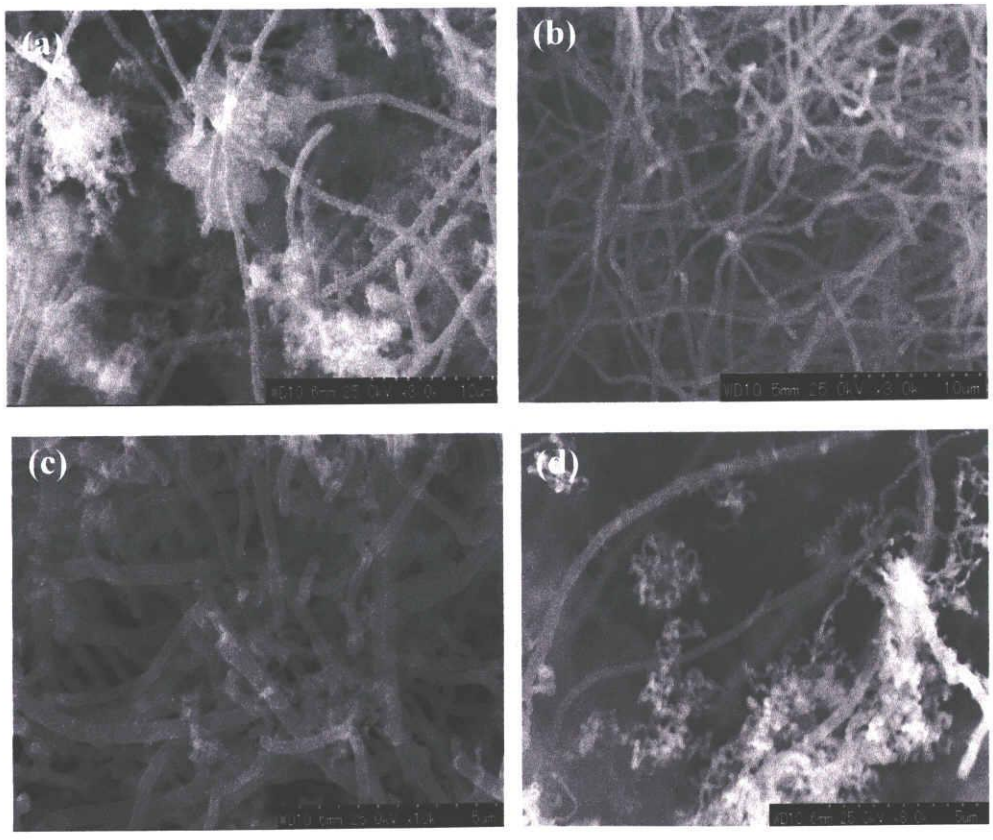

Fig. 1. SEM images of as-grown CNFs prepared at different sulfur concentration (a) 10.5 at.% sulfur (b) 21 at.% sulfur (c) 31.5 at.% sulfur (d) 40 at.% sulfur.

bridge forming compartment (Fig. 2b and 2c) and very few CNFs contain sharp tip (Fig. 2b). Such CNF with sharp tip have high expectation for enhancement of field electron emission. Fig. 2d shows as-grown CNFs with hemispherical cap. In Fig. 2e, the catalyst particles were observed at the tip and inside the hollow channel of CNFs. At the initial stage of the fiber growth process, the catalyst particle flow out of their molten state which leads to the formation of internal hollow channel. Furthermore, near to the tip of the fiber, molten catalyst particle has been fragmented into two parts. Both the fragments have tapered their bodies so as to grow hollow CNFs in between themselves. In Fig. 2f, two kinds of graphene arrangement have been observed. Near to the main fiber axis (shown by arrow head), graphene sheets are parallel whereas, graphene alignment away from the main axis angled by 50-60°, shown by rectangle area. In some cases metal particles were also observed inside the hollow core of CNFs and core diameter (25 nm) is almost similar to the metal particle size (Fig. 2g). Here few metal particles sit over the fiber and they are deactivated due to the small layer of carbon coating. Some of the metal particles remain their activity alive which is responsible for short in-situ fiber growth over main fiber platform (Fig. 2h). The graphene sheets of these short CNFs are parallel to the main fiber graphene sheet. Ellipsoid catalyst particle was found at the tip of this fiber and the diameter of the CNF seems to be determined by the shape and size of the catalyst particle, as shown in Fig. 2h. Very few CNFs are open ended with outer diameter of 70 nm (Fig. 2i). At lower sulfur concentration (21 at.%), we got mostly pipe-like structure with open end and hollow core (Fig. 2k and 2l).

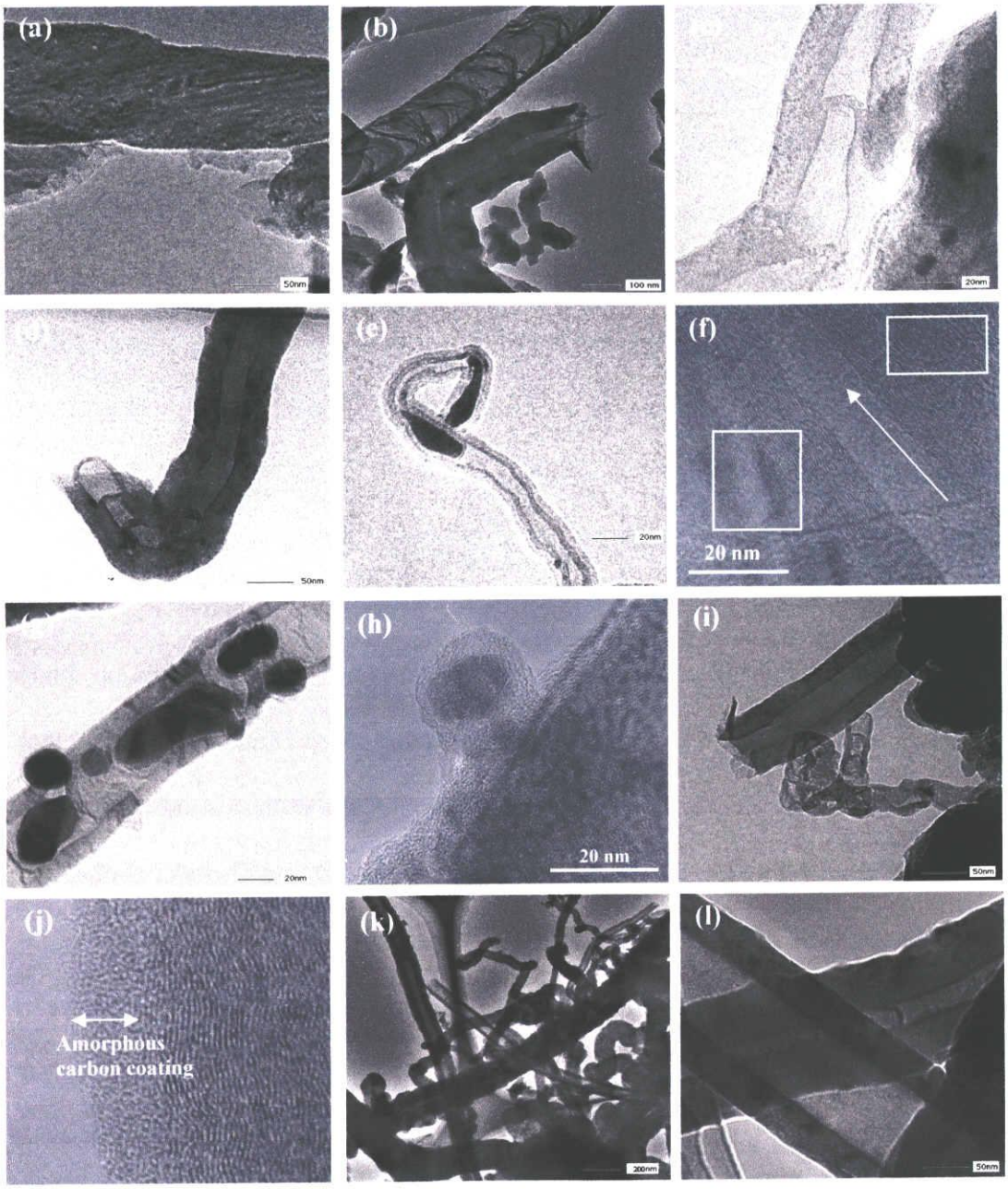

Fig. 2. TEM pictures of 31.5 at.% sulfur grown CNFs (a) CNF with a wide and variable diameter (b) bamboo-shaped and sharp tip CNF (c) CNF with transverse bridge compartment (d) CNF with hemispherical cap (e) a 25 nm CNF with metal particle at the tip and hollow channel of CNF (f) two kinds of graphene arrangement in CNF (g) a 47 nm CNF with metal particle inside the hollow core (h) a short fiber grown over a fiber (i) open ended CNF with diameter of 75 nm (j) CNF with amorphous carbon coating (k) general overview of 21 at.% sulfur grown CNF (l) wide CNF, grown using 21 at.% of sulfur.

3.3.2 Raman spectroscopy analysis of as-grown CNFs

Raman spectroscopy is widely used to characterize the structural and phase disorder information in carbon related material. Fig. 3 shows Raman spectroscopy (using a green laser with an excitation wavelength of 532 nm and power of 14.4 mW) in a range of Raman shift from 1100 to 1800 cm^{-1} of the as-grown CNFs, prepared at different sulfur concentration. Each spectrum was performed with 30 s acquisition time with an illumination spot size of 1 μm. In the Raman-shift range (1100-1800 cm^{-1}), two peaks were observed at approximately 1345 and 1573 cm^{-1} region, which corresponds to the D- and G-band respectively. The G-band is attributed to the Raman active E_{2g} in-plane oscillation mode and D-band corresponds to the A_{1g} in-plane breathing vibration mode due to structural defects in the graphite crystal. The rather sharp D and G-band, together with the evident high frequency shoulder of the G-peak, indicates the order and crystallinity of the CNFs [17,18]. Relative intensity ratio of D and G-peaks (I_D/I_G) is a measure of amount of disorder in the CNFs. It is well known that low intensity of D-band relative to G-band indicates a low amount of amorphous carbon or lower defect in the CNFs. The I_D/I_G value was found to be ~1 for CNFs prepared at different sulfur concentration, indicating a large quantity of defects in the CNFs structure. The defects in the as-grown CNFs are due to the presence of amorphous carbon coating which is shown in Fig. 2j.

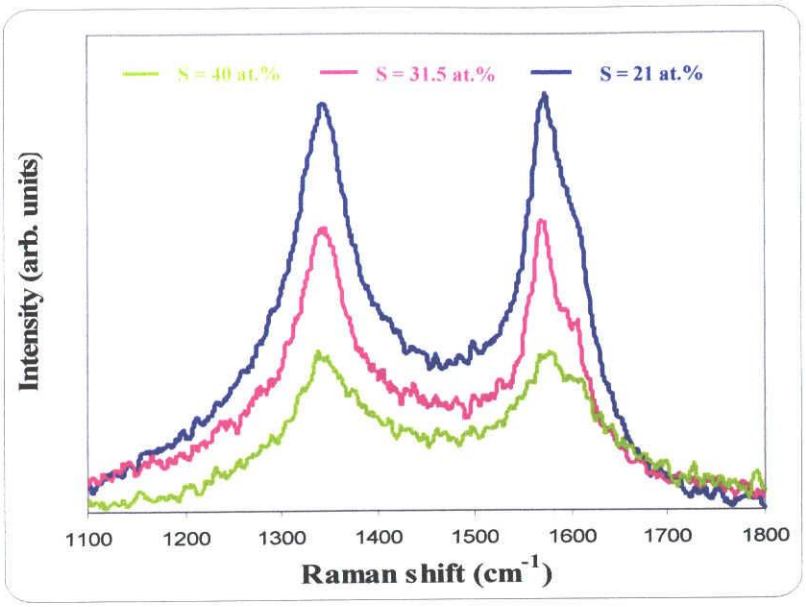

Fig. 3. Raman spectroscopy of as-grown CNFs prepared using different sulfur concentration.

3.3.3 Thermogravimetric analysis of as-grown CNFs

Thermogravimetric analysis and corresponding DTA curves of as-grown CNFs are shown in Fig. 4. Detail study shows that all the CNFs grown at different sulfur concentration mostly show their oxidation temperature at around 620 °C. This temperature is decomposition temperature of as-prepared CNFs. The apparent mass loss below 400 °C is due to mainly oxidation of amorphous carbon. At very low sulfur concentration (10.5 at.%) we have got some oxidation peaks at 400 and 498 °C. We assume that these peaks are mainly responsible for low diameter nanofiber. With increasing sulfur concentration from 21 at.% to 31.5 at.%, DTA maxima shifted towards lower value. This shift of DTA maxima by changing the sulfur concentration from 21

at.% to 31.5 at.%, is attributed to the lower diameter CNFs, that has been observed in TEM analysis. The high diameter and less deformity in fibril structure are less susceptible to oxidize.

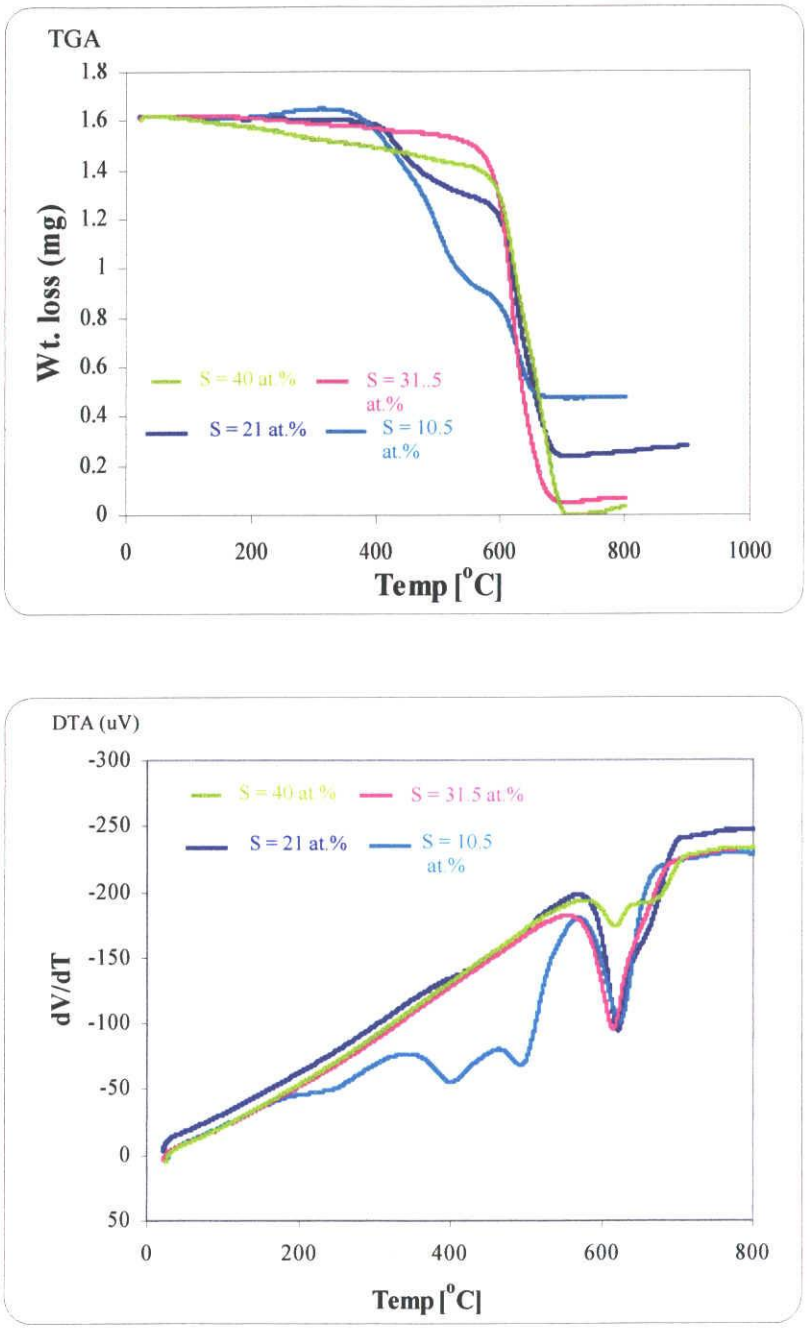

Fig. 4. Thermogravimetric analysis and corresponding derivative profile of as-prepared CNFs.

3.3.4 Surface characteristic studies of as-grown CNFs

To determine the effective surface area of as-grown CNFs, nitrogen cryo-adsorption isotherm was carried out. Fig. 5 shows the nitrogen cryo-adsorption isotherm of CNFs prepared from 31.5 at.% of sulfur concentration. Monolayer adsorption occurs at low relative pressure range. At higher relative pressure range ($P/P_o > 0.7$), the hysteresis loop appears which is responsible for capillary condensation in the mesopores. The calculated BET surface area was found to be 23.6 m^2/g. The low surface area is due to high diameter and the presence of amorphous carbon coating (Fig. 2j) in the outer wall of as-prepared CNFs that decreases the porosity of CNFs which is well evident from TEM analysis.

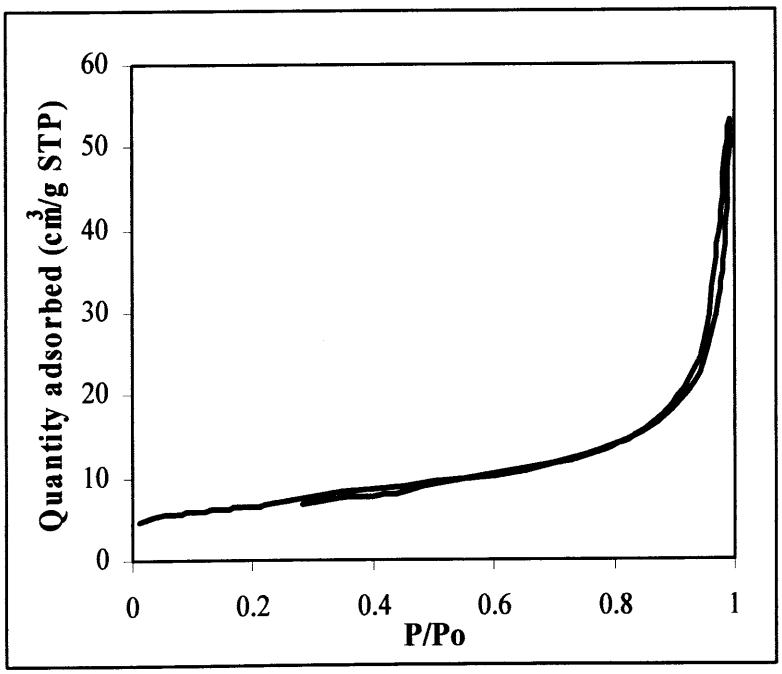

Fig. 5. Nitrogen adsorption isotherm of 31.5 at.% sulfur grown CNFs.

3.4 Role of sulfur for the growth of CNFs

The role of sulfur accompanied with transition metal catalyst (Fe, Ni) for the formation of CNFs has been observed by several groups [9,11]. From Fe-S binary alloys phase diagram it is clear that solubility of sulfur in Fe is very low, while sulfur can partially react with Fe to form a FeS-Fe eutectic alloys phase and lower down the local region surface free energy for the catalytic formation of CNFs than that of the bare α-Fe phase. In our reaction condition we have shown the concentration dependent enhancement and poisoning of Fe catalyst particle in the growth process of CNF by sulfur using turpentine oil as carbon precursor and ferrocene as a dissolved catalyst. It is well evident that CNFs are susceptible to nucleate and grow from the molten catalyst surface where sulfur of 42 at.% concentration effectively reacts with Fe particle to decrease the melting point of the local region around 980 °C which is very close to our reaction temperature. This molten state of metal particle catalytically enhances the dissolution of carbon atom leading to the high growth of fiber material through VLS mechanism. Catalytic enhancement of growth process with increasing sulfur concentration reduces the residence time which inhibit the non catalytic CVD coating. At low sulfur concentration (10.5 at.%), fiber growth is very less with lot of non-catalytic CVD coating. In our experiment it has been observed that with 21 and 31.5 at.% of sulfur produces CNFs of higher yield compared to that of very low and very high concentration of sulfur. At these two intermediate concentration of sulfur (21 and 31.5 at.%), the surface of the as-grown CNFs are very smooth and some amount of amorphous carbon are occasionally observed which is in accordance with SEM, TEM and TGA/DTA analysis. The depression of

freezing point of binary alloy system (Fe-S) has a linear relationship with concentration of sulfur up to a certain limit. The yield of the CNFs gradually increases with increasing sulfur concentration and reaches to a maxima at 31.5 at.% of sulfur. There is a steady fall of fiber growth rate at sulfur concentration of 40 at.%. In this case the amount of CNFs is very low, which is observed from SEM analysis. This clearly shows that not only the sulfur has the promoting effect for fiber growth over Fe catalyst but after a certain limiting concentration it acts as an inhibitor due to poisoning of catalyst leading to product of low yield.

3.5 Conclusion

CNFs with diameters of 20-130 nm were grown successfully when turpentine oil containing ferrocene and sulfur was used as feedstock in the growth process. The morphology and yield of the as-grown CNFs strongly influenced by the concentration of the promoting agent. The results indicate that addition of sulfur to the ferrocene catalyst can increase the yield of fiber. Optimum amount of sulfur has a promoting effect for the growth of CNFs. However, addition of large quantity of sulfur decreases the efficiency of the catalyst and only few CNFs were formed. In our case, we obtained CNF of higher yield with sulfur atomic concentration of 21 and 31.5 at.%. The result shows that turpentine oil is an ideal natural carbon feedstock for synthesis of CNFs. The as-prepared CNFs of different morphologies may significantly contribute for their potential applications. The CNFs containing sharp tip may exhibit enhanced field emission property and CNFs with open ended is possibly benefit to the gas storage.

References

1. C. Park, P.E. Anderson, A. Chambers, C.D. Tan, R. Hidalgo, N.M. Rodriguez, J. Phys. Chem. B 103 (1999) 10572.
2. G.G. Tibbetts, J.J. McHugh, J. Mater. Res. 14 (1999) 2871.
3. H. Dai, Acc. Chem. Res. 35 (2002) 1035.
4. A. Hoque, M.K. Alam, G.G. Tibbetts, Chem. Eng. Sci. 56 (2001) 4233.
5. T. Kato, K. Kusakabe, S. Morooka, J. Mater. Sci. Lett. 11 (1992) 674 .
6. L.Ci, Y. Li, B.Wei, J. Liang, C. Xu, D. Wu, Carbon 38 (2000) 1933.
7. T. Koyama, Carbon 10 (1972) 757.
8. H. Katsuki, K. Matsunaga, M. Egashira, S. Kawasumi, Carbon 19 (1981) 148.
9. G.G. Tibbetts, C.A. Bernardo, D.W. Gorkiewicz, R.L. Alig, Carbon 32 (1994) 569.
10. F. Benissad-Aissani, H. Aït-Amar, M.C. Schouler, P. Gadelle, Carbon 42 (2004) 2163.
11. Ignacio Martin-Gullon, José Vera, Juan A. Conesa, José L. González, César Merino, Carbon 44 (2006) 1572.
12. M. Endo, Y.A. Kim, T. Takeda, S.H. Hong, T. Matusita, T. Hayashi, M.S. Dresselhaus, Carbon 39 (2001) 2003.
13. R.A. Afre, T. Soga, T. Jimbo, M. Kumar, Y. Ando, M. Sharon, Chem. Phys. Lett. 414 (2005) 6.
14. R.A. Afre, T. Soga, T. Jimbo, M. Kumar, Y. Ando, M. Sharon, International Journal of Modern Physics B 20 (2006) 4965.

15. R.A. Afre, T. Soga, T. Jimbo, M. Kumar, Y. Ando, M. Sharon, P.R. Somani, M. Umeno, Microporous and Mesoporous Materials 96 (2006) 184.

16. Pradip Ghosh, T. Soga, R.A. Afre, T. Jimbo, Journal of Alloys and Compounds 462 (2008) 289.

17. M. Chhowalla, K.B.K. Teo, C. Ducati, N.L. Rupesinghe, G.A.J. Amaratunga, A.C. Ferrari, D. Roy, J. Robertson, W.I. Miline, J. Appl. Phys. 90 (2001) 5308.

18. A.C. Ferrari and J. Robertson, Phys. Rev. B 61 (2000) 14095.

Chapter 4

Synthesis of vertically aligned CN_x nanotubes using turpentine oil and pyridine derivative

4.1 Introduction

The discovery of CNTs by Iijima in 1991 [1] has created an immense interest due to their unique physical properties and potential application in electronic devices. CNTs show a variety of electronic behavior from metallic to semiconducting, depending on their composition, chirality etc [2]. However, it is still remained a big challenge to control precisely these parameters during the growth process of CNTs. The deliberate incorporation of defects and impurities (dopants) into the CNTs could offer a possible route to change and tune its electronic properties in a well defined way. Heteroatoms (boron, nitrogen, cobalt, potassium, silicon, phosphorous, oxygen) doping into graphitic carbon lattices effect various properties of sp^2 carbon material [3-9]. The advantage of such nanotubes is that their electronic properties are primarily determined by composition and thus relatively easy to control. Among these heteroatoms boron and nitrogen atoms are the most effective dopant because of their small atomic size. Boron-doped CNTs were reported to be uniformly metallic via theoretical calculation [10]. On the other hand, CN_x nanotubes were found to be either metallic or semiconducting with a narrow energy gap [11]. Recent research in that field reveals that incorporated nitrogen atom in carbon nanostructure can enhance the mechanical, electrical properties and increase the energy storage capacity [12]. Synthesis of CN_x nanotubes has created a considerable attention because it offers the possibility of greater electrical conductivity as compare to pure CNTs. The additional lone pairs of electrons on nitrogen atom with respect to the delocalized π-system of a graphite-like hexagonal framework can enhance its electron conducting properties [12].

Heteroatom-doped nanotubes were synthesized by laser ablation [13], arc discharge [14], and CVD method [15]. Among these methods, CVD method is considered as the best method for synthesizing heteroatom-doped carbon nanotubes. This method is very effective to synthesize well-aligned CN_x nanotubes. Most of the syntheses were carried out by the catalytic decomposition of C/N sources [16-18]. Rao and his co-workers prepared high yield of well-aligned CN_x nanotubes by pyrolysis of pyridine over iron or cobalt nanoparticle catalysts [19]. Point et al. produced aligned CN_x nanotubes using a mixture of acetylene and ammonia by plasma-enhanced chemical vapor deposition method [20].

Apart from these conventional methods, spray pyrolysis method is another promising method to produce CN_x nanotubes. This method is very simple and inexpensive compared to that of CVD method. It is the sister method of CVD method. Recently our group reported the synthesis of SWNTs [21], MWNTs [22] and vertically aligned MWNTs [23] using this simple technique. However, aligned CN_x nanotubes by this simple technique using turpentine oil, pyridine derivative and ferrocene as dissolved catalyst has so far not been achieved.

Turpentine oil is a natural precursor and mainly distilled from various species of pine (Pinus). It is well known for large scale industrial and medicinal application, not only as a solvent but a good precursor for organic synthesis. Very recently it proves its important attendance as a nano-technological feedstock. The 4-tert-butylpyridine was chosen as a nitrogen precursor as it is highly miscible with turpentine oil. Again the boiling point of turpentine oil and 4-tert-butylpyridine are almost similar. So during deposition they evaporated at almost the same rate.

In the present chapter, an efficient method to synthesize vertically aligned CN_x nanotubes on silicon and quartz substrate using turpentine oil as carbon feedstock, pyridine derivative as nitrogen source and ferrocene as dissolved catalyst in an inert atmosphere have been discussed.

4.2 Experimental

Vertically aligned CN_x nanotubes were synthesized by pyrolyzing ferrocene/ turpentine oil/4-tert-butylpyridine solution at 700 °C under the flow of nitrogen gas. The concentration of ferrocene was 0.03 g/ml in the mixture of turpentine oil and pyridine derivative. The solution was sonicated for 1 minute to prepare the homogeneous mixture. The spray pyrolysis system is illustrated in Fig. 1. Quartz tubing of 25 mm inner diameter and 500 mm length was placed in a horizontal furnace whose temperature was controlled to the accuracy of 1% at 1100 °C. The one end of this tube was attached with spray nozzle. The other part of the quartz tube was attached with standard B-24 join which was attached with water bubbler through rubber tube. The spray gun made of quartz having inner and outer diameter of 0.5 and 2 mm respectively. The inner part of the spray gun was used to pass the solution containing ferrocene, turpentine oil and pyridine derivative into the reaction zone. Nitrogen gas comes through outer part and helps the solution to spray. The inlet of the inner part was attached with container containing the solution mixture. Quartz and n-type silicon (100) of size 10 mm × 10 mm were used as the substrates. Before used, substrates were cleaned properly in acetone by ultrasonication followed by deionized water and finally dried using nitrogen blower. The substrates were

kept in quartz boat which was then placed at the center of the quartz tube. Before switch on the furnace, nitrogen gas was purged for 15 minutes for complete removal of the air from the quartz tube. After that furnace was switched on and allowed to the desired deposition temperature. When the temperature in the reaction zone reached to 700 °C, the solution was fed continuously into the quartz reactor through spray nozzle at a feed rate of 0.2 ml/min. The flow rate of the nitrogen gas was 100 cm^3/min. The reaction was usually maintained for 60 min. After deposition the furnace was cooled down to the room temperature under the flow of nitrogen gas. Finally, the substrates containing aligned nanotubes were removed from the quartz tube for characterization. The as-grown CN_x nanotubes were characterized by scanning electron microscopy (SEM), transmission electron microscopy (TEM), X-ray photoelectron spectroscopy (XPS), electron probe micro analysis (EPMA), thermogravimetric analysis (TGA) and Raman spectroscopy. Scanning electron microscopy (SEM) images were recorded using a Hitachi S-3000H, scanning electron microscope. Substrates were mounted using a conductive double-sided sticky silver tape. Transmission electron microscopy (TEM) images were recorded on a JEOL JEM-3010 electron microscope operating at 200 kV. Samples for analysis were prepared by spreading them in methanol and suspension was dropped on a holey carbon grid. TGA was performed with DTG-60, Shimadzu, TA-60 WS thermal analyzer with a heating rate of 10 °C/min with 100 cm^3/min flow of air. Raman spectroscopy was measured with 532 nm excitation wavelength from a green laser with typical acquisition time of 300 s. X-ray photoelectron spectroscopy (XPS) was measured by SSX-100 XPS spectrometer using Al Kα X-ray source (1486.6 eV) under high vacuum condition of about 10^{-10} Torr.

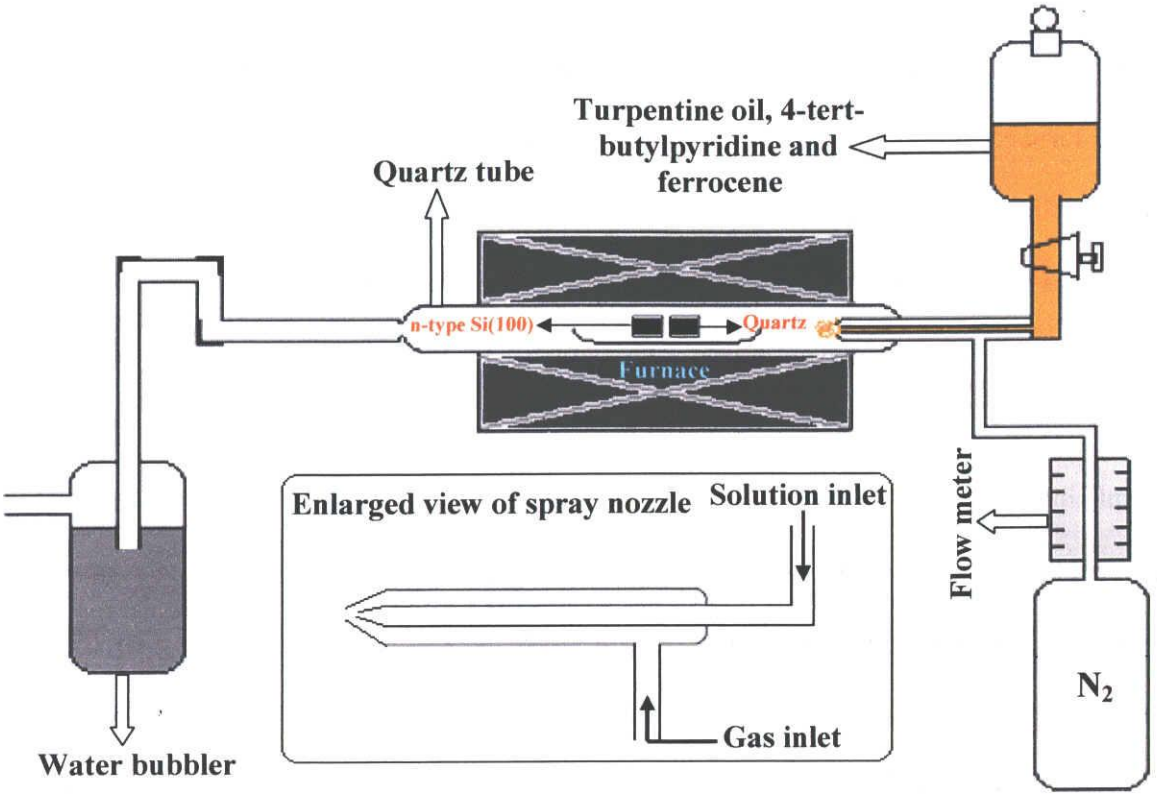

Fig. 1. Schematic diagram of spray pyrolysis system to grow CN_x nanotubes.

4.3 Results and discussion

4.3.1 Electron microscopy characterization

The morphology of the products is shown in Fig. 2. Fig. 2a, 2b and 2c, 2d depicts the SEM images of aligned CN_x nanotubes grown on silicon and quartz substrate, respectively. It is showing a large area of well-aligned CN_x nanotubes perpendicular to the surface of the substrate. SEM images clearly reveal that nanotubes are densely packed and this is the result of Van der Waals interactions between the neighboring nanotubes.

From SEM images it has been observed that the lengths of the as-grown CN_x nanotubes were 12 and 9 μm on silicon and quartz substrate, respectively.

TEM images of the as-prepared samples are shown in Fig. 3. From TEM images it is found that most of the nanotubes are bamboo-like with transverse carbon bridge compartments. The nanotubes consist of compartment layers and cylindrical shells of almost constant outer diameter. It has been demonstrated that multi-walled bamboo-like morphologies arise from the incorporation of pyridine-like N atoms within the carbon framework. It has been proved theoretically that substitutional nitrogen atoms could result in significant local deformations within the hexagonal lattice framework [24]. The detailed structure of the multi-walled CN_x nanotubes grown on silicon and quartz were characterized by HRTEM images (inset of Fig. 3b and 3d). The overall structure of the CN_x nanotube mainly depends upon the nitrogen concentration on carbon nanotubes. Nitrogen atoms tend to introduce disorders in the graphene planes, even at relatively low concentration. As the nitrogen incorporates into the graphene sheets, the crystalline perfection of the graphene sheets was deteriorated.

From TEM images it is revealed that the graphitization of nanotubes grown on silicon is better than nanotubes grown on quartz substrate. The outer wall of the nanotube is little bit rough and distorted (Fig. 3b and 3d). Amorphous carbonaceous layer was also observed on outer surface of the carbon nanotubes. The defects and disorders of as-prepared samples are related to the presence of nitrogen atom in the MWNTs. HRTEM images clearly indicate that crystalline perfection of the nanotubes grown on silicon was

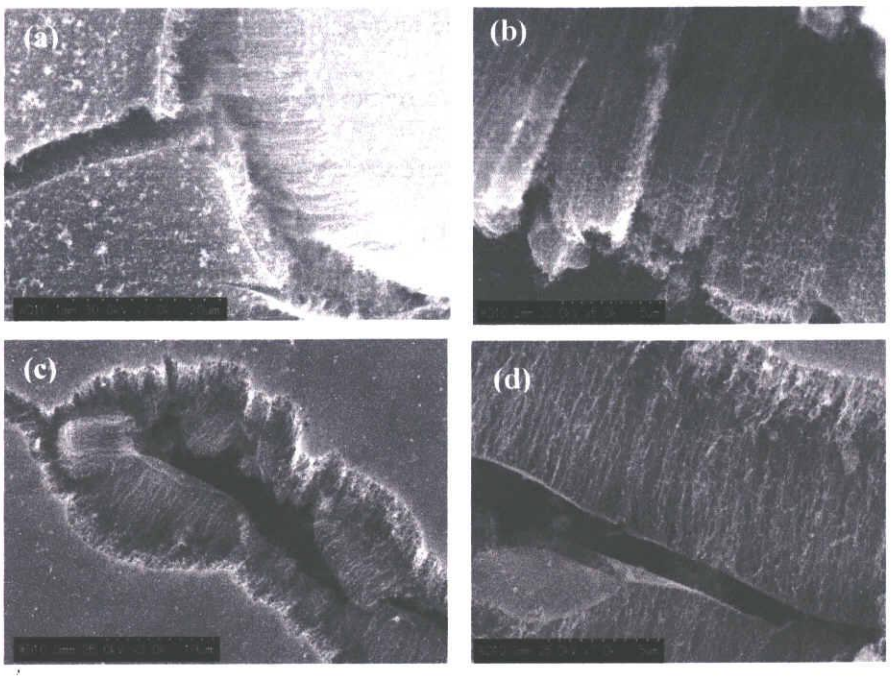

Fig. 2. SEM images of CN_x nanotubes grown on silicon substrate (a) and (b) and on quartz substrate (c) and (d) at 700 °C.

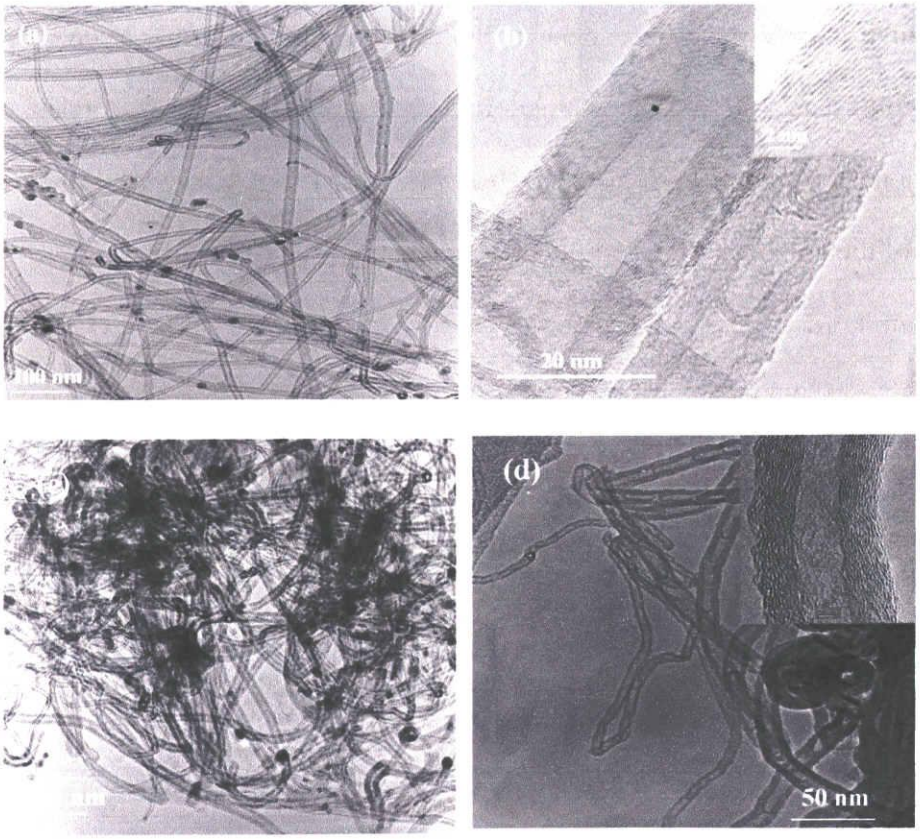

Fig. 3. TEM images of as-grown CN_x nanotubes grown on silicon (a) and (b) and on quartz substrate (c) and (d).

enhanced than the nanotubes grown on quartz (inset of Fig. 3b and 3d). This is mainly attributed to the higher nitrogen concentration on nanotubes grown on quartz than on silicon.

In addition, the diameter distribution of the CN_x nanotubes grown on quartz substrate was carefully examined from the TEM images. The diameter distribution of as-grown CN_x nanotubes grown on quartz substrate is shown in Fig. 4. There is not so remarkable difference of diameter distributions between the nanotubes grown on silicon and quartz nanotubes.

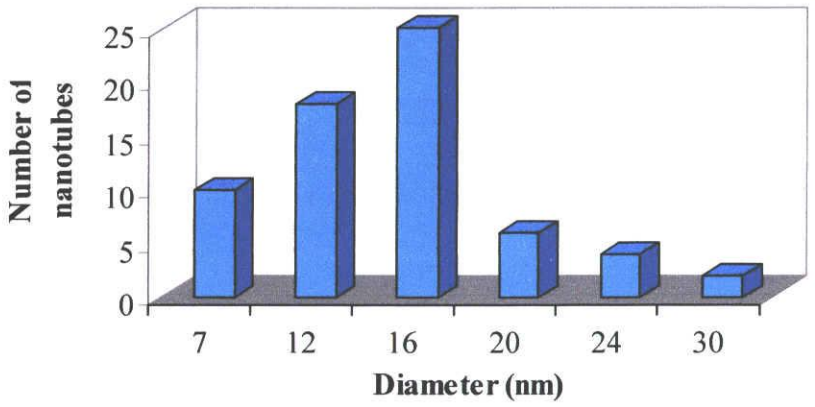

Fig. 4. Diameter distribution of CN_x nanotubes grown on quartz substrate.

4.3.2 XPS analysis of as-grown CN_x nanotubes

The XPS spectra of the CN_x nanotubes are shown in Fig. 5. XPS analysis is an effective tool to know the information on the nitrogen content and bonding environment in the as-prepared samples. An XPS spectrum shows the presence of carbon, nitrogen and oxygen in the as-grown samples deposited on silicon and quartz substrate. The C1s peak was observed at ca. 284.4 eV and 285.2 eV for both samples and this is consistent with

sp^2 graphitic carbon and carbon-nitrogen bond, respectively [25]. The O 1s peak appears at 532.4 eV might arise from SiO_2 layer on silicon substrate or from air adsorbed on the surface of the as-prepared nanotubes. From XPS spectra it has been revealed that N 1s signal was split into two peaks centered at 398.2 and 400.4 eV. The two peaks at 398.2 and 400.4 eV are related to the two different chemical environments of the nitrogen atoms in the as-prepared sample. The band at 398.2 eV corresponds to the "pyridinic" nitrogen whereas band at 400.4 eV correspond to "graphitic" nitrogen [11,26-29]. It is found that "graphitic" nitrogen structure is more dominant than "pyridinic" nitrogen. The similarity of the N 1s peak position for both samples indicates the similar structures and chemical environment in the as-synthesized material. The term "pyridinic" is used to refer to the N atoms that contribute to the π-system with one p-electron. The "graphitic" nitrogen corresponds to highly coordinated N atoms substituting inner C atoms on the graphite layers [30]. The N content on as-grown nanotubes was calculated to be 1.6 and 2 at.% on silicon and quartz substrate, respectively.

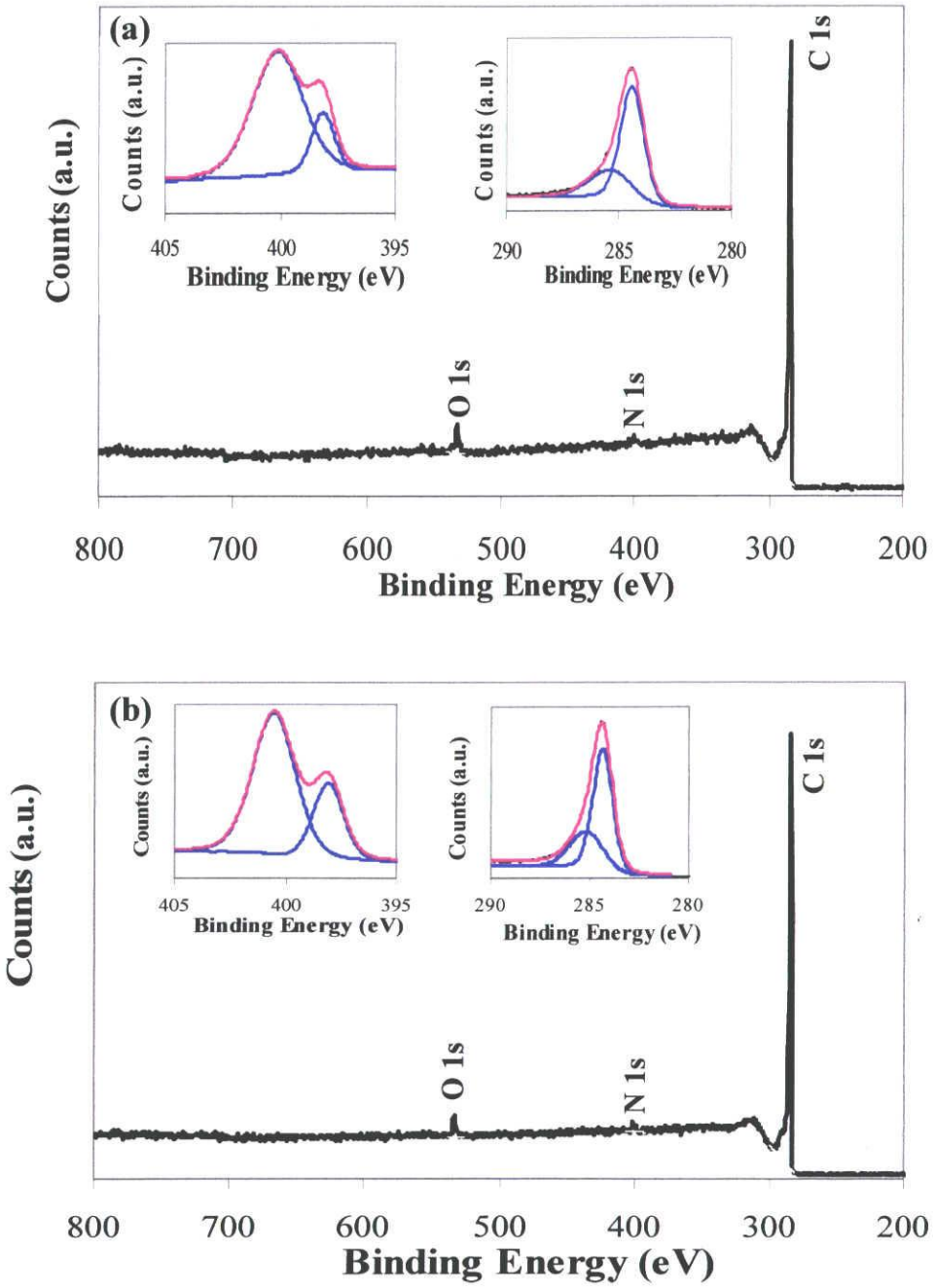

Fig. 5. XPS spectra of CN_x nanotubes grown on (a) silicon and (b) quartz substrate.

4.3.3 Raman spectroscopy analysis of as-grown CN_x nanotubes

Raman spectroscopy is a powerful tool to identify and evaluate the quality of as-grown CN_x nanotubes. Fig. 6a and 6b shows the typical Raman spectra of CN_x nanotubes grown on silicon and quartz substrate respectively. The G-bands appear at 1589 cm^{-1} for silicon substrate and 1583 cm^{-1} for quartz substrate and this band is usually regarded as in-plane oscillation of carbon atoms in the graphene wall of CNTs. The D-band at 1353 cm^{-1} for silicon substrate and 1344 cm^{-1} for quartz substrate corresponds to degree of defects or dangling bonds [31]. The G-line mode is ascribed to E_{2g} mode of graphite lattice and D-peak is assigned to A_{1g} mode due to the existence of structural defects of the graphite lattice [32,33].

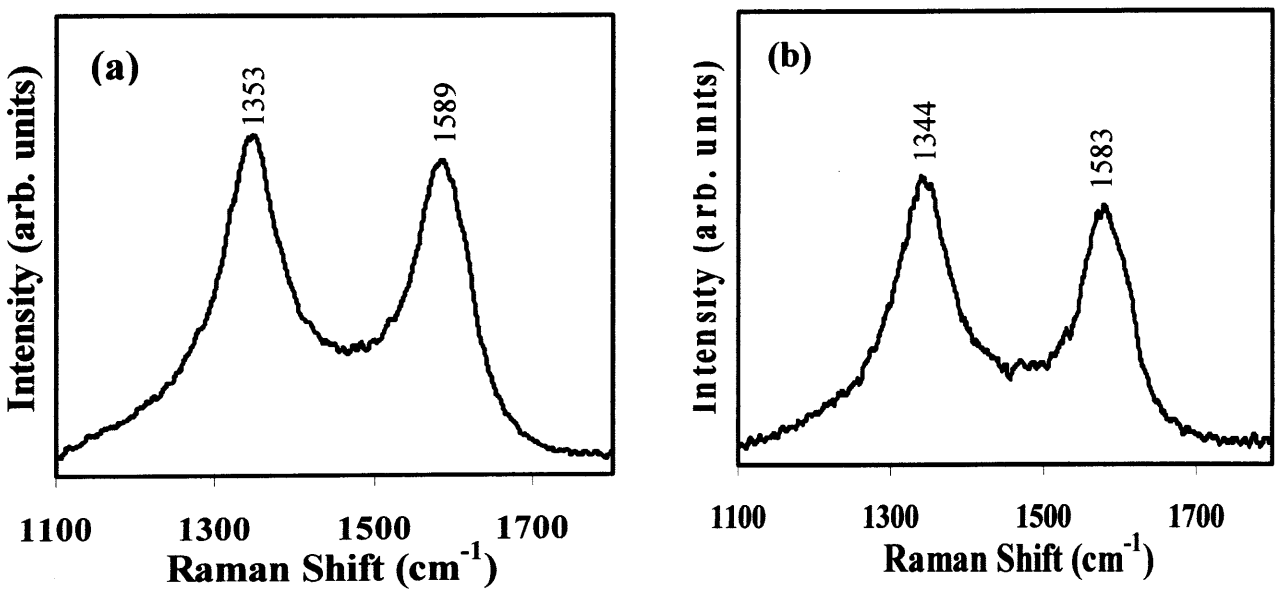

Fig. 6. Raman spectra of as-grown CN_x nanotubes deposited on (a) silicon and (b) quartz substrate.

The presence of wider D-band in the Raman spectrum of both samples arises from defects and disorder in graphene sheets and is consistent with the presence of MWNTs. From Raman spectroscopy, the I_D/I_G value was calculated to be 1.08 and 1.13 for the as-prepared sample deposited on silicon and quartz substrate, respectively. The higher I_D/I_G value suggests that more defects and disorders are introduced in the curved graphene sheets or in sp^2-hybridized carbon. This defects and disorders are due to presence of nitrogen atom in the carbon nanotubes. The higher I_D/I_G value of CN_x nanotubes deposited on quartz substrate in relative to that of nanotubes deposited on silicon substrate reveal that the degree of long-range ordered crystalline perfection of nanotubes was improved on silicon than on quartz substrate.

4.3.4 Thermogravimetric analysis of as-grown CN_x nanotubes

TGA and corresponding DTA curve of the CN_x nanotubes are shown in Fig. 7. From TGA analysis it has been observed that nanotubes grown on quartz substrate shows weight loss from 50 °C. The weight loss below 400 °C is attributed to the evaporation of volatile compounds, adsorbed gas molecule and thermal decomposition of amorphous carbon. A second weight loss was observed in the temperature range of 400-~600 °C. This main weight loss is attributed to the oxidation of CN_x nanotubes. The mass loss maxima (obtained from DTA profiles, Fig. 7) was observed at 557.1 °C and 538.74 °C of CN_x nanotubes grown on silicon and quartz substrate, respectively. From DTA profile it has been observed that peak maxima shifted to higher value in the case of nanotubes grown on silicon than the nanotubes grown on quartz substrate.

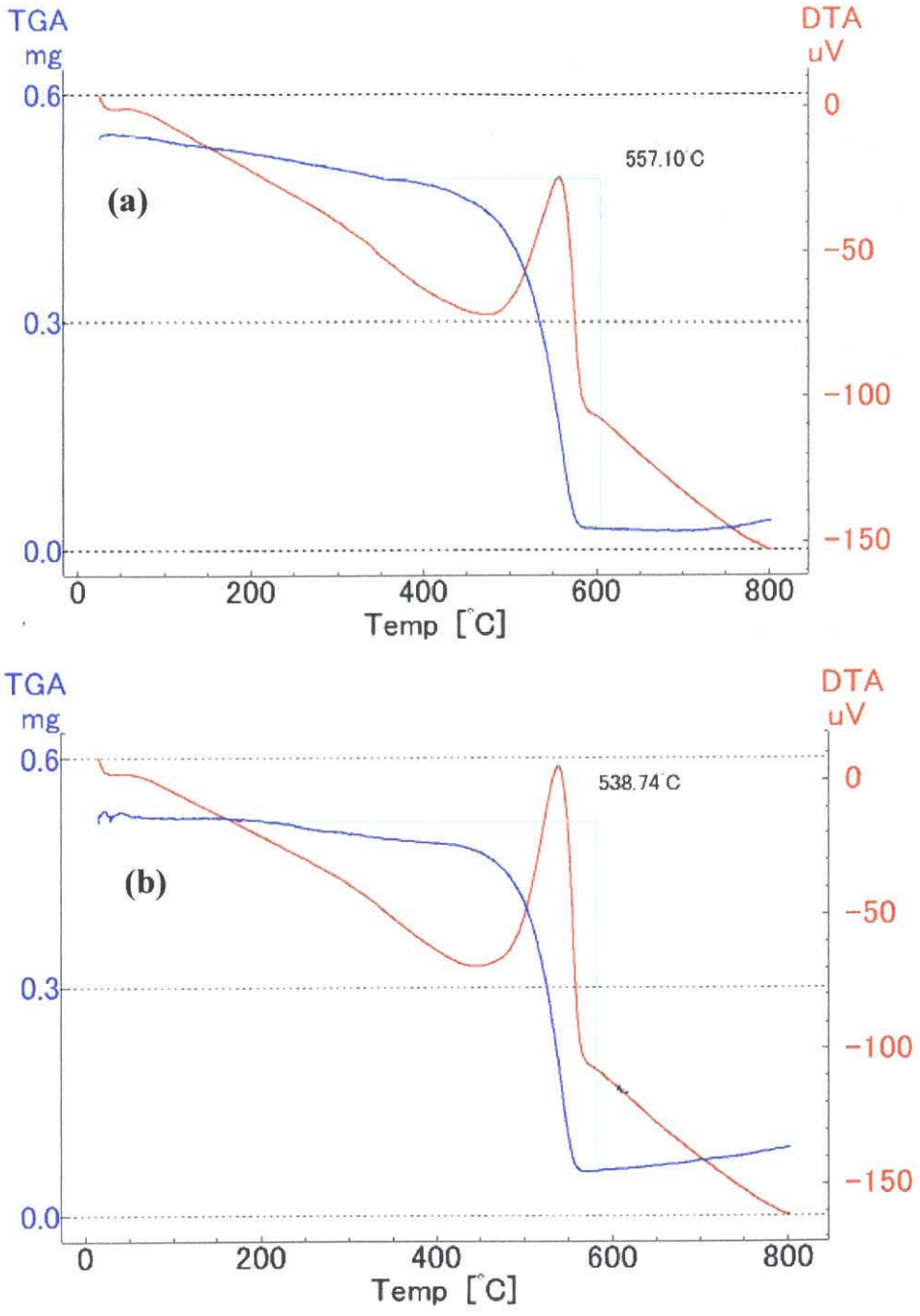

Fig. 7. TGA/DTA curves of CN_x nanotubes grown on (a) silicon and (b) quartz substrate.

The higher shift of DTA peak maxima from 538.74 °C to 557.10 °C suggests that nanotubes grown on silicon substrate contain less defects and disorders in relative to the nanotubes grown on quartz substrate, which is in agreement with HRTEM and Raman spectroscopy analysis.

4.4 Conclusion

Vertically aligned CN_x nanotubes were synthesized by spray pyrolysis of turpentine oil, 4-tert-butylpyridine and ferrocene mixture at 700 °C on silicon and quartz substrate. Experimental results indicated that the nitrogen content on silicon and quartz substrate was 1.6 and 2 at.%, respectively. The length of the as-prepared material was 12 and 9 μm on silicon and quartz substrate, respectively. Raman spectroscopy indicates that graphitization of CN_x nanotubes grown on silicon is better than the nanotubes grown on quartz substrate. The CN_x nanotubes exhibited high level of thermal stability in air, confirmed by TGA/DTA analysis. Such an aligned CN_x nanotubes may be suitable for fabrication in different electronic devices, field emission display, sensors etc.

References

1. S. Iijima, Nature 354 (1991) 56.
2. K. Saito, M. Fujita, G. Dresselhaus, M.S. Dresselhaus, Appl. Phys. Lett. 60 (1992) 2204.
3. M. Endo, T. Hayashi, S.H. Hong, T. Enoki, M.S. Dresselhaus, J. Appl. Phys. 90 (2001) 5670.
4. S. Glenis, A.J. Nelson, M.M. Labes, J. Appl. Phys. 86 (1999) 4464.
5. K. Lafdi, A. Chin, N. Ali, J.F. Despres, J. Appl. Phys. 79 (1996) 6007.
6. J. Kong, C. Zhou, E. Yenilmez, H. Dai, Appl. Phys. Lett. 77 (2000) 3977.
7. S.B. Fagan, R. Mota, Antonio J.R. da Silva, A. Fazzio, Nano Lett. 4 (2004) 975.
8. V. Jourdain, O. Stephan, M. Castignolles, A. Loiseau, P. Bernier, Adv. Mater. 16 (2004) 447.
9. D.J. Manna and M.D. Halls, J. Chem. Phys. 116 (2002) 9014.
10. D.L. Carroll, Ph. Redlich, X. Blase, J.C. Charlier, S. Curran, P.M. Ajayan, S. Roth, M. Rühle, Phys. Rev. Lett. 81 (1998) 2332.
11. M.S. He, S. Zhou, J. Zhang, Z.F. Liu, C. Robinson, J. Phys. Chem. B 109 (2005) 9275.
12. M. Terrones, P.M. Ajayan, F. Banhart, X.D. Blase, L. Carroll, J.C. Charlier, R. Czerw, B. Foley, N. Grobert, R. Kamalakaran, P. Kohler-Redlich, M. Rühle, T. Seeger, H. Terrones, Appl. Phys. A 74 (2002) 355.
13. Y. Zhang, H. Gu, K. Suenaga, S. Iijima, Chem. Phys. Lett. 279 (1997) 264.

14. Z. Weng-Sieh, K. Cherrey, N.G. Chopra, X. Blase, Y. Miyamoto, A. Rubio, M.L. Cohen, S.G. Louie, A. Zettl, R. Gronsky, Phys. Rev. B 51 (1995) 11229.

15. X.Y. Tao, X.B. Zhang, F.Y. Sun, J.P. Cheng, F. Liu, Z.Q. Luo, Diamond Relat. Mater. 16 (2007) 425.

16. M. Terrones, N. Grobert, J. Olivares, J.P. Zhang, H. Terrones, K. Kordatos, W.K. Hsu, J.P. Hare, P.D. Townsend, K. Prassides, A.K. Cheetham, H.W. Kroto, D.R.M. Walton, Nature 388 (1997) 52.

17. W.Q. Han, P. Kohler-Redlich, T. Seeger, F. Ernst, M. Rühle, N. Grobert, W.K. Hsu, B.H. Chang, Y.Q. Zhu, H.W. Kroto, D.R.M. Walton, M. Terrones, H. Terrones, Appl. Phys. Lett. 77 (2000) 1807.

18. S.H. Lim, H.I. Elim, X.Y. Gao, A.T.S. Wee, W. Ji, J.Y. Lee, J. Lin, Phy. Rev. B 73 (2006) 045402.

19. M. Nath, B.C. Satishkumar, A. Govindaraj, C.P. Vinod, C.N.R. Rao, Chem. Phys. Lett. 322 (2000) 333.

20. S. Point, T. Minea, B. Bouchet-Fabre, A. Granier, G. Turban, Diamond Relat. Mater. 14 (2005) 891.

21. Pradip Ghosh, T. Soga, R.A. Afre, T. Jimbo, Journal of Alloys and Compounds 462 (2008) 289.

22. R.A. Afre, T. Soga, T. Jimbo, M. Kumar, Y. Ando, M. Sharon, P.R. Somani, M. Umeno, Microporous and Mesoporous Materials 96 (2006) 184.

23. R.A. Afre, T. Soga, T. Jimbo, M. Kumar, Y. Ando, M. Sharon, Chem. Phys. Lett. 414 (2005) 6.

24. M. Terrones, H. Terrones, N. Grobert, W.K. Hsu, Y.Q. Zhu, J.P. Hare, H.W. Kroto, D.R.M. Walton, Ph. Kohler-Redlich, M. Rühle, J.P. Zhang, A.K. Cheetham, Appl. Phys. Lett. 75 (1999) 3932.

25. S. Maldonado, S. Morin, K.J. Stevenson, Carbon 44 (2006) 1429.

26. Y. Xia and R. Mokaya, Adv. Mater. 16 (2004) 886.

27. Y. Xia, Z. Yang, R. Mokaya, J. Phys. Chem. B 108 (2004) 19293.

28. R. Sen, B.C. Satishkumar, A. Govindaraj, K.R. Harikumar, M.K. Renganathan, C.N.R. Rao, J. Mater. Chem. 7 (1997) 2335.

29. S. Stafstrom, Appl. Phys. Lett. 77 (2000) 3941.

30. Z. Yang, Y. Xia, R. Mokaya, Chem. Mater. 17 (2005) 4502.

31. R. Saito, G. Dresselhaus, M.S. Dresselhaus, Physical Properties of Carbon Nanotubes, Imperial College Press, London, 1998.

32. M. Yudasaka, R. Kikuchi, T. Matsui, H. Kamo, Y. Ohki, E. Ota, S. Yoshimura, Appl. Phys. Lett. 64 (1994) 842.

33. D.C. Li, L. Dai, S. Huang, A.W.H. Mau, Z.L. Wang, Chem. Phys. Lett. 316 (2000) 349.

Chapter 5

Vertically aligned carbon nanotubes synthesized from natural precursors and their field electron emission properties

5.1 Introduction

During the past few years, CNTs have attracted much attention because of their unique electrical properties [1,2] and potential applications in various devices such as field emission devices and nanoelectronics [3,4]. CNTs exhibit excellent field emission property because of their high aspect ratio, small radius of curvature at the tip, mechanical strength and chemical inertness [5-7]. If CNTs are to be used as future building blocks in flat panel displays, it is imperative to enhance the field emission efficiency and decrease the turn-on and threshold electric field. From application point of view it is highly desirable to synthesize well-ordered arrays of nanotubes at low cost. In general, CNTs are mainly synthesized by arc discharge, laser ablation and CVD method [8-10]. Compared with other methods, CVD method is very effective technique because of low cost production, controllable and highly dense synthesis of nanotubes at lower temperature on various substrates [11,12]. Terrones et al. obtained aligned CNTs by pyrolyzing organic precursor at 950 °C [13]. Zhang et al. synthesized aligned CNTs arrays with high density by catalytic decomposition of ferrocene/xylene mixture at 850 °C on quartz substrate [14]. Kumar et al. synthesized well-aligned CNTs by pyrolyzing camphor and ferrocene mixture at 850 °C by CVD method [15]. Spray pyrolysis method is also an effective method to grow well-aligned CNTs at low temperature [16]. This method is a sister method of CVD and very simple and cost-effective in relative to CVD method. Recently vertically aligned CNTs [16], MWNTs [17] and SWNTs [18] were synthesized by this simple method using natural precursor as a carbon feedstock. The advantages of the natural precursors over conventional precursors (methane, acetylene,

alcohol, benzene etc.) have been discussed in our earlier reports [16-18]. There are still few reports about the synthesis of CNTs from natural precursors and study of their field emission property. Kumar et al. reported the synthesis of three dimensional well-aligned CNTs from a botanical hydrocarbon: camphor and studied their field electron emission performance [15]. In the present investigation attempts were carried out to prepare the well-aligned CNTs using natural precursors (turpentine oil, eucalyptus oil) as a carbon feedstock and studied their field emission performance.

In this chapter, we reported the synthesis of well-aligned CNT arrays from botanical hydrocarbons: turpentine oil and eucalyptus oil by simple and inexpensive spray pyrolysis technique at 700 °C and their field emission property have been studied.

5.2 Experimental

Vertically aligned CNTs were grown by spray pyrolysis method using turpentine oil and eucalyptus oil as carbon feedstock on n-type silicon (100) substrate with an area of 10 mm × 10 mm. The details of experimental set up are described in chapter 4. Before deposition, silicon substrates were ultrasonically cleaned by acetone followed by methanol and deionized water. 3 wt% of ferrocene was dissolved in turpentine oil and eucalyptus oil and passed through spray nozzle to the CVD reactor by nitrogen as a carrier gas (100 cm^3/min) and pyrolyzed at 700 °C for 60 min. The deposited material was annealed for 10 minutes at the same temperature and allowed to cool down to room temperature under the same nitrogen gas flow (100 cm^3/min). This simple technique results in uniform and thick layer of CNTs on Si substrate. Turpentine oil and eucalyptus

oil grown CNTs are designated as TGCNTs and EGCNTs, respectively. The as-grown materials were collected from the reactor and characterized by scanning electron microscopy (Hitachi S-3000H, scanning electron microscope), transmission electron microscopy (HITACHI HF 2000 with an acceleration voltage 200 kV), Raman spectroscopy (JASCO, NRS-1500W) and thermogravimetric analysis (Rigaku, THERMOFLEX, TAS 300, TG 8101D) with a heating rate of 10 °C/min in an air. Field emission measurements were performed in a vacuum chamber at a pressure less than 3×10^{-9} Torr within UHV-SEM (JAMP-7100). The cathode consisted of as-grown CNTs on n-type Si substrate, and anode was a polished stainless steel rod (1 mm in diameter). The distance between cathode and anode was 300 μm and the gap distance was carefully monitored in-situ with the aid of UHV-SEM. The macroscopic field was determined by dividing the applied voltage by the sample-anode distance. To detect very low field emission current at respective applied voltages, the voltage drop on a 100 kΩ series resistor connected to the sample was monitored.

5.3 Results and discussion

5.3.1 Electron microscopy characterization

Fig. 1a and 1c shows the typical SEM images of CNTs grown by pyrolyzing turpentine and eucalyptus oil, respectively with a growth time of 60 min.

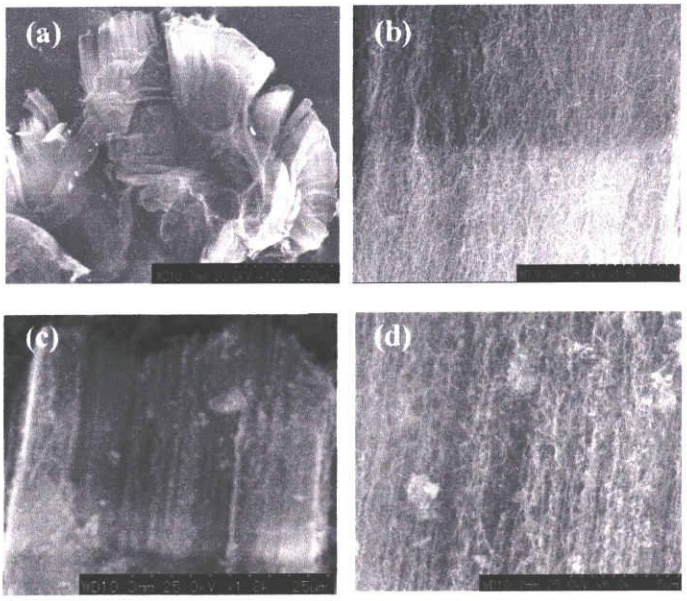

Fig. 1. SEM images of TGCNTs (a) Low magnification image (b) high magnification image (c) low magnification image of EGCNTs (d) high magnification image of EGCNTs.

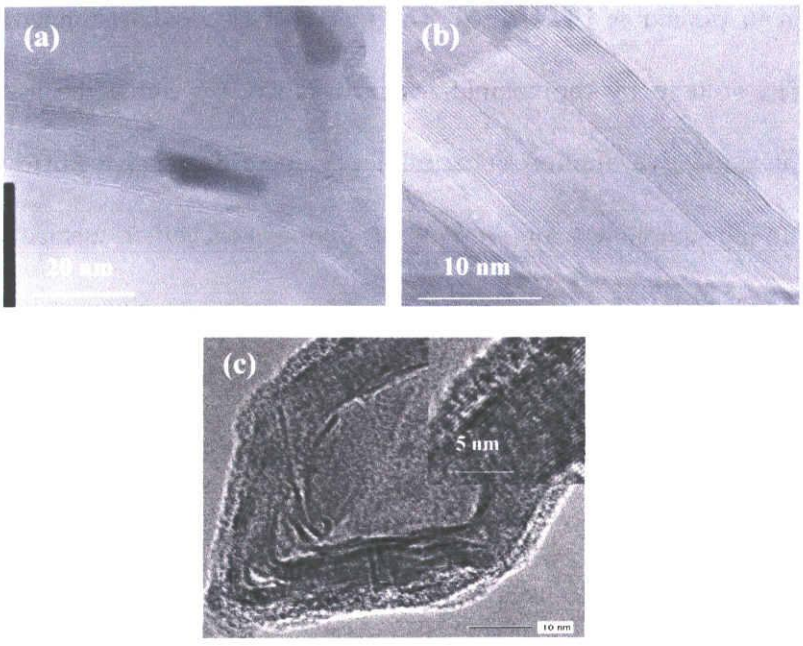

Fig. 2. (a) TEM image of TGCNTs with sharp tip and column-like Fe particle encapsulated in the cavity of CNTs (b) HRTEM image of TGCNTs (c) HRTEM image of EGCNTs. The outer wall of the tube is shown in inset.

Fig 1b and 1d shows the enlarged images of aligned CNTs of TGCNTs and EGCNTs, respectively. It shows highly dense and well-aligned CNTs on silicon substrate. However,

the density and length are different for turpentine oil and eucalyptus oil grown CNTs. It was found that the lengths of as-grown CNTs were 300 and 30 μm for TGCNTs and EGCNTs, respectively. HRTEM images clearly show the morphology of the as-grown CNTs. The nanotubes grown from turpentine oil have sharp tip which is shown in Fig. 2a. This kind of sharp tip of nanotubes helps to enhance the field emission property of CNTs. Again, from TEM images it is revealed that diameter of the as-prepared CNTs are in the range of 15-25 nm. Fig. 2a shows some metal particle encapsulation on CNTs. TEM observation shows that the metal particles are column-like shape in the cavities of CNTs. This is attributed to the high pressure created by the wall of CNTs [14]. This leads to the deformation of metal particles to the column-shape and diameter of the metal particles determines the inner diameter of CNTs. The growth of CNTs has not stopped with the stop of metal particles. It is also confirmed from HRTEM image that the as-prepared TGCNTs have high degree of graphitization with clearly resolved concentric shells of graphite sheets, and amorphous carbon was rarely found on the outer surface of CNTs (Fig. 2b). However, CNTs grown from eucalyptus oil show wavy graphene structures and some defects over long range (Fig. 2c).

5.3.2 Raman spectroscopy analysis of as-grown CNTs

Raman spectrum (JASCO, NRS-1500W) was measured with an excitation wavelength of 532 nm from a green laser with typical acquisition time of 60 sec to characterize the graphitization of as-grown CNTs. The Raman spectra of as-grown CNTs are shown in Fig. 3, which mainly consists of two main groups of peaks called D-band

and G-band. D-band indicates the disorder-induced features or lattice distortion and G-band is mainly attributed to the Raman active in-plane atomic displacement E_{2g} mode. Generally I_D/I_G value can be used as an indicator of the extent of defect or disorder within the CNTs. From Fig. 3, it is found that I_D/I_G value is higher for EGCNTs compared to TGCNTs. The I_D/I_G value was found to be 0.73 and 1.07 for TGCNTs and EGCNTs, respectively. This indicates that defect level is higher for EGCNTs than TGCNTs.

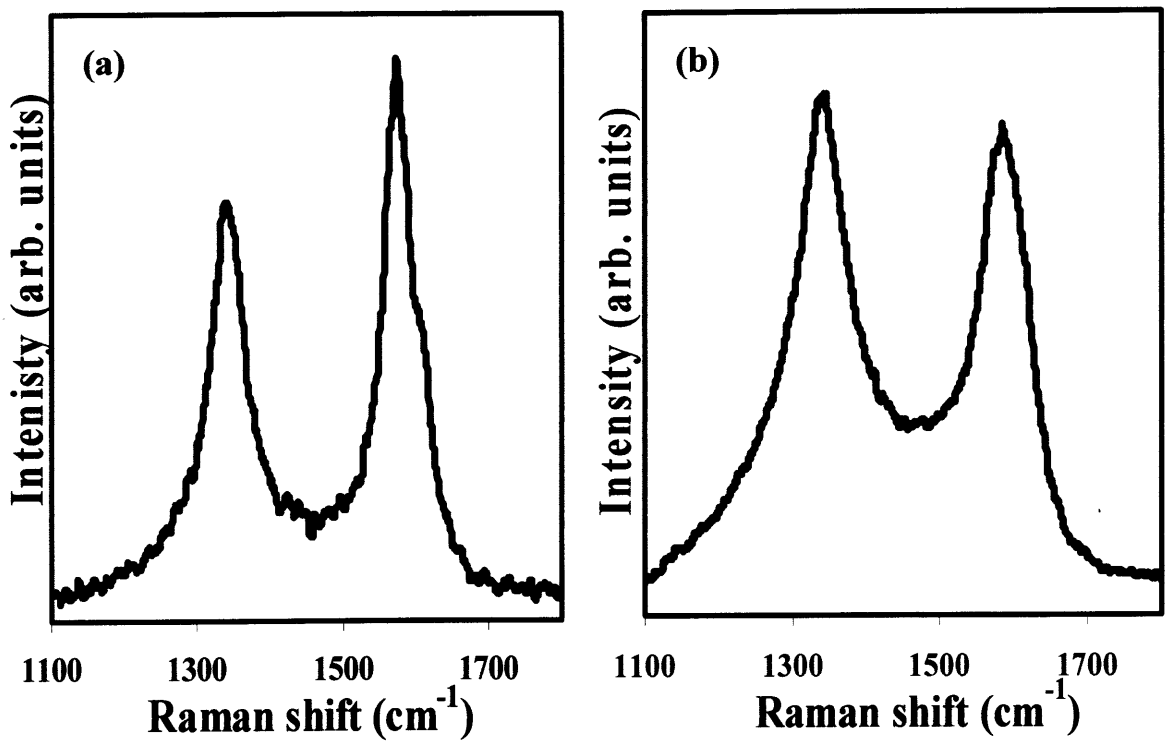

Fig. 3. Raman spectra of (a) TGCNTs and (b) EGCNTs grown at 700 °C. The exciton wavelength was 532 nm from a green laser.

5.3.3 Thermogravimetric analysis of as-grown CNTs

Thermogravimetric analysis is a very useful technique to determine the degree of crystallinity of the as-grown CNTs. The TGCNTs and EGCNTs were thermally analyzed in an air with a heating rate of 10 °C/min. Fig. 4a shows the TGA curve of

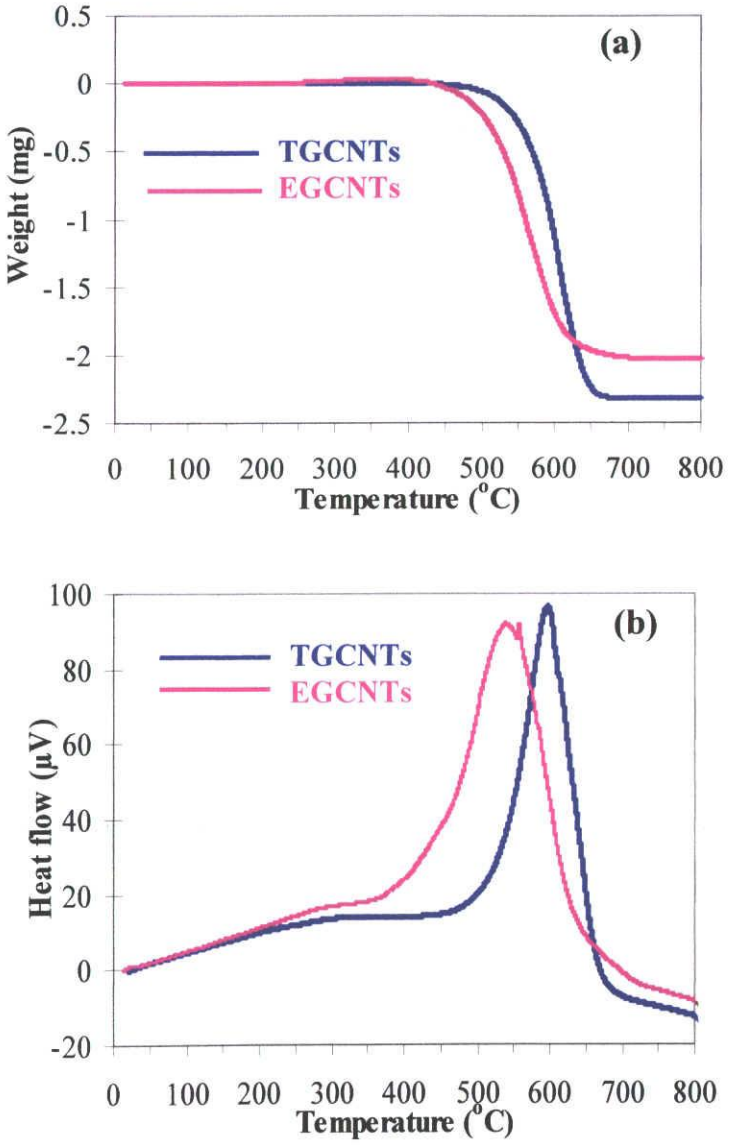

Fig. 4. Thermogravimetric analysis of TGCNTs and EGCNTs (a) TGA curves and (b) corresponding DTA profiles.

TGCNTs and EGCNTs. TGA curves clearly indicate that the thermal stability of TGCNT is higher than of EGCNT. The lower thermal stability of EGCNTs compared to TGCNTs is due to the presence of more defects and disorders of the EGCNTs. The corresponding DTA profiles of TGCNTs and EGCNTs are shown in Fig. 4b. The mass loss maxima were observed at 601 °C and 549 °C of TGCNTs and EGCNTs, respectively. The higher shift of DTA peak for TGCNTs suggests that CNTs grown from turpentine oil have higher degree of crystallinity compared with the CNTs grown from eucalyptus oil, which is in agreement with TEM and Raman analysis.

The structure of the main components of turpentine oil and eucalyptus oil are shown in Fig. 5. α- pinene and β- pinene are major components of the turpentine oil and 1, 8-cineole is the major component of the eucalyptus oil. The main component of the eucalyptus oil contains one oxygen atom per molecule whereas there is no such oxygen atom present in turpentine oil. It was assumed that the CNTs grown from oxygen containing natural precursor (eucalyptus oil) will be well graphitized in comparison with the CNTs prepared from natural precursor containing no oxygen atom (turpentine oil). Raman spectra indicated that the I_D/I_G value for TGCNTs (containing no oxygen atom) is lower than EGCNTs (containing one oxygen atom). Thus the presence of oxygen atom in the natural precursor (eucalyptus oil) does not help to increase the quality of the as-grown CNTs.

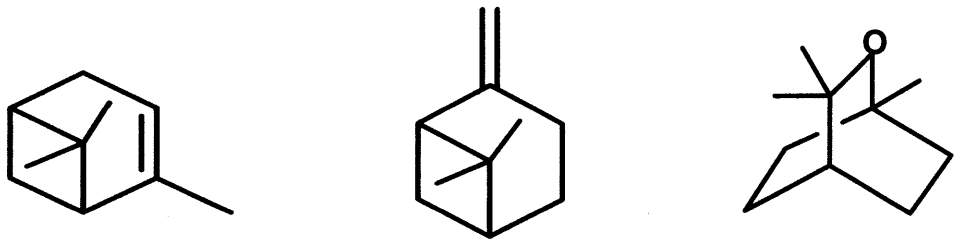

α- pinene β- pinene 1, 8- cineole

Fig. 5. The major components of turpentine oil (α- pinene and β- pinene) and eucalyptus oil (1, 8 cineole).

5.3.4 Field emission properties of turpentine oil and eucalyptus oil grown CNTs

Field emission performance of the as-grown CNTs obtained from turpentine oil and eucalyptus oil is shown in Fig. 6. During field emission measurements it was found that once voltages were removed and applied again, the process could be repeated with a slight change in current value. This performance indicated a stable and reproducible field emission behavior. The fluctuation of current in the first cycle may be due to uneven CNTs. The turn-on field defined as the field that is required to extract a current density of 10 $\mu A/cm^2$ is 1.7 and 1.93 V/μm for TGCNTs and EGCNTs, respectively. The threshold field corresponds to the current density of 1 mA/cm^2 and was 2.13 and 2.9 V/μm for CNTs obtained from turpentine oil and eucalyptus oil, respectively. The important point is that both nanotubes exhibited current density of mA/cm^2 order at moderate field and it is less for EGCNTs in comparison to TGCNTs. The TGCNTs shows maximum current density of 15.3 mA/cm^2 at ~3 V/μm whereas it is 1.6 mA/cm^2 for EGCNTs. This value is comparable to the recent reports of natural precursor (camphor) grown CNTs [15,19]. Although direct comparison is very difficult unless the nanotubes produced by different methods are investigated on the same field emission experimental set up. The Fowler-

Nordheim (F-N) plot is obtained by plotting ln (J/E^2) vs. 1/E, and the linear relationship indicates that measured current is indeed the result of field emission. The field enhancement factor β can be calculated using the F-N equation: $J = A (\beta^2 E^2/\varphi) \exp(-B\varphi^{3/2}/\beta E)$, where J is the emission current density, β is the field enhancement factor, φ is the work function and the value is assuming to be ~5 eV and E is the electric field, A and B are constant and the value of $B = 6.83 \times 10^9 eV^{-3/2}Vm^{-1}$. The field enhancement factor β was calculated to be 1845 and 1157 for TGCNTs and EGCNTs, respectively. The higher field enhancement factor of TGCNTs in relative to EGCNTs is supposed to be due to the presence of sharp tip of TGCNTs as suggested by Bonard et al. [20]. Moreover, TGCNTs indicate much higher emission current density at a low electric field than EGCNTs. Jung and co-workers observed that DWNTs with lower I_D/I_G value and high crystallinity show better field emission in relative to the less crystalline sample [21]. From Raman spectroscopy it is observed that I_D/I_G value is higher for EGCNTs than for TGCNTs. The high field emission performance of TGCNTs might be due to higher crystallinity and fewer defects compared to EGCNTs. Again it has been observed from SEM images that the average length of the nanotubes grown from turpentine oil is greater than of those grown from eucalyptus oil. SEM images also indicate that the density of is different for TGCNTs and EGCNTs. This indicates that the overall morphology of the TGCNTs differ from the EGCNTs. Therefore one of the reasons for getting enhanced field emission performance in turpentine oil grown CNTs may also be due to the greater length of the TGCNTs.

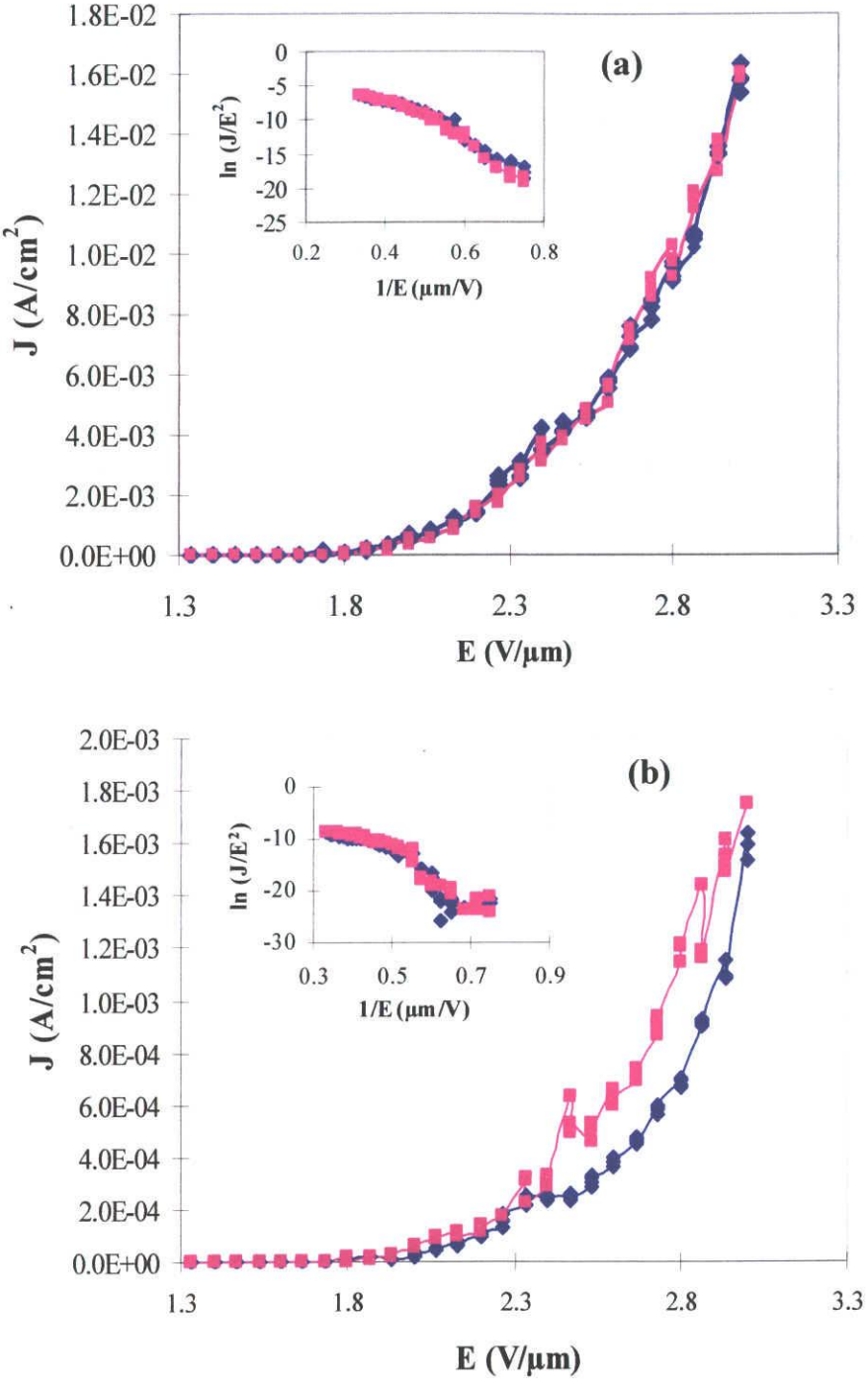

Fig. 6. Current density vs. electric field characteristics of (a) TGCNTs (b) EGCNTs. Inset shows corresponding Fowler-Nordheim plot.

5.4 Conclusion

We have presented a simple technique of growing well-aligned CNTs by using cheap and eco-friendly precursors on Si substrate as low as 700 °C at atmospheric pressure and studied their field electron emission properties. Nature of the precursor strongly affects graphitization and the field emission property of CNTs. The observed turn-on and threshold field of aligned CNTs, grown from turpentine oil and eucalyptus oil was 1.7, 1.93 and 2.13, 2.9 V/μm, respectively. Raman spectroscopy revealed that I_D/I_G is lower for TGCNTs than EGCNTs. The enhancement of field emission property of TGCNTs is attributed to the improved crystallinity and greater length compared to the EGCNTs. The natural precursor grown CNTs arrays using simple spray pyrolysis method will be useful for application in field emission displays. The spray pyrolysis method is so simple, versatile and effective technique that it can be adopted in any laboratory for the production of aligned CNTs from eco-friendly precursors and their performance on field electron emission

References

1. M.S. Dresselhaus, Nature 358 (1992) 195.
2. R. Saito, M. Fujita, G. Dresselhaus, M.S. Dresselhaus, Appl. Phys. Lett. 60 (1992) 2204.
3. M. Hirakawa, S. Sonoda, C. Tanaka, H. Murakami, H. Yamakawa, Appl. Surf. Sci. 169 (2001) 662.
4. W.A. de Heer, A. Chatelain, D. Ugart, Science 270 (1995) 1179.
5. M. Chhowalla, C. Ducati, N.L. Rupesinghe, K.B.K. Teo, G.A.J. Amaratunga, Appl. Phys. Lett. 79 (2001) 2079.
6. J.M. Bonard, J.P. Salvetat, T. Stockli, W.A. de Heer, L. Forro, A. Chatelain, Appl. Phys. Lett. 73 (1998) 918.
7. S. Hofmann, C. Ducati, B. Kleinsorge, J. Robertson, Appl. Phys. Lett. 83 (2003) 4661.
8. C. Journet, W.K. Maser, P. Bernier, A. Loiseau, M.L. de la Chapelle, S. Lefrant, et al., Nature 388 (1997) 756.
9. T. Guo, P. Nikoleav, A. Thess, D.T. Colbert, R.E. Smalley, Chem. Phys. Lett. 243 (1995) 49.
10. A. Cassell, N. Franklin, E. Chan, J. Han, H. Dai, J. Am. Chem. Soc. 121 (1999) 7959.
11. Z.W. Pan, S.S. Xie, B.H. Chang, C.Y. Wang, L. Lu, W. Wu, W.Y. Zhou, W.Z. Li, L.X. Qian, Nature 394 (1998) 631.
12. S. Fan, M.G. Chapline, N.R. Franklin, T.W. Tombler, A.M. Cassell, H. Dai,

Science 283 (1999) 512.

13. M. Terrones, N. Grobert, J. Olivares, J.P. Zhang, H. terrones, K. Kordatos, W.K. Hsu, J.P. Hare, P.D. Townsend, K. Prassides, A.K. Cheeetham, H.W. Kroto, D.R.M. Walton, Nature 388 (1997) 52.

14. X. Zhang, A. Cao, B. Wei, Y. Li, J. Wei, C. Xu, D. Wu, Chem. Phys. Lett. 362 (2002) 285.

15. M. Kumar, K. Kamaku, T. Okazaki, Y. Ando, Chem. Phys. Lett. 385 (2004) 161.

16. R.A. Afre, T. Soga, T. Jimbo, M. Kumar, Y. Ando, M. Sharon, Chem. Phys. Lett. 414 (2005) 6.

17. R.A. Afre, T. Soga, T. Jimbo, M. Kumar, Y. Ando, M. Sharon, P.R. Somani, M. Umeno, Microporous and Mesoporous Materials 96 (2006) 184.

18. Pradip Ghosh, T. Soga, R.A. Afre, T. Jmbo, Journal of Alloys and Compounds 462 (2008) 289.

19. M. Kumar, T. Okazaki, M. Hiramatsu, Y. Ando, Carbon 45 (2007) 1899.

20. J.M. Bonard, J.P. Salvetat, T. Stöckli, W.A.de Heer, L. Forŕo, A. Chatelain, Appl. Phys. Lett. 73 (1998) 918.

21. Seung Il Jung, S.H. Jo, H.S. Moon, J.M. Kim, Dong-Sik Zang, C.J. Lee, J. Phys. Chem. C 111 (2007) 4175.

Chapter 6

Bamboo-shaped aligned CN_x nanotubes synthesized by catalytic pyrolysis of monoethanolamine and their field electron emission

6.1 Introduction

Pure CNTs receive a continually growing interest because of many potential applications in nanoscale semiconductor devices [1], energy storage devices [2] and hydrogen storage media [3]. The increase of interest for this nanostructured material is related to their unique mechanical and electronic properties [4,5]. It has been predicted that incorporation of nitrogen atom on CNTs significantly changes their hardness, electrical conductivity and chemical reactivity [6,7]. CN_x nanotubes are very important material for nanoelectronics because their electronic properties can be controlled easily by changing the dopant concentration. The additional lone pair of electrons on nitrogen atom that acts as a donor with respect to the delocalized π system of the hexagonal framework can enhance the conducting property of CN_x nanotubes [8]. Incorporation of nitrogen atom on CNTs modifies the structure of the CNTs and forming mostly bamboo-like structure.

Variety of growth techniques including arc discharge [9,10], microwave plasma enhanced chemical vapor deposition [11], magnetron sputtering [12], and catalytic pyrolysis of organic precursors includes pyridine [13], acetonitrile [14], triazine [15] etc. have been reported to prepare CN_x nanotubes. CVD method offers most commercially viable technique towards the formation of highly dense and well-aligned CN_x nanotubes by catalytic decomposition of suitable C/N sources. CN_x nanotubes are mainly synthesized by using multi precursors. Lee et al. grew bamboo-shaped CNTs by heating the gas mixture of C_xH_y and NH_3 over the $FeCl_2 \cdot 4H_2O$ coated substrates [16]. The maximum dopant concentration was found to be 2-6 at.% over the temperature range

900-1100 °C. Han et al. obtained bamboo-shaped CNTs by pyrolyzing C_{60} mixed with ferrocene in ammonia [17]. Jang et al. prepared bamboo-shaped CN_x nanotubes of maximum 5 at.% of nitrogen by catalytic decomposition of C_2H_2/NH_3 mixture on SiO_2 substrates at 850 °C [18]. Recently, Wang and co-workers reported the vertically aligned CN_x nanotubes using the pyrolysis of iron phthalocyanine under the ammonia atmosphere [19]. Liu et al. studied the effect of ammonia on nitrogen content and doping environment of CNTs prepared by pyrolysis of pyridine and ferrocene [20]. They showed that nitrogen concentration and doping environment could be controlled by changing the flow rate of ammonia. They also showed that presence of ammonia not only increases the nitrogen concentration on CNTs but also increases the pyridine-like nitrogen doping on CNTs. Various study indicated that ammonia is an effective nitrogen source for synthesizing CN_x nanotubes. It has been observed that ammonia was passed separately as a nitrogen precursor with carbon feedstock to prepare CN_x nanotubes and this process is quite difficult. Considering the above facts, we have suggested that precursor containing C-N bond and which results ammonia after decomposition at the growth temperature may be more helpful to synthesize CN_x nanotubes of high dopant concentration. In our case we have chosen monoethanolamine as a C/N feedstock to prepare CN_x nanotubes that fulfill the above criteria. Theoretical and experimental studies showed that incorporation of nitrogen atom on CNTs enhances the local density of states near the Fermi level which in turn improve the field emission characteristics and emit electron at relatively lower field [21,22]. The motivation of this study was to prepare well-aligned CN_x nanotubes using a simple precursor and studied their field electron emission.

In this chapter, we have reported an efficient way to synthesize highly aligned nitrogen-doped bamboo-shaped CN_x nanotubes by catalytic pyrolysis of monoethanolamine/ferrocene mixture over the temperature range 700-900 °C by CVD method. Configuration, structural characteristics, composition and thermal stability have been investigated using electron microscopy, Raman spectroscopy, X-ray photoelectron spectroscopy (XPS) and thermogravimetric analysis. Field emission measurements were performed in a vacuum chamber at a pressure less than 3×10^{-9} Torr within UHV-SEM (JAMP-7100). The cathode consisted of as-grown CN_x nanotubes on quartz substrate, and anode was a polished stainless steel rod (1 mm in diameter). The distance between cathode and anode was 300 μm and the gap distance was carefully monitored in-situ with the aid of UHV-SEM. The macroscopic field was determined by dividing the applied voltage by the sample-anode distance. To detect very low field emission current at respective applied voltages, the voltage drop on a 100 kΩ series resistor connected to the sample was monitored.

6.2 Experimental

The CN_x nanotubes were synthesized by CVD technique using monoethanolamine as carbon and nitrogen feedstock and ferrocene as a catalyst. Our experimental set-up is a two-stage furnace system fitted with a quartz tube (length: 1 m and inner diameter: 25 mm). The tube was kept inside the two horizontal electric furnaces. Commercial grade quartz and n-type silicon (100) of 1 cm × 1 cm was used as a substrate. Before deposition of CN_x nanotubes, substrates were cleaned ultrasonically by acetone

followed by deionized water. Quartz and silicon substrate were placed in the quartz boat and kept at the center of the second furnace. The reactor was purged using nitrogen flow during heating up the furnace. Monoethanolamine/ferrocene mixture was sublimed in the first furnace at the temperature of 100 °C. The sublimed vapor was carried by the flow of nitrogen gas (100 cm^3/min) into the second furnace. The temperature of the second furnace was varied from 700-900 °C. The pressure inside the quartz reactor was held constant at 1 atmosphere for all the experiments. The deposition time was kept for 60 min followed by 10 min annealing at the reaction temperature. The reactor was cooled to room temperature under nitrogen atmosphere and the as-grown materials were collected for characterization.

The as-grown CN_x nanotubes were characterized by scanning electron microscopy (Hitachi S-3000H, scanning electron microscope), transmission electron microscopy (HITACHI HF 2000 with an acceleration voltage 200 kV), Raman spectroscopy (JASCO, NRS-1500W, green laser with exciton wavelength of 532 nm), X-ray photoelectron spectroscopy (SSX-100 XPS spectrometer using Al Kα X-ray source (1486.6 eV) under high vacuum condition of about 10^{-10} Torr, thermogravimetric analysis (Rigaku, THERMOFLEX, TAS 300, TG 8101D, with a heating rate of 10 °C/min in air).

6.3 Results and discussion

6.3.1 Morphologies of as-grown CN_x nanotubes

Fig. 1a-c displays the SEM images of CN_x nanotubes prepared using monoethanolamine as C/N feedstock and ferrocene as a catalyst on quartz substrate at

various CVD temperatures while other growth conditions are the same. SEM images confirmed that the samples consisted of highly ordered arrays of MWNTs, with very low amount of amorphous carbon. Due to such high density, crowding effect and Van der walls attraction between neighboring nanotubes, nanotubes deposited on substrate are well aligned. At lower temperature, for example, at 700 °C, the nanotubes are well aligned and very dense. The density and alignment decreases with increasing the deposition temperature which is clearly observed from SEM images. From SEM images it is revealed that the length of the nanotubes grown at 700 and 800 °C does not change significantly and at these two temperatures the length of the nanotubes has been found to be about 20 μm. But the length of the nanotubes changes dramatically from 20 to about 100 μm with rising growth temperature from 800 to 900 °C. Fig. 1d shows SEM image of CN_x nanotubes deposited on Si(100) substrate at 900 °C. The length of the as-prepared carbon nanotubes was found to be approximately 50 μm.

Fig. 2a shows the low resolution TEM image of as-grown CN_x nanotubes of 5.8 at.% of nitrogen concentration prepared at 800 °C. TEM analysis indicated that nanotubes mainly exhibited bamboo-like morphology in which nanotubes inside are separated into a series of compartments. It has been observed from TEM analysis that the average diameter of the nanotubes changes from ~15 nm to 60 nm with increasing the deposition temperature from 700 to 900 °C. From TEM observation it was also revealed that the tube morphology and graphitization is directly related to the growth temperature and the level of dopant concentration. The detailed structures of the bamboo-shaped CN_x nanotubes were examined by high resolution transmission electron microscopy (HRTEM). Fig. 2b-d shows the HRTEM images of CN_x prepared at 700, 800 and 900 °C respectively.

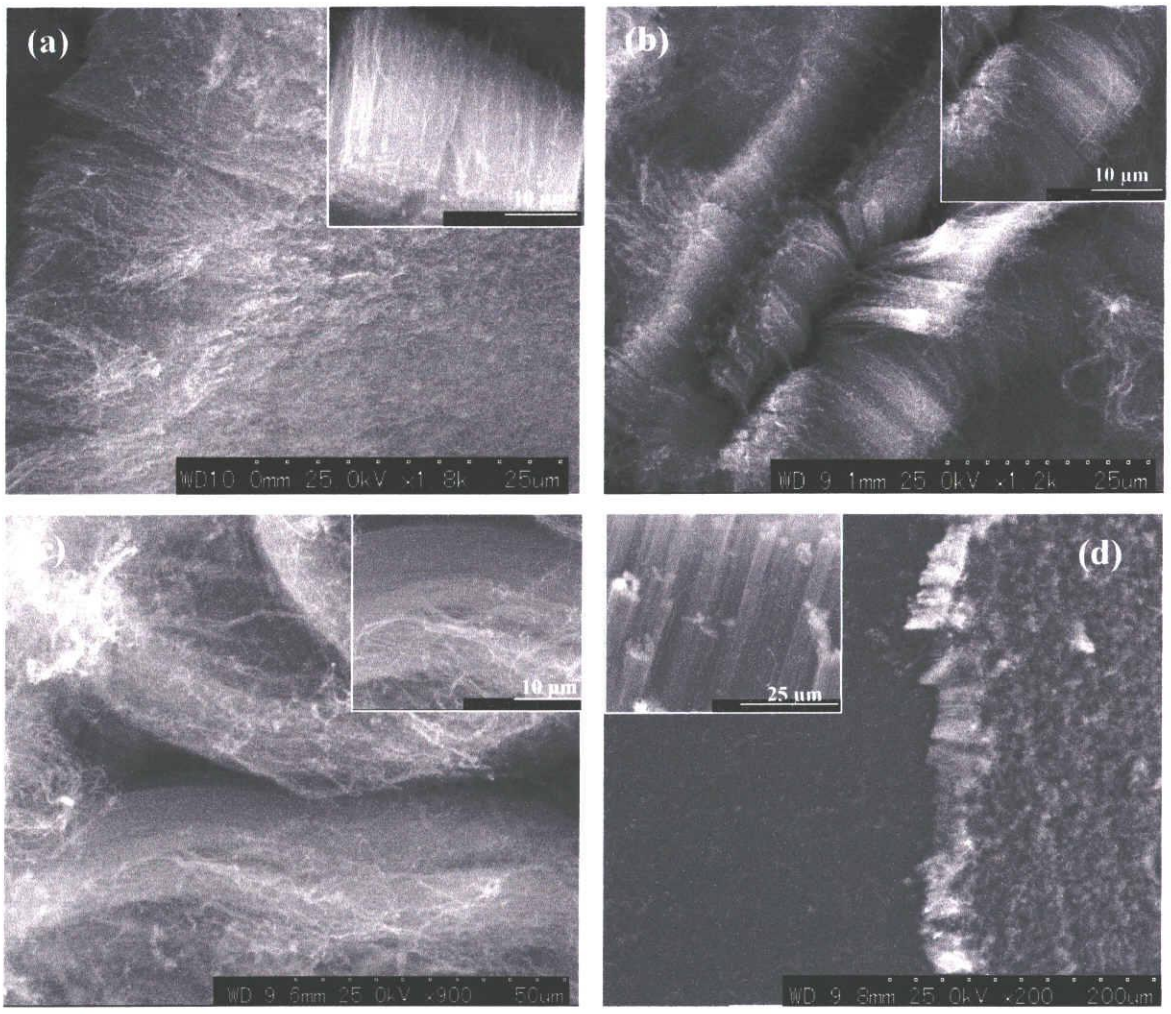

Fig. 1. SEM images of as-grown CN_x nanotubes synthesized at (a) 700 °C (b) 800 °C (c) 900 °C on quartz substrate. (d) CN_x nanotubes on Si(100) substrate at 900 °C. Corresponding magnified images are shown in inset.

The outer wall of CN_x nanotubes prepared at 700 °C are more rough and waved over a long range (Fig. 2b), showing the lower degree of crystalline perfection in relative to the nanotubes prepared at 800 and 900 °C (Fig. 2c and 2d). The compartment layers within the tubes showed interlinked morphology. The reduced temperature (700 °C) yielded bamboo-shaped CN_x nanotubes of poor crystallized compatible layers in relative to 800 and 900 °C, produced bamboo-shaped CN_x nanotubes. At 900 °C, CN_x nanotubes grown on quartz substrate are shown to be more crystalline and less defective due to lighter

nitrogen doping and high growth temperature. HRTEM image of silicon grown carbon nanotubes showed bamboo-like morphology with some amorphous carbon coating in outer layer of nanotubes (Fig. 2e).

6.3.2 Nitrogen content in the as-prepared CN_x nanotubes

XPS analysis was carried out in order to detect the element content and bonding environment of the as-grown CN_x nanotubes grown at different temperatures. Fig. 3 shows the wide scan XPS spectra of as-grown CN_x nanotubes and it shows the distinct C, N and O 1s peaks. The nitrogen concentration of as-prepared samples were determined to be 5.6, 5.8 and 4.8 at.% at 700, 800 and 900 °C respectively. The high intensity of C 1s signal confirms the formation of carbonaceous material. To know the bonding environment of the as-prepared CN_x nanotubes, a deep analysis of C 1s and N 1s signals were carried out in more details. The C 1s peak of CN_x nanotubes can be observed at 284.5, 285.5 and ~288 eV. The peak at 284.5 eV indicates that carbon is mostly in the form of graphite and assigned to sp^2 aromatic hydrocarbons [23]. The peak at 285.5 eV is assigned to sp^3 tetrahedral carbon or C-N bond and the peak at ~288 eV resulting from the carbon bridging nitrogen atoms [24]. The N 1s spectrums of CN_x nanotubes consist of three distinct peaks: N1 at 398.3 eV, N2 at 400.5 eV and N3 at 404.4 eV. The peak at N1 and N2 are known to represent "pyridinic" and "graphitic"-like structure respectively [25-29]. The peak at 404.4 eV is assigned to some oxidized N-species. The O 1s peak appears at 532.3 eV might arise from air adsorbed on the surface of the as-prepared CN_x

nanotubes. From XPS spectra nitrogen concentration of CN_x nanotubes grown on silicon substrate was calculated to be 6.6 at.%.

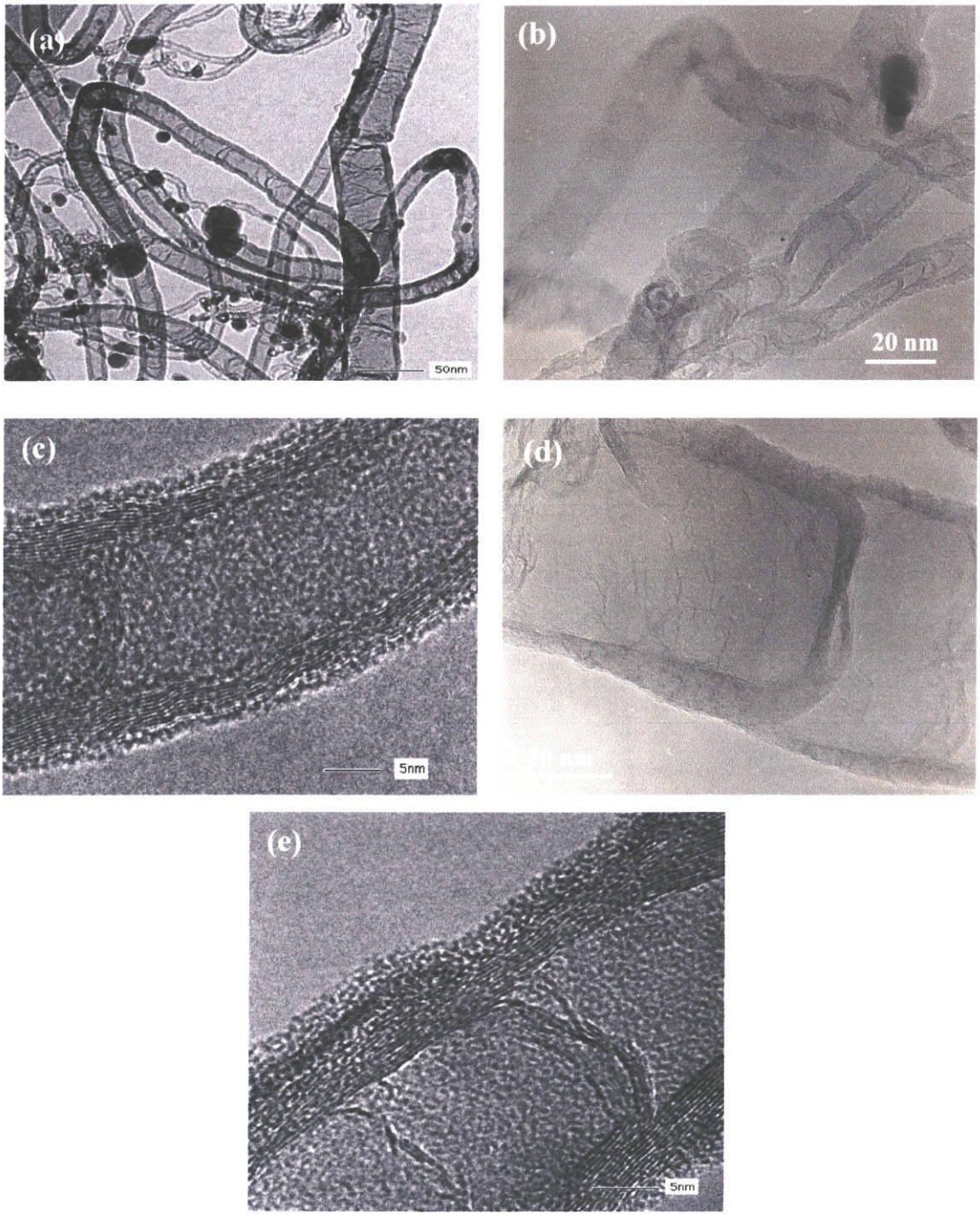

Fig. 2. TEM/HRTEM images of CN_x nanotubes grown on quartz substrate at different temperatures (a) TEM image of CN_x nanotubes prepared at 800 °C. HRTEM images of CN_x nanotubes grown on quartz substrate at (b) 700 °C (c) 800 °C (d) 900 °C. (e) HRTEM images of CN_x nanotubes grown on Si(100) substrate at 900 °C.

6.3.3 The effect of temperature and dopant concentration on the crystallinity of CN_x nanotubes

A Raman spectrum is an effective tool to evaluate the graphitization and crystallinity of the as-prepared CN_x nanotubes. The Raman spectra of the as-grown CN_x nanotubes synthesized at different temperatures are displayed in Fig. 4. The spectrum shows mainly two bands called D-band and G-band. The G-band originates from an in-plane oscillation of carbon atom in the sp^2 graphene sheets. The origin of D-band has been explained as degree of defects or dangling bonds contained in the sp^2 arrangement of graphene planes or lattice distortion. From Raman spectra it was observed that with decreasing temperature the D-band becomes stronger and broader. This indicates that more defects and disorders are introduced as the growth temperature decreases. The graphitization and crystallinity of the as-grown CN_x nanotubes are determined by two factors: growth temperature and nitrogen concentration on CNTs. XPS result indicated that with rising temperature from 700 to 800 °C, the nitrogen concentration increases from 5.6 to 5.8 at.%. But when temperature was increased from 800 to 900 °C, nitrogen concentration on as-prepared CN_x nanotubes decreases from 5.8 at.% to 4.8 at.%. It is obvious that CN_x nanotubes prepared at higher temperature with low dopant concentration shows high degree of crystallinity. The ratio of I_D/I_G value can be taken as crystalline order in the graphene planes where I_D represents the intensity of the disordered band and I_G represents the intensity of the graphitic band. As the value of I_D/I_G increases, more defects are introduced into the CN_x nanotubes. With increasing growth temperature from 700 to 900 °C, the I_D/I_G value decreases from 1.10 to 0.92. This indicates that CN_x

nanotubes prepared at high temperature containing low nitrogen concentration have high degree of graphitization compared to CN_x nanotubes prepared at low temperature.

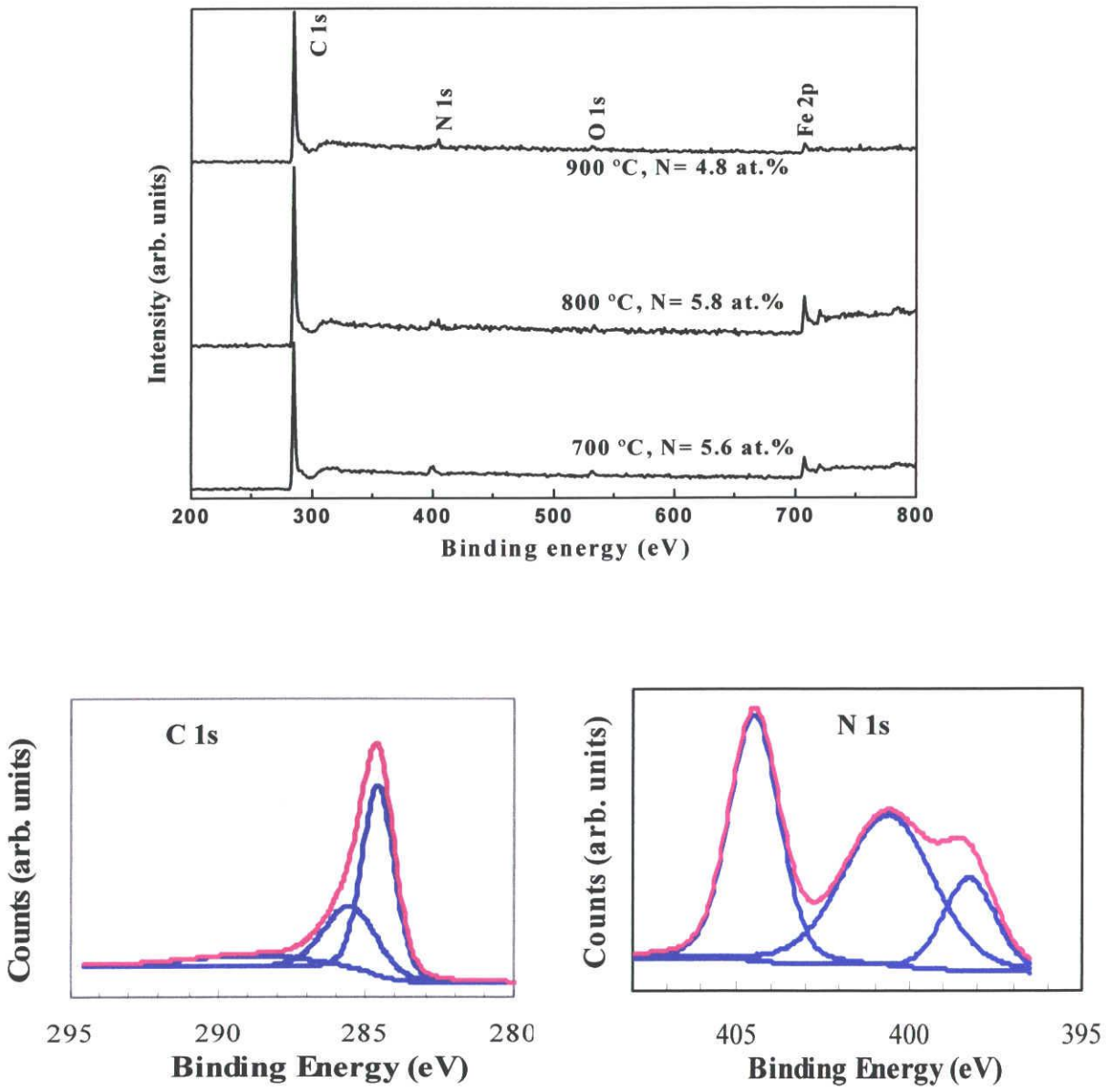

Fig. 3. Wide scan XPS spectra of CN_x nanotubes synthesized at different temperatures on quartz substrate. C 1s and N 1s signal for CN_x nanotubes grown at 800 °C.

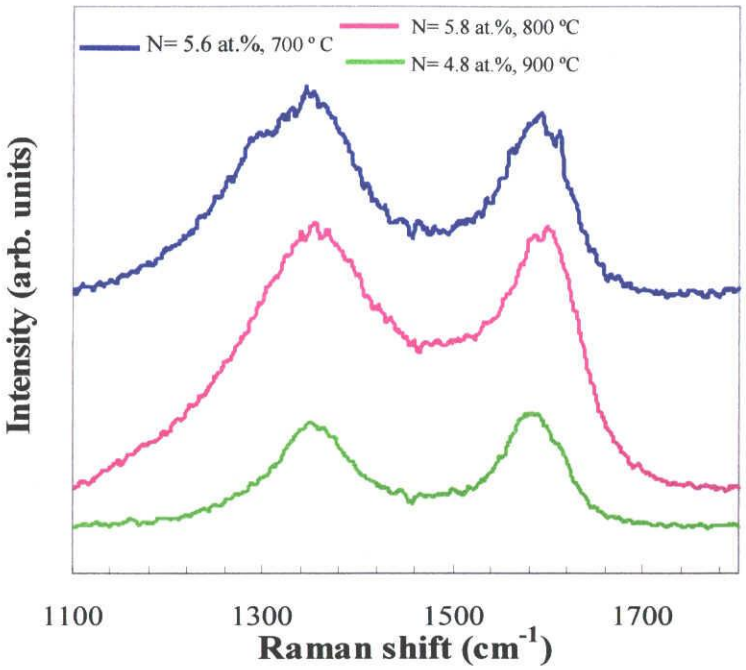

Fig. 4. Raman spectra of as-grown CN_x nanotubes synthesized at different temperatures on quartz substrate.

6.3.4 Thermal stability of as-prepared CN_x nanotubes

TGA and the derivative curve of the weight loss (DTA) are often used to investigate the level of graphitization of as-prepared CN_x nanotubes. Fig. 5 shows the TGA and corresponding DTA curve of as-prepared CN_x nanotubes synthesized at 700-900 °C on quartz substrate. TGA curves show that there is a mass loss of CN_x nanotubes below 300 °C for the sample prepared at 700 °C (Fig. 5a). This apparent mass loss is attributed to the combustion of amorphous carbon in air. But there was no such mass loss was found for CN_x nanotubes prepared at 800 and 900 °C. This indicates that amorphous carbon was rarely observed in these two specimens. The DTA curves of the as-grown CN_x nanotubes are shown in Fig. 5b. When the deposition temperature was increased

from 700 to 800 °C, there is a higher shift of DTA peak maxima from 438 to 452 °C. The higher shift of DTA peak maxima indicates the higher thermal stability of CN_x nanotubes prepared at 800 °C compared to CN_x prepared at 700 °C. The DTA maxima shifted from 452 to 550 °C with increase in CVD temperature from 800 to 900 °C. This shift can be explained in terms of higher degree of graphitization and crystallinity of CN_x nanotubes synthesized at 900 °C, which is in agreement with HRTEM and Raman analysis.

6.3.5 Field emission performance of CN_x nanotubes

The field emission performance was carried out for CN_x nanotubes grown over quartz substrate at three different temperatures. The field emission properties of the CN_x nanotubes depend upon various factors such as level of dopant concentration and overall structure of the CN_x nanotubes film which includes height, density, spacing etc. The field emission performance of CN_x nanotubes prepared at 800 °C showed better results compared to the CN_x nanotubes grown at 700 and 900 °C. The superior field emission performance of the CN_x nanotubes grown at 800 °C might be due to proper alignment and higher level of dopant concentration on CN_x nanotubes. Fig. 6 shows the field emission characteristics of as-grown CN_x nanotubes prepared at 800 °C. For reliability of data, measurements were recorded four times: while increasing the voltage (1st up), while decreasing the voltage (1st down), and similarly again for the next cycle (2nd up and 2nd down). The corresponding Fowler-Nordheim plot is shown in the inset of Fig. 6. The turn-on and threshold field was found to be 1.6 and 2.3 V/μm, respectively for the CN_x nanotubes prepared at 800 °C. Here the turn-on field and threshold field were defined as

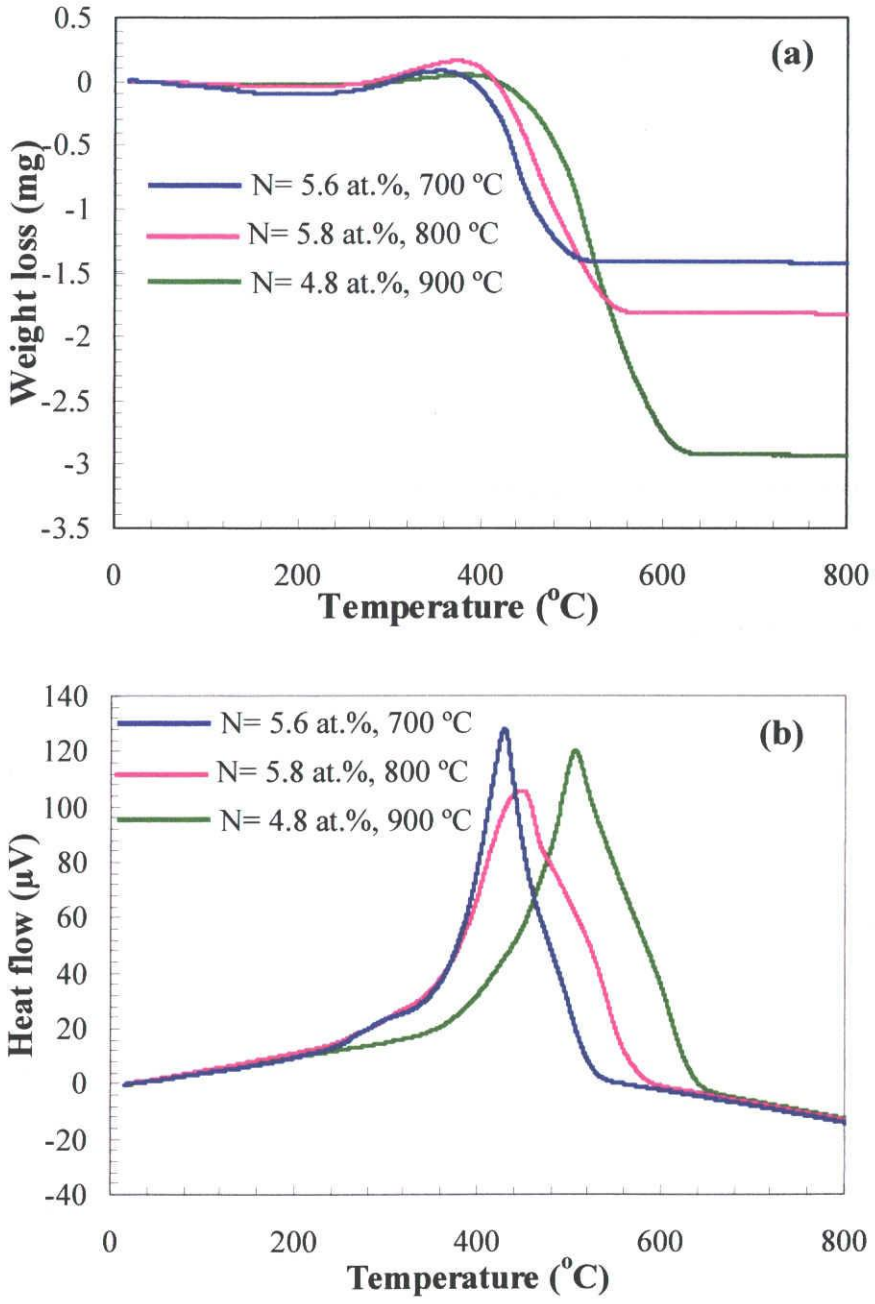

Fig. 5. (a) TGA and corresponding (b) DTA curves of CN_x nanotubes synthesized at different temperatures on quartz substrate.

the fields at which current density reaches 10 μA/cm^2 and 1 mA/cm^2, respectively. The plot of ln(J/E^2) versus 1/E characteristics (inset of Fig. 6) shows straight line, suggesting

that the current indeed results from the field emission of the CN_x nanotubes. Moreover, CN_x nanotubes indicate much higher emission current density at a low electric field (10 mA/cm^2 at ~3 V/μm), which is suitable to apply to various field emission devices.

In past, there are few studies of field electron emission of CN_x nanotubes synthesized by different techniques using different precursors. Recently, Srivastava et al. studied the field emission behavior of CN_x nanotubes. Field emission measurement of CN_x nanotubes indicated that turn-on and threshold field is in the range of 1.5-1.95 and 2.65-3.55 V/μm, respectively [11]. In our case the turn-on and threshold field was observed to be 1.6 and 2.3 V/μm, respectively. Wang et al. measured the field electron emission of CN_x nanotubes and they observed that the CN_x nanotubes began to emit electrons at an electric field of 1.5 V/μm, and current densities of 80 $\mu A/cm^2$ have been realized at an applied field as low as 2.6 V/μm [19]. Similarly Che et al. showed superior field emission characteristics of horizontally aligned CNTs and it was found that the turn-on field of the CN_x nanotubes is at least ~2 V/μm less and the field conversion factor under low bias voltage is about four times more than that of the CNTs [30]. The field electron emission behavior of our CN_x nanotubes is comparable or even better with some of the earlier published reports [11,19]. Such a nice field emission performance of the CN_x nanotubes synthesized at 800 °C might be due to high nitrogen concentration and suitable density of the as-grown CN_x nanotubes on substrate. The results demonstrate that monoethanolamine is an effective precursor for growing highly dense and aligned CN_x nanotubes and their performance on field electron emission. Such nanomaterials might be a promising material for field electron emission applications.

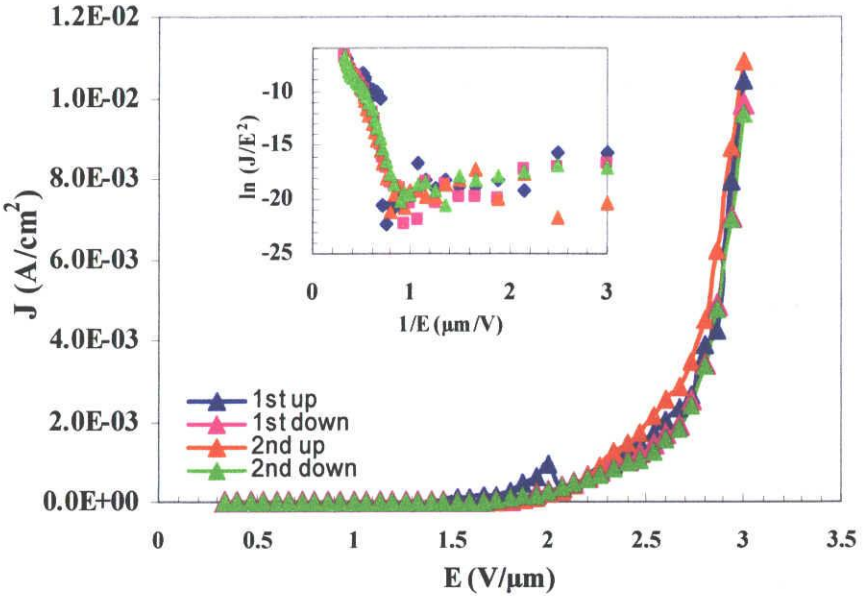

Fig. 6. Plot of emission current density versus electric field of CN_x nanotubes on quartz substrate prepared at 800 °C. The inset shows the corresponding Fowler-Nordheim plot of emission current.

6.4 Conclusion

In summary, highly aligned bamboo-shaped CN_x nanotubes were synthesized via pyrolysis of monoethanolamine/ferrocene mixture in the temperature range 700-900 °C. The difficulty of using multi precursors during CVD can be avoided easily using monoethanolamine as a single C/N feedstock to grow aligned bamboo-shaped CN_x nanotubes. Again during deposition monoethanolamine decomposes to form ammonia which is very effective for growing CN_x nanotubes. HRTEM and Raman spectroscopy reveals that degree of graphitization increases with increasing the growth temperature. XPS results revealed that three different types of nitrogen atoms are present in the as-prepared material. The as-grown CN_x nanotubes show superior field emission characteristics and high current density at low field (turn-on field: 1.6 V/μm, threshold

field: 2.3 V/μm and maximum current density: 10 mA/cm^2 at ~3 V/μm). The results demonstrate that monoethanolamine is an effective precursor for growing CN_x nanotubes and such nanomaterials might be a promising material for field electron emission applications. For further exploitation of this promising material as an FEE source, detailed study of the morphology and dopant concentration of the emitters will be necessary.

References

1. W. Liang, M. Bockrath, D. Bozovic, J.H. Hafner, M. Tinkham, H. Park, Nature 411 (2001) 665.
2. K.H. An, W.S. Kim, Y.S. Park, J.M. Moon, D.J. Bae, S.C. Lim, Y.S. Lee, Y.H. Lee, Adv. Funct. Mater. 11 (2001) 387.
3. C. Liu, Y.Y. Fan, M. Liu, H.T. Cong, H.M. Cheng, M.S. Dresselhaus, Science 286 (1999) 1127.
4. M.S. Dresselhaus, G. Dresselhaus, P.C. Eklund, Science of Fullerene and carbon nanostructures, Academic press, San Diego, 1996.
5. M.S. Dresselhaus, G. Dresselhaus, Ph. Avouris Eds., Carbon Nanotubes Synthesis, Structure, Properties, And Applications, Springer Verlag, Berlin, 2001.
6. A.H. Nevidomskyy, G. Csanyi, M.C. Payne, Phys. Rev. Lett. 91 (2003) 105502.
7. M.C. dos Santos and F. Alvarez, Phys. Rev. B 58 (1998) 13918.
8. M. Terrones, P.M. Ajayan, F. Banhart, X. Blase, D.L. Carroll, J.C. Charlier, et al., Appl. Phys. A 74 (2002) 355.
9. R.Droppa Jr., C.T.M. Ribeiro, A.R. Zanatta, M.C. dos Santos, F. Alvarez, Phys. Rev. B 69 (2004) 045405.
10. M. Glerup, J. Steinmetz, D. Samaille, O. Stephan, S. Enouz, A. Loiseau, S. Roth, P. Bernier, Chem. Phys. Lett. 387 (2004) 193.
11. S.K. Srivastava, V.D. Vankar, D.V. Sridhar Rao, V. Kumar, Thin Solid Films 515 (2006) 1851.

12. K. Suenaga, M.P. Johansson, N. Hellgren, E. Broitman, L.R. Wallenberg, C. Colliex, J. Sundgren, L. Hultman, Chem. Phys. Lett. 300 (1999) 695.

13. R. Sen, B.C. Satishkumar, A. Govindaraj, K.R. Harikumar, G. Raina, J.P. Zhang, et al., Chem. Phys. Lett. 287 (1998) 671.

14. S.H. Lim, H.I. Elim, X.Y. Gao, A.T.S. Wee, W. Ji, J.Y. Lee, J. Lin, Phy. Rev. B 73 (2006) 045402.

15. M. Terrones, N. Grobert, J. Olivares, J.P. Zhang, H. Terrones, K. Kordatos, W.K. Hsu, J.P. Hare, P.D. Townsend, K. Prassides, A.K. Cheetham, H.W. Kroto, D.R.M. Walton, Nature 388 (1997) 52.

16. Y.T. Lee, N.S. Kim, S.Y. Bae, J. Park, S.C. Yu, H. Ryu, H.J. Lee, J. Phys. Chem. B 107 (2003) 12958.

17. W.Q. Han, P. Kohler-Redlich, T. Seeger, F. Ernst, M. Rühle, N. Grobert, W.K. Hsu, B.H. Chang, Y.Q. Zhu, H.W. Kroto, D.R.M. Walton, M. Terrones, H. Terrones, Appl. Phys. Lett. 77 (2000) 1807.

18. J.W. Jang, C.E. Lee, S.C. Lyu, T.J. Lee, C.J. Lee, Appl. Phys. Lett. 84 (2004) 2877.

19. X. Wang, Y. Liu, D. Zhu, L. Zhang, H. Ma, N. Yao, B. Zhang, J. Phys. Chem. B 106 (2002) 2186.

20. J. Liu, S. Webster, D.L. Carroll, J. Phys. B 109 (2005) 15769.

21. G. Zhang, W. Duan, B. Gu, Appl. Phys. Lett. 80 (2002) 2589.

22. H.-L. Sun, J.F. Jia, D. Zhong, Q.T. Shen, M. Sun, Q.K. Xue, E.G. Wang, Phys. Rev. B 66 (2002) 085423.

23. Y. Xia and R. Mokaya, Adv. Mater. 16 (2004) 1553.

24. B. Bouchet-Fabre, E. Marino, G. Lazar, K. Zellama, M. Clin, D. Ballutaud, F. Abel, C. Godet, Thin Solid Films 482 (2005) 167.

25. H.C. Choi, J. Park, B. Kim, J. Phys. Chem. B 109 (2005) 4333.

26. M. Nath, B.C. Satishkumar, A. Govindaraj, C.P. Vinod, C.N.R. Rao, Chem. Phys. Lett. 322 (2000) 333.

27. M. Terrones, P. Redlich, N. Grobert, S. Trasobares, W.K. Hsu, H. Terrones, Y.Q. Zhu, J.P. Hare, C.L. Reeves, A.K. Cheetham, M. Rühle, H.W. Kroto, D.R.M. Walton, Adv. Mater. 11 (1999) 655.

28. R. Sen, B.C. Satishkumar, A. Govindaraj, K.R. Harikumar, M.K. Renganathan, C. N.R. Rao, J. Mater. Chem. 7 (1997) 2335.

29. M. Terrones, P.M. Ajayan, F. Banhart, X. Blase, D.L. Carroll, J.C. Charlier, R. Czerw, B. Foley, N. Grobert, R. Kamalakaran, P. Kohler-Redlich, M. Ruhle, T. Seeger, H. Terrones, Appl. Phys. A: Mater. Sci. Process. 74 (2002) 355.

30. R.C. Che, L.M. Peng, M.S. Wang, Appl. Phys. Lett. 85 (2004) 4753.

Chapter 7

Growth of Y-junction bamboo-shaped CN_x nanotubes and their field electron emission

7.1 Introduction

CNTs with junction are likely to be a basic building unit for nanoelectronic devices. This kind of junction material show novel mechanical [1], electrical [2] and thermal [3] properties. Andriotis et al. postulated that Y-junction nanotubes may exhibit the gating behavior characteristics of transistors [4] and this prediction was proved by Rao and his co-workers [5]. This kind of material is difficult to synthesize than the normal CNTs. The first synthesis of Y-junction CNTs was reported in 1995 by a catalytic arc discharge method [6]. Since then, varieties of method have been developed to synthesize Y-junction CNTs. Y-junction CNTs are synthesized by Y-shaped nanochannel alumina templates in the presence of cobalt particles [7], CVD method [8-13], reduction of hydrocarbon in stainless autoclave [14] etc.

The doping of CNTs with nitrogen atom is a practical and effective ways to tailor their electronic properties. Incorporation of nitrogen atom on CNTs changes electrical properties and chemical reactivity of CNTs [15,16]. CN_x nanotubes render them n-type material regardless of tube chirality [17] and nitrogen in doped CNTs act as a donor. In particular, CN_x nanotubes are effective field emitter and it has been proved that CN_x nanotubes show lower turn-on and higher current density than undoped CNTs [18]. Like unbranched CNTs, Y-junction nitrogen-doped carbon nanotubes (Y-CN_x) are also one of the promising materials in the upcoming field of nanoelectronics. There are few reports available in the literature on the synthesis of Y-CN_x nanotubes. Deepak et al. synthesized Y-CN_x nanotubes by pyrolysis of a Ni-phthalocyanine and thiophene mixture and studied

their electronic properties [19]. The main focus of the current research was to prepare Y-CN_x nanotubes and their application in field electron emission.

Up to now, several methods such as arc discharge [20], microwave plasma enhanced chemical vapor deposition [21], magnetron sputtering [22], and CVD method have been carried out to synthesize CN_x nanotubes [23]. Among these methods, CVD method is the preferred technique for low cost production of CNTs. CN_x nanotube is mainly synthesized by catalytic pyrolysis of multi feedstock which has been discussed in our earlier chapter. Lee et al. synthesized CN_x nanotubes by pyrolysis of C_2H_2 and NH_3 using $Fe(CO)_5$ as Fe catalyst [24] and they confirmed that ammonia is an effective nitrogen source for doping of CNTs. Jang et al. prepared bamboo-shaped CN_x nanotubes of maximum 5 at.% of nitrogen by catalytic decomposition of C_2H_2/NH_3 mixture on SiO_2 substrates at 850 °C [25]. Han et al. obtained bamboo-shaped CN_x nanotubes by pyrolyzing C_{60} mixed with ferrocene in ammonia [26]. Wang and co-workers synthesized the vertically aligned CN_x nanotubes by pyrolysis of iron phthalocyanine under the ammonia atmosphere [18]. Liu et al. studied the effect of ammonia on nitrogen content and doping environment of CNTs prepared by pyrolysis of pyridine and ferrocene [27]. It has been proved that ammonia is an effective nitrogen source for preparing CN_x nanotubes. It has been observed that in every case ammonia gas was passed separately as a nitrogen precursor with carbon feedstock to prepare CN_x nanotubes. In the present investigation, we have chosen monoethanolamine as a C/N feedstock to prepare Y-CN_x nanotubes. The main advantage of using monoethanolamine is that during the growth condition it decomposes to produce ammonia which might be very effective for incorporation of high nitrogen concentration on CNTs.

A variety of growth mechanisms have been proposed to explain the formation of Y-junction CNTs. Luo et al. proposed that when CNTs with metal particle collide from different direction (Fig. 1) that leads to formation of CNTs of different junctions [28].

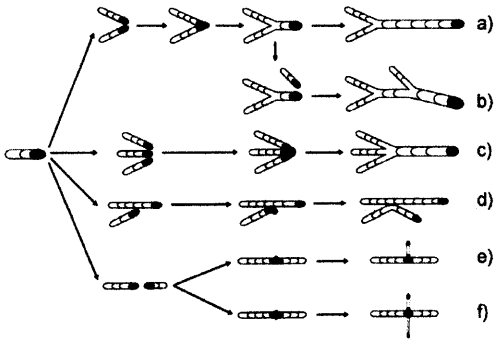

Fig. 1. Schematic representation of the growth processes of various CNT junctions. (a) a Y-junction CNT (b) a multilevel Y-junction CNT (c) a multi-terminal Y-junction CNT (d) an L-junction CNT (e) a needle-like branched T-junction CNT and (f) a four-terminal crossed-junction CNT.

Tsai et al. described the growth as a welding process. The nanoparticles on the top of the CNTs may merge into one because of surface tension and after that the joining CNTs grow steadily to form junction CNTs [29]. The schematic diagram of the mechanism of formation of Y-CNTs proposed by Heyning et al. is shown in Fig. 2 [30].

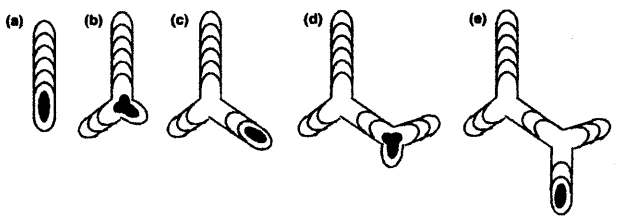

Fig. 2. (a) The formation of a normal nanotube. (b) The catalyst particle stops and the growth of a branch is formed (end-growth), the angle between the backbone and the branch is on 120°. (c) The catalyst particle continues moving while growing the back-bone tip-growth. (d, e) The sequence (b, c) is repeated until the growth of the whole tube is terminated.

In this chapter, we have reported an efficient way to synthesize Y-CN_x nanotubes on GaAs substrate using a single feedstock by thermal CVD method and studied their field electron emission performance. To the best of our knowledge this is the first approach to synthesize Y-CN_x nanotubes by catalytic pyrolysis of monoethanolamine/ferrocene mixture on GaAs substrate. The development of new idea to grow Y-CN_x nanotubes over GaAs substrate using monoethanolamine as a C/N feedstock would be significant for further investigation in this field.

7.2 Experimental

CN_x nanotubes were prepared by catalytic pyrolysis of monoethanolamine ($NH_2CH_2CH_2OH$) and ferrocene mixture at 950 °C pressure by CVD method. The schematic diagram of the CVD system is shown in Fig. 3.

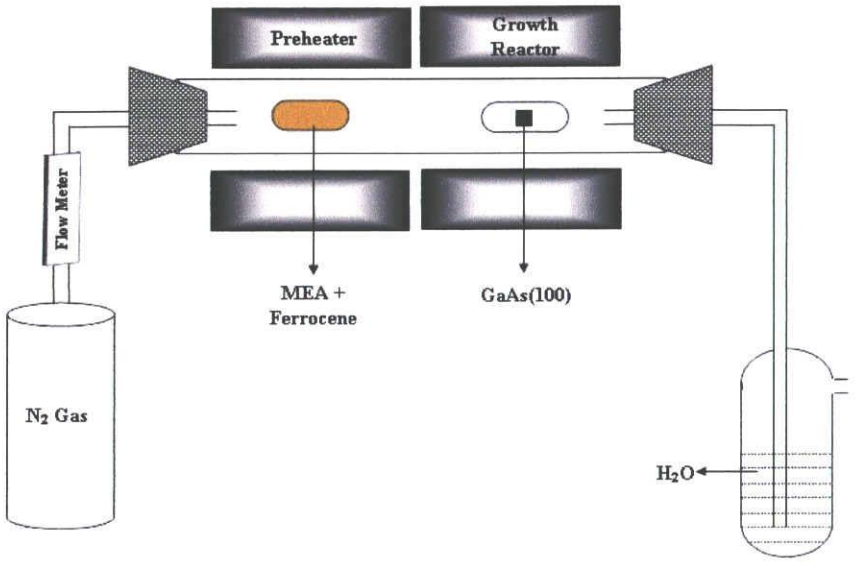

Fig. 3. Schematic diagram of CVD system.

The CVD system consists of two electric furnaces, one is preheater and other is growth reactor. GaAs substrate was ultrasonically cleaned by acetone followed deionized water. The cleaned substrate was kept in the quartz boat and placed at the middle of the growth reactor. Before switch on the furnaces, nitrogen gas was purged for few minutes to expel out the air inside the quartz tube. Monoethanolamine/ferrocene mixture was vaporized at 100 °C in the preheater and pyrolyzed at 950 °C in the second furnace (growth reactor) under nitrogen atmosphere (flow rate: 100 cm^3/min). After 90 min, the furnaces were switched off and allowed to cool to room temperature under nitrogen atmosphere. The deposited material was characterized by SEM, TEM and XPS and Raman spectroscopy analysis. Field emission measurements were performed in a vacuum chamber at a pressure less than 3×10^{-9} Torr within UHV-SEM (JAMP-7100). The cathode consisted of as-grown CN_x nanotube on GaAs substrate, and anode was a polished stainless steel rod (1 mm in diameter). The distance between cathode and anode was 300 μm.

7.3 Results and discussion

7.3.1 Electron microscopy analysis

Fig. 4 shows the scanning electron microscopy image (Hitachi S-3000H, scanning electron microscope) of as-synthesized Y-CN_x nanotubes. Both normal and branched CNTs were observed in the as-prepared material. There is also combination of junctions, for example a Y-junction is connected to another Y-junction (Fig. 4b). SEM images clearly show that metal particle often present at the tip or outside of the tip of the nanotubes. Due to the presence of metal particle at the tip, the as-grown nanotubes can be

purified easily by mild acid treatment for devices fabrication. Inset of Fig. 4a shows Y-CN_x nanotubes of non uniform branches diameter. Detail interior structure of the Y-CN_x nanotube was investigated by TEM (HITACHI HF 2000 with an acceleration voltage 200 kV) and it was shown in Fig. 5.

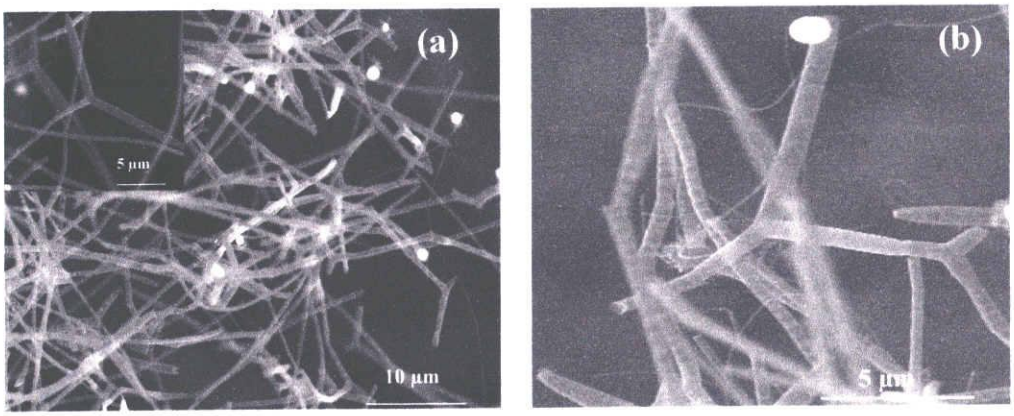

Fig. 4. SEM images of (a) Y-CN_x nanotubes grown on GaAs substrate. Inset shows Y-CN_x of non uniform branches diameter (b) a Y-junction connected with another junction.

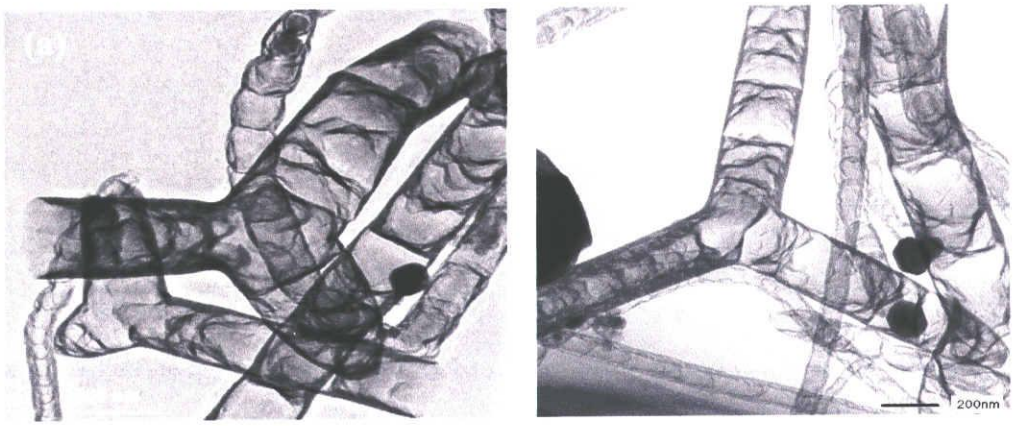

Fig. 5. TEM images of Y-CN_x nanotubes with bamboo like structure with compartment grown on GaAs substrate (a) with two open ended and (b) with no metal particle presence in the junction of the nanotube.

Bamboo-like nanotubes with well separated compartments was observed from TEM analysis (Fig. 5a and 5b). It was realized that the observation of bamboo-like morphology was due to the doping of nitrogen in the CN_x [31]. From TEM images, it is also noted that

no catalyst particles are present at the junction of CNTs and two ends of the junction nanotubes are opened (Fig. 5a and 5b). This gives an indication that during the growth process catalyst particle pushed away from the tip and come outside of the tube and makes the tube open ended. It was observed that catalyst particle lift off from the substrate during the growth of CN_x. We speculated that during the growth process catalyst particle move upward and divided into two parts. These two particles were moved forward in different direction and incorporation of carbon clusters forms the Y-CN_x nanotubes. If the catalyst particle comes outside of the tube, the formation of

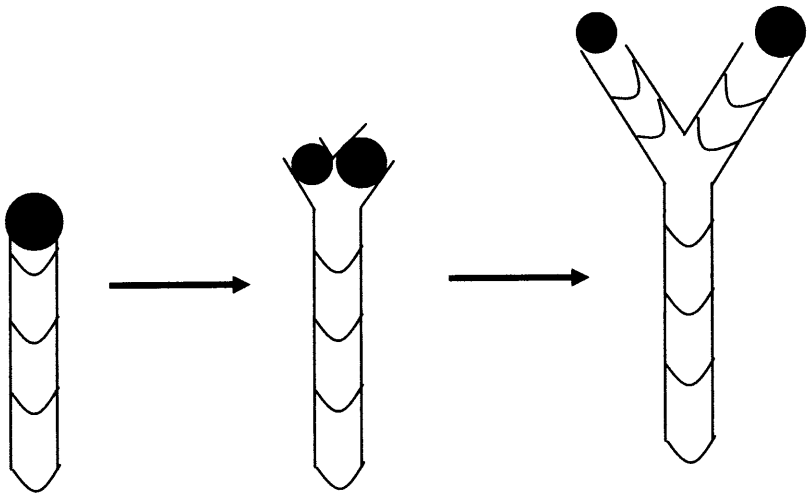

Fig. 6. Schematic representation of Y-CN_x growth sequences.

nanotubes will be terminated. The schematic diagram of the proposed mechanism is depicted in Fig. 6.

7.3.2 XPS analysis of as-grown CN_x nanotubes

The composition of the CN_x nanotubes was determined by XPS (SSX-100 XPS spectrometer) analysis. The XPS spectrum of the sample indicated that product consists of carbon, nitrogen and small amount of oxygen.

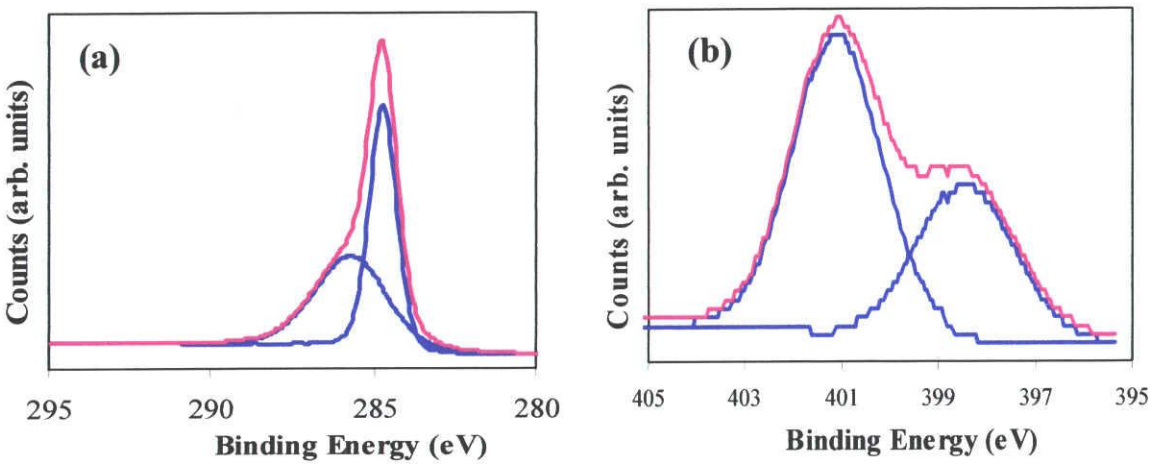

Fig. 7. XPS spectra of (a) C 1s signal and (b) N 1s signal of CN_x nanotubes grown on GaAs substrate. It depicts the presence of two different types of nitrogen environment and the nitrogen content can be estimated as 7.8 at.%.

The oxygen peak might arise from air adsorbed at the specimen surface (not shown here). C 1s and N 1s spectrum of CN_x nanotube is shown in Fig. 7a and 7b respectively. The C 1s peak was observed at 284.6 and 285.6 eV. The peak at 284.6 eV indicates that carbon is mostly in the form of graphite [32] and the peak at 285.6 eV indicates the presence of C-N bond [33]. The N 1s peak at 398.4 eV and 401.1 eV is ascribed due to the "pyridinic" and "graphitic" nitrogen, respectively [34]. From XPS analysis nitrogen concentration on CN_x nanotubes was estimated to be 7.8 at.% and the nitrogen concentration is higher than the earlier reported value [24,25].

7.3.3 Raman spectroscopy analysis of as-synthesized CN_x nanotubes

Raman spectroscopy is an effective way to evaluate the quality of the as-prepared CN_x nanotubes. Fig. 8 shows the Raman spectra of as-grown CN_x nanotubes. The spectrum shows two bands at ca. 1355 cm^{-1} (D-band) and ca. 1590 cm^{-1} (G-band). The D-band corresponds to the defects and disordered in the graphene sheets. The G-band is attributed to the well graphitized CNTs [35]. The intensity ratio of D-band and G-band determines the quality of the CNTs. For CN_x nanotubes I_D/I_G was found to be ~1.

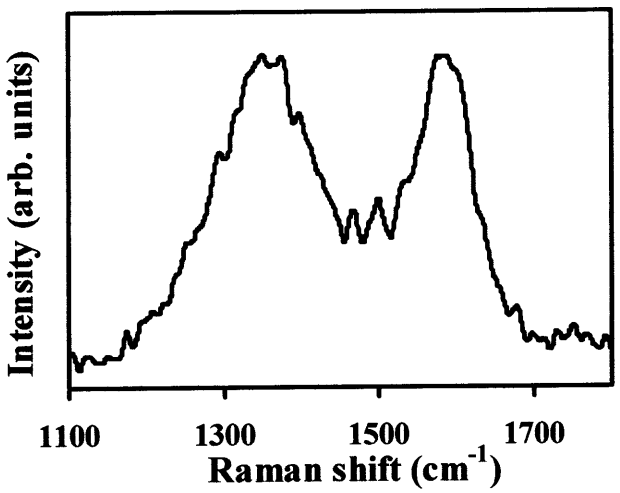

Fig. 8. Raman spectra of as-grown CN_x nanotubes.

7.3.4 Field emission behavior of CN_x nanotubes

The emission current density versus electric field curve of as-grown CN_x nanotube is shown in Fig. 9. The turn-on field, corresponding to the current density of 10 $\mu A/cm^2$ is 1.6 V/μm and threshold field, which correspond to the current density of 1 mA/cm^2 is 2.63 V/μm. The maximum current density was found to be 2 mA/cm^2 at ~3

V/μm. Inset of the Fig. 9 shows F-N plot. The emission characteristics were comparable or better than those reported for CN_x nanotubes [18,21]. The Y-CN_x nanotubes grown on GaAs substrate are quite advantageous to reduce the screening effect because of sufficient distance between the adjacent CNTs.

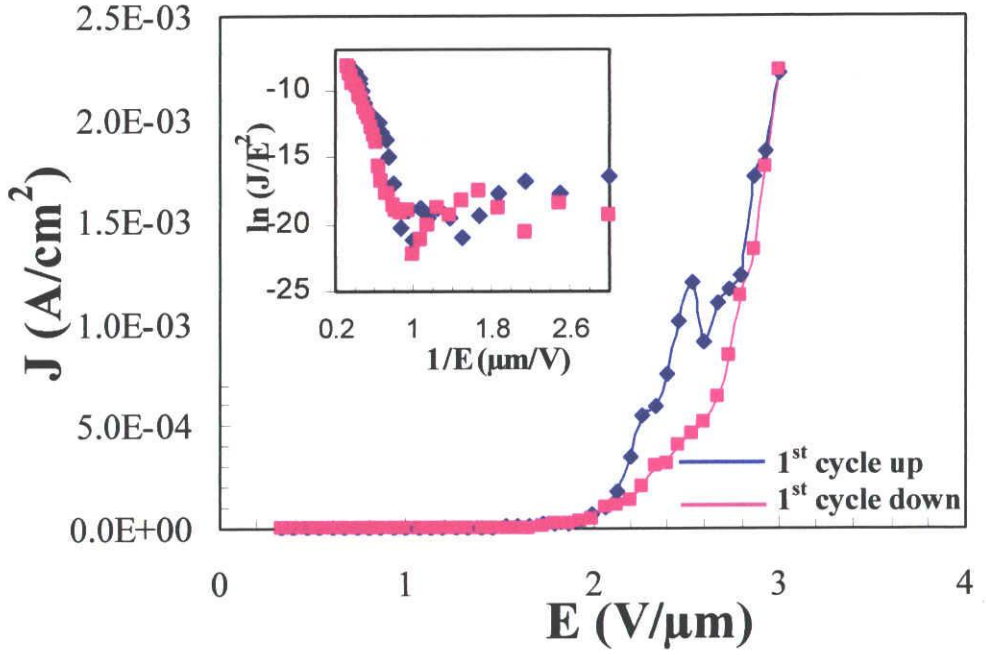

Fig. 9. Field electron emission behavior of CN_x nanotubes deposited on GaAs substrate.

The yield of Y-CN_x nanotube is still low and we believe that proper adjustment of reaction conditions, it is possible to increase the selectivity of Y-junction N-doped nanotubes. For further exploitation of this promising material as a field electron emission source, detailed study would provide a more details of role of junction nanotubes.

7.4 Conclusion

Bamboo-shaped Y-CN_x of 7.8 at.% nitrogen concentration were synthesized by pyrolysis of monoethanolamine and ferrocene mixture at 950 °C on GaAs substrate. The use of single feedstock as a C/N feedstock to prepare the Y-CN_x nanotubes makes the reaction simpler and feasible. Field emission measurements indicated that as-grown CN_x nanotubes are very effective for field electron emission. The as-grown CN_x nanotubes on GaAs showed good field emission characteristics with turn-on and threshold field is 1.6 and 2.63 V/μm, respectively and maximum current density was observed 2.2 mA/cm^2 at ~3 V/μm. Thus Y-CN_x nanotube grown on GaAs substrate was thought to be quite promising as field electron emission source.

References

1. B.C. Satishkumar, P.J. Thomas, A. Govindaraj, C.N.R. Rao, Appl. Phys. Lett. 77 (2000) 2530.
2. C. Papadopoulos, A. Rakitin, J. Li, A.S. Vedeneev, J.M. Xu, Phys. Rev. Lett. 85 (2000) 3476.
3. A. Cummings, M.A. Osman, D. Srivastava, M. Menon, Phys. Rev. B 70 (2004) 115405.
4. A.N. Andriotis, M. Menon, D. Srivastava, L. Chernozatonskii, Phys. Rev. Lett. 87 (2001) 066802.
5. P.R. Bandaru, C. Daraio, S. Jin, A.M. Rao, Nature Mater. 4 (2005) 663.
6. D. Zhou and S. Seraphin, Chem. Phys. Lett. 238 (1995) 286.
7. J. Li, C. Papadopoulos, J. Xu, Nature 402 (1999) 253.
8. Q. Liu, W. Liu, Z.M. Cui, W.G. Song, L.J. Wan, Carbon 45 (2007) 268.
9. O.T. Heyning, P. Bernier, M. Glerup, Chem. Phys. Lett. 409 (2005) 43.
10. L.F. Su, J.N. Wang, F. Yu, Z.M. Sheng, Chem. Vapor. Depos. 11 (2005) 351.
11. D.Y. Ding, J.N. Wang, F. Yu, L.F. Su, Appl. Phys. A-Mater. 81 (2005) 805.
12. F.L. Deepak, A. Govindaraj, C.N.R. Rao, Chem. Phys. Lett. 345 (2001) 5.
13. H.W. Zhu, L.J. Ci, C.L. Xu, J. Liang, D.H. Wu, Diamond Relat. Mater. 11 (2002) 1349.
14. J.W. Liu, M.W. Shao, X.Y. Chen, W.C. Yu, X.M. Liu, Y.T. Qian, J. Am. Chem. Soc. 125 (2003) 8088.

15. D.P. Kim, C.L. Lin, T. Mihalisin, P. Heiney, M.M. Labes, Chem. Mater. 3 (1991) 686.

16. M.C. dos Santos and F. Alvarez, Phys. Rev. B 58 (1998) 13918.

17. R. Czerw, M. Terrones, J.C. Charlier, X. Blase, B. Foley, R. Kamalakaran, N. Grobert, H. Terrones, D. Tekleab, P.M. Ajayan, W. Blau, M. Rühle, D.L. Carroll, Nano Lett. 1 (2001) 457.

18. X. Wang, Y. Liu, D. Zhu, L. Zhang, H. Ma, N. Yao, B. Zhang, J. Phys. Chem. B 106 (2002) 2186.

19. F.L. Deepak, N.S. John, A. Govindaraj, G.U. Kulkarni, C.N.R. Rao, Chem. Phys. Lett. 411 (2005) 468.

20. M. Glerup, J. Steinmetz, D. Samaille, O. Stephan, S. Enouz, A. Loiseau, S. Roth, P. Bernier, Chem. Phys. Lett. 387 (2004) 193.

21. S.K. Srivastava, V.D. Vankar, D.V. Sridhar Rao, V. Kumar, Thin Solid Films 515 (2006) 1851.

22. K. Suenaga, M.P. Johansson, N. Hellgren, E. Broitman, L.R. Wallenberg, C. Colliex, J. Sundgren, L. Hultman, Chem. Phys. Lett. 300 (1999) 695.

23. S.H. Lim, H.I. Elim, X.Y. Gao, A.T.S. Wee, W. Ji, J.Y. Lee, J. Lin, Phy. Rev. B 73 (2006) 045402.

24. C.J. Lee, S.C. Lyu, H.W. Kim, H.J. Lee, K.I. Cho, Chem. Phys. Lett. 359 (2002) 115.

25. J.W. Jang, C.E. Lee, S.C. Lyu, T.J. Lee, C.J. Lee, Appl. Phys. Lett. 84 (2004) 2877.

26. W.Q. Han, P. Kohler-Redlich, T. Seeger, F. Ernst, M. Rühle, N. Grobert, W.K. Hsu, B.H. Chang, Y.Q. Zhu, H.W. Kroto, D.R.M. Walton, M. Terrones, H. Terrones, Appl. Phys. Lett. 77 (2000) 1807.

27. J. Liu, S. Webster, D.L. Carroll, J. Phys. B 109 (2005) 15769.

28. C. Luo, L. Liu, K. Jiang, L. Zhang, Q. Li, S. Fan, Carbon 46 (2008) 440.

29. S.H. Tsai, C.T. Shiu, W.J. Jong, H.C. Shih, Carbon 38 (2000) 1899.

30. O.T. Heyning, P. Bernier, M. Glerup, Chem. Phys. Lett. 409 (2005) 43.

31. M. Terrones, P. Redlich, N. Grobert, S. Trasobares, W.K. Hsu, H. Terrones, Y.Q. Zhu, J.P. Hare, C.L. Reeves, A.K. Cheetham, M. Rühle, H.W. Kroto, D.R.M. Walton, Adv. Mater. 11 (1999) 655.

32. J.R. Pels, F. Kapteijn, J.A. Moulijn, Q. Zhu, K.M. Thomas, Carbon 33 (1995) 1641.

33. S. Point, T. Minea, B. Bouchet-Fabre, A. Granier, G. Turban, Diamond Relat. Mater. 14 (2005) 891.

34. Y. Xia and R. Mokaya, Chem. Mater. 17 (2005) 1553.

35. A.M. Rao, E. Richter, S. Bandow, B. Chase, P.C. Eklund, K.A. Williams, et al., Science 275 (1997) 187.

Chapter 8

Summary and suggestions for future work

8.1 Summary of the present work

Recently undoped CNTs/CNFs and doped CNTs have created a much attention due to their unique physical and chemical properties and potential application in various devices. This thesis mainly deals with the synthesis of undoped CNTs/CNFs and CN_x nanotubes from conventional and unconventional precursors and their application in field electron devices. Till date, CNTs and CNFs have been synthesized by using different precursors (mainly organic precursors). Natural precursors grown CNTs showed its importance due to their advantages over conventional precursors. The natural precursors are regenerative, easily available and no chance of shortage in the coming future. The synthesis of CNTs/CNFs from natural precursors is very rare. Recent studies indicated that natural precursor grown CNTs are very effective for field electron emission. Here we described the synthesis of vertically aligned CNTs from turpentine oil and eucalyptus oil by simple spray pyrolysis method. The result showed that the nanotubes grown from natural precursors are superior for field electron emission. We also successfully synthesized CNFs from turpentine oil using ferrocene as dissolved catalyst and sulfur as a promoter.

Not only undoped but doped CNTs are also very effective material for nanodevices. Till date, people synthesized CN_x nanotubes using a single and multi precursors. I have been successfully synthesized vertically aligned CN_x nanotubes using a single and multi feedstock. For synthesis of CN_x nanotubes using multi feedstock, we used turpentine oil as one of the carbon source. The using of natural precursor over organic precursor as a carbon feedstock is advantageous which is described earlier.

Results showed that turpentine oil is also effective precursor for synthesizing CN_x nanotubes. CN_x nanotubes were synthesized by a single feedstock, monoethanolamine, on various substrates (silicon, quartz, GaAs) and studied their electron field emission. It has been proved that ammonia is an effective precursor to incorporate nitrogen on CNTs. However, literature reports indicated that mostly ammonia gas was passed separately with carbon precursor to synthesize CN_x nanotubes. This make the process little bit difficult. Instead of using ammonia as a separate source we have chosen a precursor which itself produces ammonia after decomposition at high temperature. Monoethanolamine fulfill this requirement. At high temperature it decomposes to produce ammonia that helps to incorporate nitrogen on CNTs easily. It has been observed that monoethanolamine is a suitable precursor to synthesize highly doped CN_x nanotubes by simple CVD method. CN_x nanotubes have predicted as possible candidates for nanosized electronic, photonic devices and mechanical materials in the future applications. CN_x nanotubes grown from monoethanolamine exhibited nice field emission characteristics with turn-on and threshold field are in the literature report range or better than that value. This indicates that monoethanolamine might be a suitable precursor to grow CN_x nanotubes for future field electron devices. The dissertation is summarized below.

Chapter 2 to 7 illustrates the synthesis and characterization of undoped CNTs/CNFs and CN_x nanotubes by spray pyrolysis and CVD method and their application in field electron emission.

SWNTs were prepared by catalytic decomposition of turpentine oil and eucalyptus oil over Fe-Co and Fe-Mo/zeolite catalyst by simple spray pyrolysis method at

850 °C at atmospheric pressure. The result showed that like conventional precursor, turpentine oil and eucalyptus oil is also suitable hydrocarbons for SWNTs synthesis.

CNFs were synthesized from turpentine oil using sulfur as a promoter and ferrocene as dissolved catalyst by spray pyrolysis method. Results indicated that sulfur plays a profound role to promote or inhibit the growth of CNFs. It has been observed that up to certain concentration of sulfur, it promote the growth of CNFs. But the yield of CNFs is very less at high concentration of sulfur which is due to poison of Fe catalyst.

CN_x nanotubes have been synthesized using multi feedstock (turpentine oil and 4-tert-butylpyridine) on silicon and quartz substrate by spray CVD method. The nitrogen concentration on silicon and quartz was found to be 1.6 and 2 at.%, respectively. It was observed that CN_x nanotubes grown on silicon substrate are well graphitized and thermally stable compared to the nanotubes grown on quartz substrate.

Vertically aligned CNTs were deposited on silicon substrate by catalytic pyrolysis of turpentine oil and eucalyptus oil by spray pyrolysis method. CNTs grown from turpentine oil are more graphitized than the CNTs grown from eucalyptus oil. The field emission measurement showed that turpentine oil grown CNTs are better field emitter than eucalyptus oil grown CNTs. This is mainly attributed to the higher degree of crystallinity and greater length of turpentine oil grown CNTs compared to the CNTs grown from eucalyptus oil.

The well-aligned CN_x nanotubes were grown on silicon and quartz substrate from a single feedstock (monoethanolamine) using iron as a catalyst at different temperatures. The CN_x nanotubes grown on quartz substrate have been studied extensively. It is observed that alignment gradually decreases with increasing the

deposition temperature. The as-grown CN_x nanotubes material showed nice field emission behavior.

GaAs substrate was found to be one of the important semiconducting materials for the synthesis of CN_x nanotubes. Y-CN_x nanotubes with 7.8 at.% of nitrogen were prepared on GaAs substrate from monoethanolamine by simple CVD method. The Y-CN_x nanotubes grown on GaAs substrate are good field emitter with a turn-on and threshold field of 1.6 and 2.63 V/μm, respectively. Our result demonstrates that Y-CN_x nanotubes can be suitable to fabricate field emitter for various field emission devices.

8.2 Suggestions for future work

1. To synthesize DWNTs by simple spray pyrolysis method and their application in field electron emission.
2. To synthesize nitrogen-doped SWNTs and DWNTs from a single feedstock: monoethanolamine and studied their field electron emission properties.
3. The detail comparison of field electron emission of nitrogen-doped SWNTs, DWNTs and MWNTs will be carried out.
4. To synthesize boron and alkali metal doped CNTs by simple and inexpensive spray pyrolysis method and their application in field electron emission.
5. To synthesize nitrogen-doped CNFs and the comparison of field emission properties with undoped CNFs will be studied.

Acknowledgement

This thesis would not appear in its present form without the kind assistance, encouragement and support from my supervisor, my family and my colleagues. I am extremely indebted to my Ph.D. supervisor ***Prof. Tetsuo Soga, Department of Environmental Technology and Urban Planning, Nagoya Institute of Technology (NIT).*** With his enthusiasm, constant inspiration, and his efforts to explain things clearly and simply, he helped to make the subject easy for me. Throughout my thesis writing period, he provided advice, good company, and lots of good ideas to me. I am thankful to ***Prof. T. Jimbo*** for his prayers, invaluable guidance, helpful suggestions and support, which have sustained me during these past few years. I must send thanks to ***Prof. M. Tanemura*** for his intellectual advice and giving me the opportunity to use their field emission measurement instrument. ***Prof. M. Tanemura*** was also a particular good leader and motivator, enabling me to face the hard work with a smile on the lips. The discussions, encouragement and critiques made by him were of essence to the progress of this work. I am thankful to ***Dr. Y. Hayashi*** for his constant motivation and inspiration throughout the research period. My sincere thanks and gratitude to ***Prof. Y. Ando of Meijo University*** and ***Prof. K. Sumiyama of NIT*** for their experimental support. I gratefully acknowledge to ***Mr. Y. Fujimoto*** for his assistance in TEM observation.

My special thanks and gratitude to ***Dr. P.R. Somani*** and ***Mrs. S.P. Somani*** who helped me a lot and made my life easier at the initial stage in Japan. I am grateful to ***Dr. R. A. Afre, Dr. Mukul Kumar, Mr. M. Subramanian, Dr. M.K. Pandey, Dr. P. Pradhan, M. Zamri, Dr. S.P. Singh, Mr. Sahabuthin, Mr. Sarvanan, Mr. Kaushik Ghosh, Dr. K.P.O. Mahesh, Dr. Bhaskar, Mr. I. Khatri, Mr. Sudhakar Reddy, Mr. Sridhar Babu, Mr. K.***

Jeyakodi, Mr. Madan, Mr. Maneesh, Mr. V. Reddy, Dr. R. Katoh, Mr. Golap Kalita, Mr. Santosh Satbhai, Ms. Josephine, Ms. Subana, Mrs. Minal, Mrs. Shewta, Mrs. Bharati, Dr. K. Uma, Mrs. Nazreen and all of my lab mates for their kind help, suggestions and cooperation and academic discussions. Many thanks to my friends ***Mr. Taponendu Ghosh, Dr. Jayanta Basu, Mr. Nihar Ranjan Roy, Dr. Basudeb Haldar, Dr. Arabinda Mallick, Mr. Chinmoy Nandi, Mr. Krishanu Sarkar, Mr. Abhijit Dan, Dr. Satyajyoti Senapati, Dr. Debdut Roy, Dr. Kartick Mandal, Dr. B.R. Sarkar, Dr. Nirmalya Kumar Chaki, Mr. Sugata Chowdhury, Dr. Prabal Banerjee, Dr. Anirban Kar, Dr. Anirban Ghosh, Dr. Prabhas Jana, Mr. Arijit Bag, Dr. Suresh Kumar*** for standing by me in good and bad times.

I would like to acknowledge ***21st century COE program and JASSO scholarship*** for providing me fellowship during my PhD period, without this financial support it would have not been possible to complete this degree.

I wish to thank my entire family ***(my late grandfather, my grandmother, my elder brothers, my cousin brothers, my cousin sisters, my sister-in-law, my brother-in-law, my uncle, my aunty, my paternal uncle and aunty)*** for providing a loving environment for me. I owe my loving thanks to ***Madhumanti (Sweety).*** She raised me, supported me, taught me and loved me. Lastly, and most importantly, I wish to thank my parents, ***Mr. Madhusudan Ghosh*** and ***Mrs. Sulekha Ghosh*** for creating an environment in which following this path seemed so natural.

List of Publications

1. **Pradip Ghosh,** Rakesh A. Afre, T. Soga, T. Jimbo, "A simple method of producing single-walled carbon nanotubes from a natural precursor: Eucalyptus oil", Mater. Lett., 61 (2007) 3768.

2. **Pradip Ghosh,** T. Soga, Rakesh A. Afre, T. Jimbo, "Simplified synthesis of single-walled carbon nanotubes from a botanical hydrocarbon: Turpentine oil", Journal of Alloys and Compd. 462 (2008) 289.

3. **Pradip Ghosh,** M. Tanemura, T. Soga, M. Zamri, T. Jimbo, "Field emission property of N-doped aligned carbon nanotubes grown by pyrolysis of monoethanolamine", Solid State Commun. 147 (2008) 15.

4. **Pradip Ghosh,** Tetsuo Soga, Kaushik Ghosh, Rakesh A. Afre, Takashi Jimbo, Yoshinori Ando, "Vertically aligned N-doped carbon nanotubes by spray pyrolysis of turpentine oil and pyridine derivative with dissolved ferrocene", J. Non-Cryst. Solids, 354 (2008) 4101.

5. **Pradip Ghosh,** M. Zamri, M. Subramanian, T. Soga, T. Jimbo, R. Katoh, M. Tanemura, "Bamboo-shaped aligned CN_x nanotubes synthesized using single feedstock at different temperatures and studied their field electron emission", J. Phys. D: Appl. Phys. 41 (2008) 155405.

6. **Pradip Ghosh,** Tetsuo Soga, Kaushik Ghosh, Takashi Jimbo, Ryoji Katoh, Kenji Sumiyama, Yoshinori Ando, "Effect of sulfur concentration on the morphology of carbon nanofibers produced from a botanical hydrocarbon", Nanoscale Res. Lett. 3 (2008) 242.

7. **Pradip Ghosh,** T. Soga, M. Tanemura, M. Zamri, T. Jimbo, R. Katoh, K. Sumiyama, "Vertically aligned carbon nanotubes from natural precursors by spray pyrolysis method and studied their field emission properties", Appl. Phys. A: Material Science and Processing (DOI 10.1007/s00339-008-4856-9).

8. **Pradip Ghosh,** M. Subramanian, M. Zamri, T. Soga, T. Jimbo, M. Tanemura, "Synthesis of Y-junction N-doped carbon nanotubes and their field electron emission" (Submitted to Solid State Commun.).

Conference presentations

National Conference

1. **Pradip Ghosh,** Rakesh A. Afre, T. Soga, T. Jimbo, "Synthesis of single-walled carbon nanotubes by spray pyrolysis of natural precursors", IWAC 2006, Oct. 30-Nov. 3, 2006, NIT, Nagoya, Japan.

International Conferences

1. **Pradip Ghosh,** Rakesh A. Afre, Prakash R. Somani, M. Umeno, T. Jimbo, T. Soga, "Synthesis of carbon nanotubes with narrow diameter-distribution by spray pyrolysis of a natural precursor: Turpentine oil", Nanotube-2006 (NT'06), June 18-June 23, 2006, Nagano, Japan.
2. **Pradip Ghosh,** Rakesh A. Afre, T. Soga, T. Jimbo, "A simple method of producing single-walled carbon nanotubes from natural precursors", New Diamond and Nano Carbons (NDNC 2007), May 28-May 31, 2007, Osaka, Japan.
3. Tetsuo Soga, **Pradip Ghosh,** Rakesh A. Afre, Takashi Jimbo, "Synthesis of Carbon Nanotubes by Spray Pyrolysis of Natural Precursors", International Conference on Advancement of Materials and Nanotechnology (ICAMN) 2007, Malaysia.